

AD-A068 425

NATIONAL SEVERE STORMS LAB NORMAN OKLA
THUNDERSTORM GUST FONTS--OBSERVATIONS AND MODELING.(U)
DEC 78 J T LEE, J STOKES, Y SASAKI, T BAXTER DOT-FA76WAI-622

F/G 4/2

UNCLASSIFIED

FAA/RD-78/145

NL

1 OF 2
ADA
068425



Report No. FAA-RD-78-145

LEVEL *II*

B.S. 12

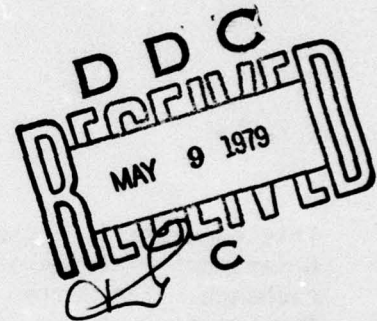
THUNDERSTORM GUST FRONTS— OBSERVATIONS AND MODELING

J.T. Lee

J. Stokes

Y. Sasaki

T. Baxter



December 1978

FINAL REPORT

Document is available to the U.S. public through
the National Technical Information Service,
Springfield, Virginia 22161.

Prepared for

U.S. DEPARTMENT OF TRANSPORTATION
FEDERAL AVIATION ADMINISTRATION
Systems Research & Development Service
Washington, D.C. 20590

79 04 05 020

AD A068425

DDC FILE COPY

NOTICE

This document is disseminated under the sponsorship of the Department of Transportation in the interest of information exchange. The United States Government assumes no liability for its contents or use thereof.

(18) FAA/RD (19) 78/145

Technical Report Documentation Page

1. Report No. FAA-RD-78-145	2. Government Accession No.	3. Recipient's Catalog No.
4. Title and Subtitle THUNDERSTORM GUST FRONTS--OBSERVATIONS AND MODELING	5. Report Date December 1978	6. Performing Organization Code
7. Author(s) J. T. Lee, J. Stokes, Y. Sasaki, T. Baxter*	8. Performing Organization Report No.	9. Work Unit No. (TRAIS) 154-451-014
10. Performing Organization Name and Address U. S. Department of Commerce National Oceanic and Atmospheric Administration National Severe Storms Laboratory 1313 Halley Circle Norman, Oklahoma 73069	11. Contract or Grant No. DOT-FA76WAI-622 Task II	12. Type of Report and Period Covered Final Report March 1976 - December 1978
13. Sponsoring Agency Name and Address U. S. Department of Transportation Federal Aviation Administration Systems Research and Development Service, Airport Div. Washington, D.C. 20590	14. Sponsoring Agency Code FAA/ARD-450	
15. Supplementary Notes Prepared under FAA Interagency Agreement No. DOT-FA76WAI-622, managed by the Aviation Weather Branch, ARD-450.		
*University of Oklahoma, Norman, Oklahoma.		
16. Abstract Gust front structures as observed and as modeled are reviewed and a mean model presented. Integrated observations from the 461 m meteorologically instrumented tower at Oklahoma City, OK, aircraft, weather satellites and Doppler radar are compared to one and two-dimensional models to provide a better understanding of the gust front. In the mean, updrafts of 3 m s^{-1} accompany the gust front's approach. Horizontal wind shears are 8 m s^{-1} per km. Gust front cases in 1976 and 1977 are presented along with a data log of tower observations. Aircraft observations during gust front flights are also presented.		
17. Key Words Thunderstorm Gust Front Wind Shear		18. Distribution Statement Document is available to the U. S. public through the National Technical Information Service, Springfield, Virginia 22151.
19. Security Classif. (of this report) Unclassified	20. Security Classif. (of this page) Unclassified	21. No. of Pages 116
22. Price		

Form DOT F 1700.7 (8-72)

Reproduction of completed page authorized

111

244 670

slt

PREFACE

The authors are indebted to the many who have assisted in the data collection, analysis and preparation of this report. In particular we wish to recognize Mr. Glen Anderson, Mr. Dale Sirmans and Mr. Larry Hennington for their work with the Doppler radar and Mr. Jesse Jennings for the operation of the WSR-57. Mr. Leonard Johnson and Mr. Jack Reece are responsible for the tower data's high quality. The assistance of Mr. Charles Clark and Ms. Jennifer Moore in the preparation of the illustrations is greatly appreciated.

ACCESSION for	White Section <input checked="" type="checkbox"/>	Black Section <input type="checkbox"/>
NTIS		
DDC		
UNANNOUNCED		
JUSTICE		
BY		
DISTRIBUTION		
DATE		

[Handwritten signature/initials across the bottom of the form]

METRIC CONVERSION FACTORS

Approximate Conversions to Metric Measures

Symbol	When You Know	Multiply by	To Find	Symbol
LENGTH				
in	inches	2.5	centimeters	cm
ft	feet	30	centimeters	cm
yd	yards	0.9	meters	m
mi	miles	1.6	kilometers	km
AREA				
in ²	square inches	6.5	square centimeters	cm ²
ft ²	square feet	0.09	square meters	m ²
yd ²	square yards	0.8	square meters	m ²
mi ²	square miles	2.6	square kilometers	km ²
	acres	0.4	hectares	ha
MASS (weight)				
oz	ounces	28	grams	g
lb	pounds	0.45	kilograms	kg
	short tons (2000 lb)	0.9	tonnes	t
VOLUME				
teaspoon	teaspoons	5	milliliters	ml
Tablespoon	tablespoons	15	milliliters	ml
fl oz	fluid ounces	30	milliliters	ml
c	cup	0.24	liters	l
pt	pints	0.47	liters	l
qt	quarts	0.95	liters	l
gal	gallons	3.8	liters	l
ft ³	cubic feet	0.03	cubic meters	m ³
yd ³	cubic yards	0.76	cubic meters	m ³
TEMPERATURE (exact)				
°F	Fahrenheit temperature	5/9 (after subtracting 32)	Celsius temperature	°C

*1 in = 2.54 (exactly). For other exact conversions and more detailed tables, see NBS Misc. Publ. 286, Units of Weights and Measures, Price \$2.25, SD Catalog No. C13.10-286.

Symbol	When You Know	Multiply by	To Find	Symbol
LENGTH				
mm	millimeters	0.04	inches	in
cm	centimeters	0.4	inches	in
m	meters	3.3	feet	ft
km	kilometers	1.1	yards	yd
		0.6	miles	mi
AREA				
cm ²	square centimeters	0.16	square inches	in ²
m ²	square meters	1.2	square yards	yd ²
km ²	square kilometers	0.4	square miles	mi ²
ha	hectares (10,000 m ²)	2.5	acres	ac
MASS (weight)				
g	grams	0.035	ounces	oz
kg	kilograms	2.2	pounds	lb
t	tonnes (1000 kg)	1.1	short tons	st
VOLUME				
ml	milliliters	0.03	fluid ounces	fl oz
l	liters	2.1	pints	pt
l	liters	1.06	quarts	qt
l	liters	0.26	gallons	gal
m ³	cubic meters	36	cubic feet	ft ³
m ³	cubic meters	1.3	cubic yards	yd ³
TEMPERATURE (exact)				
°C	Celsius temperature	9/5 (then add 32)	Fahrenheit temperature	°F

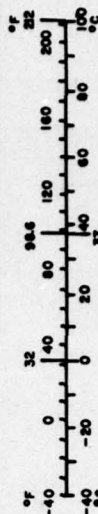


TABLE OF CONTENTS

	<u>Page</u>
TECHNICAL REPORT DOCUMENTATION PAGE	iii
PREFACE	iv
METRIC CONVERSION FACTORS	v
TABLE OF CONTENTS	vii
LIST OF ILLUSTRATIONS	viii
LIST OF TABLES	xi
LIST OF ABBREVIATIONS AND SYMBOLS	xii
1.0 INTRODUCTION	1
1.1 Background	1
1.2 Objectives and Scope	1
1.3 Research Plan	2
2.0 NEW DATA	2
2.1 May 19, 1977	3
2.2 June 12, 1977	10
2.3 June 28, 1977	13
3.0 MEAN GUST FRONT ANALYSIS	15
4.0 DYNAMICAL MODEL OF GUST FRONT	18
4.1 Gust Front Dynamics	18
4.1.1 Downdraft Simulation	22
4.1.2 Numerical Computation	23
4.2 Origin of Gust Front	31
4.2.1 Margules Process	31
4.2.2 Far-reaching Gust Fronts	38
4.3 Microphysical Processes (One Dimensional Thunderstorm Simulation)	38
4.4 Dry Air Intrusion (Two Dimensional Thunderstorm Simulation)	48
4.5 Twisted Storm Circulation (Three Dimensional Model)	55
5.0 SUMMARY	58
6.0 CONCLUSIONS AND RECOMMENDATIONS	59
APPENDIX A: Gust Front Cases, 1977	61
APPENDIX B: Index of Tower Observations	85
REFERENCES	99

LIST OF ILLUSTRATIONS

<u>Figure</u>		<u>Page</u>
2-1.	WSR-57 weather radar display for (a) 1520:17 CST and (b) 1550:15 CST May 19, 1977.	2
2-2.	May 19, 1977 KTVY-tower time-height sections of streamlines, potential temperature and wind.	3
2-3.	Dual-Doppler wind field of a gust front 19 May 1977, for (a) 1525 CST and (b) 1532 CST.	4
2-4.	Westbound winds recorded by F-4-C aircraft 1527:21-1528:40 CST May 19, 1977 at 460 m (1500 ft) AGL.	7
2-5.	Time cross section of F-4-C recorded (a) derived gust velocities and (b) vertical winds for 1527:21-1528:40 CST May 19, 1977.	7
2-6.	Winds recorded by F-4-C aircraft during approach to runway 17 at TIK 1539-1541 CST May 19, 1977.	8
2-7.	Winds recorded by F-4-C during approach to runway 17R at OKC, 1550-1552 CST May 19, 1977.	8
2-8.	WSR-57 weather radar scope presentation for 1733 CST June 12, 1977.	9
2-9.	Thunderstorm's northeastern edge taken from F-4-C on June 12, 1977, 1733 CST flying at 1520 m (5000 ft) MSL showing sharp leading edge of storm marking separation of warm air inflow and lower cold air outflow.	9
2-10.	Same storm as Figure 2-9 except central portion.	10
2-11.	Same storm as Figure 2-9 except southern portion.	11
2-12.	Derived gust velocities and vertical wind cross-section for flight above gust front. (Same storm as Figure 2-9) June 12, 1977 1736-1745 CST at 1520 m (5000 ft).	12
2-13.	Aircraft observed horizontal winds and Dual-Doppler winds for June 12, 1977.	12
2-14.	Satellite photograph taken at 1600 CST June 12, 1977.	13
2-15.	June 28, 1977 real-time Doppler radar display of (a) radar reflectivity, pattern reflectivity factor (dBZ) scale given at right and (b) Doppler radial velocity.	14

3-1.	Composite diagram of gust front.	17
4-1.	Potential temperature field at $t = 0.40$ minutes.	23
4-2a.	Potential temperature field at $t = 12.00$ minutes.	25
4-2b.	Objective analysis of a gust front associated temperature field for May 31, 1969.	25
4-3a.	Stream function at $t = 12.00$ minutes.	27
4-3b.	Same as Figure 4-2b except stream function analysis.	27
4-4a.	Horizontal velocity field at $t = 12.00$ minutes.	28
4-4b.	Same as Figure 4-2b except wind speed analysis.	28
4-5.	Vertical velocity field at $t = 12.00$ minutes.	29
4-6.	Horizontal velocity as a function of time at a fixed point at the surface for all six surface drag cases.	29
4-7.	Horizontal velocity as a function of time at a fixed point at the surface for the four cases given in Table 1.	30
4-8.	Schematic of Margules' Process.	32
4-9.	Major squall line features at 2337 CST May 31, 1969.	39
4-10.	A composite schematic model combining the features of the analyzed and deduced structure of the windshift and gust front leading the squall line of May 31, 1969.	40
4-11.	Vertical profiles of temperature and density at WKY just before and after the gust surge passed, 2300 and 2345 CST, respectively.	41
4-12.	Scheme of cloud microphysical processes in a thunderstorm.	42
4-13.	Time-height cross sections of (a) vertical velocity, (b) excess temperature, (c) liquid water content for a cloud without microphysical processes.	49
4-14.	Time height cross sections of (a) vertical velocity, (b) excess temperature, (c) liquid and solid water content, (d) content of cloud droplets, (e) content of raindrops and (f) content of ice crystals for a cloud with microphysical processes.	50
4-15.	Time-height cross sections of the rates of (a) condensation of water vapor into cloud droplets and evaporation of melting ice crystals, (b) evaporation of cloud droplets,	8

	raindrops, and ice crystals, (c) conversion of cloud droplets into raindrops and melting of ice crystals, and (d) glaciation and growth of ice crystals by sublimation.	51
4-16.	Schematic representation of the motion field within a middle latitude cumulonimbus in wind shear.	55
4-17.	Variable fields for Experiment R1 at 5.6 minutes.	56
4-18.	Same as Figure 4-17 except for R2 at 5.0 minutes and 15.7 minutes.	57
A-A-1 through A-I-2.	Gust front cases, 1977.	80
A-J-1 through A-K-1.	Cold front cases 1976 and 1977.	83

LIST OF TABLES

<u>Table</u>		<u>Page</u>
1	Gust frontal cases used in mean analysis.	16
B1	October 1976 KTVY Tower	87
B2	November 1976 KTVY Tower	88
B3	December 1976 KTVY Tower	89
B4	January 1977 KTVY Tower	90
B5	February 1977 KTVY Tower	91
B6	March 1977 KTVY Tower	92
B7	April 1977 KTVY Tower	93
B8	May 1977 KTVY Tower	94
B9	June 1977 KTVY Tower	95
B10	July 1977 KTVY Tower	96
B11	August 1977 KTVY Tower	97
B12	September 1977 KTVY Tower	98

LIST OF ABBREVIATIONS AND SYMBOLS

a_z	=	Vertical acceleration of aircraft
AGL	=	Above ground level
c	=	Frontal movement speed
C	=	Ventilation constant
C_D	=	Non-dimensional average drag coefficient
$C_{L\alpha}$	=	Change in lift coefficient with angle of attack
C_m	=	Turbulent mixing coefficient
cm	=	Centimeter
C_o	=	Reciprocal of conversion time
CST	=	Central Standard Time
c_p	=	Specific heat capacity of dry air at constant pressure
c_v	=	Specific heat capacity of dry air at constant volume.
dBZ	=	Decibel measure of radar reflectivity
e_{is}	=	Saturation vapor pressure over ice
e_{ws}	=	Saturation vapor pressure over water
E	=	Total energy per unit cross section of a column
f_o	=	Constant
F_r	=	Linear diffusion
ft	=	Feet
g	=	Acceleration attributable to gravity
G	=	The reciprocal of glaciation time
h	=	Height
H	=	Top surface of gust front simulation model
IE	=	Internal energy
K	=	$\frac{Y}{Y-T}$
$^{\circ}K$	=	Degrees Kelvin
KE	=	Kinetic energy
km	=	Kilometers
K_g	=	Gust alleviation factor
K_x, K_z	=	Diffusion constants
ℓ	=	Total horizontal dimension of Margules process system
L	=	Lateral boundary of gust front simulation model

L_v	=	Distance from accelerometer to angle of attack vane
L_f, L_s, L_v	=	Latent heats of fusion, sublimation and evaporation, respectively
\ln	=	Natural log
LTS	=	Altus Air Force Base, Oklahoma
m	=	Meter
m_1, m_2	=	Masses of cold and warm air columns, respectively
M	=	Mass
min	=	Minutes
$m\ s^{-1}$	=	Meters per second
NE	=	Northeast
n mi	=	Nautical miles
NW	=	Northwest
OKC	=	Will Rogers International Airport, Oklahoma City, Oklahoma
p	=	Pressure
$p_0(z)$	=	Initial vertical pressure profile
PE	=	Potential energy
P1	=	Condensation rate
P2	=	Rate of conversion from cloud droplets to raindrops
P3	=	Glaciation rate
P4	=	Sublimation rate
P5	=	Melting rate
P6	=	Rate of evaporation from cloud droplets to water vapor
P7	=	Rate of evaporation of raindrops
P8	=	Rate of evaporation of ice crystals
P9	=	Rate of evaporation of melting ice crystals
q_c	=	Mixing ratio of cloud droplets
q_i	=	Mixing ratio of ice crystals
q_ℓ	=	Rain water mixing ratio
q_r	=	Mixing ratio of raindrops
q_v, q_{vs}	=	Mixing ratio of water vapor and its saturated value
r	=	Radial cylindrical coordinate
R	=	Gas constant for dry air
s	=	Second
S_a	=	Aircraft wing area

SE	=	Southeast
t	=	Time
T	=	Temperature
$T_0(z)$	=	Initial vertical temperature profile
T''	=	Environmental temperature
T_v	=	Virtual temperature
T_{vo}	=	Environmental virtual temperature
TE	=	Total static energy of Margules process system
TIK	=	Tinker Air Force Base, Oklahoma
u	=	Velocity component along x-axis
u_l	=	u at 175 m
u''	=	Environmental horizontal wind component which varies only in the vertical direction
U_{de}	=	Derived gust velocity
v	=	Velocity component along y-axis
\vec{V}	=	Horizontal wind
\vec{V}_{ag}	=	Aircraft speed and heading
V_e	=	Equivalent airspeed at sea level
V_{ga}	=	Aircraft velocity with respect to ground
V_i	=	Terminal velocity of ice particles
V_T	=	Effective terminal velocity of the raindrop distribution
V_{Ta}	=	Aircraft true airspeed
V_w	=	Terminal velocity of raindrops
w	=	Velocity component along z-axis
w''	=	Environmental vertical wind component which varies only in the vertical direction
W	=	Weight of aircraft
x	=	Horizontal coordinate
y	=	Horizontal coordinate
z	=	Vertical coordinate
α	=	Angle of attack
β	=	Fraction of area of cold air column to the total area of Margules process system
β_a	=	Yaw angle
γ	=	$\frac{c_p}{c_v}$

Γ_d	=	Dry adiabatic lapse rate
Δ	=	Delta
η	=	Vorticity
θ	=	Potential temperature
θ_a	=	Aircraft pitch angle
$\dot{\theta}_a$	=	Aircraft pitch rate
λ	=	Cylindrical coordinate
ν	=	Constant
ν_x, ν_z	=	Time-space dependent horizontal and vertical eddy viscosity coefficient
ν_θ	=	Constant of thermal diffusivity
ρ	=	Density
$\rho_0(z)$	=	Initial vertical density profile
τ	=	Stress
ψ	=	Stream function
∂	=	Partial derivative

THUNDERSTORM GUST FRONTS--OBSERVATIONS AND MODELING

1.0 Introduction

1.1 Background

The gust front defined by a sudden wind shift and temperature change, is a dramatic consequence of the thunderstorm downdraft. Such a gust front is the interface between the warm, moist low-level ambient air and the cool, nearly saturated downdraft air of mid-level origin. The horizontal velocity of the mid-levels contained in the downdraft momentum is additionally accelerated by the negative (downward) buoyancy resulting from the evaporation of precipitation. This downdraft is deflected into a horizontal plane by the ground and dissipated by interaction with surrounding air and with the ground surface. The outflow is a potential hazard to aircraft due to wind shear and turbulence. A previous report (Goff, et al., 1977) provides initial details. In this report we address numerical modeling, mean models, turbulence, flow patterns and auxiliary observations.

1.2 Objectives and Scope

Several objectives are primary to this study. These are:

- (1) investigate and categorize the turbulent structure of the subcloud layer and the outflow gust front
- (2) observe aircraft response during landing approaches through thunderstorm gust fronts and
- (3) investigate suitable numerical models.

Secondary objectives are:

- (a) collection of wind and temperature data in the lower levels during gust front cases
- (b) provide a significant data bank for laboratory and computer simulation studies

- (c) determine quasi-steady state characteristics of thunderstorm outflow and gust front features and
- (d) investigate use of Doppler radar and satellites for gust front detection.

1.3 Research Plan

The basic organization is detailed in Federal Aviation Administration Report No. FAA-RD-77-119 and is not here repeated. The 461 m tower instrumented at seven levels to 444 m continued in operation during the 1977 program. Dual Doppler radars, a WSR-57 weather radar, a surface station network and an F-4-C aircraft form the 1977 research observations' base. The 1977 season had below normal thunderstorm activity and no exceptionally strong gust fronts were reported. Significant new data are discussed in the following sections.

2.0 New Data

Several interesting gust fronts were observed jointly through the use of Doppler radar, aircraft, tower, and satellite.

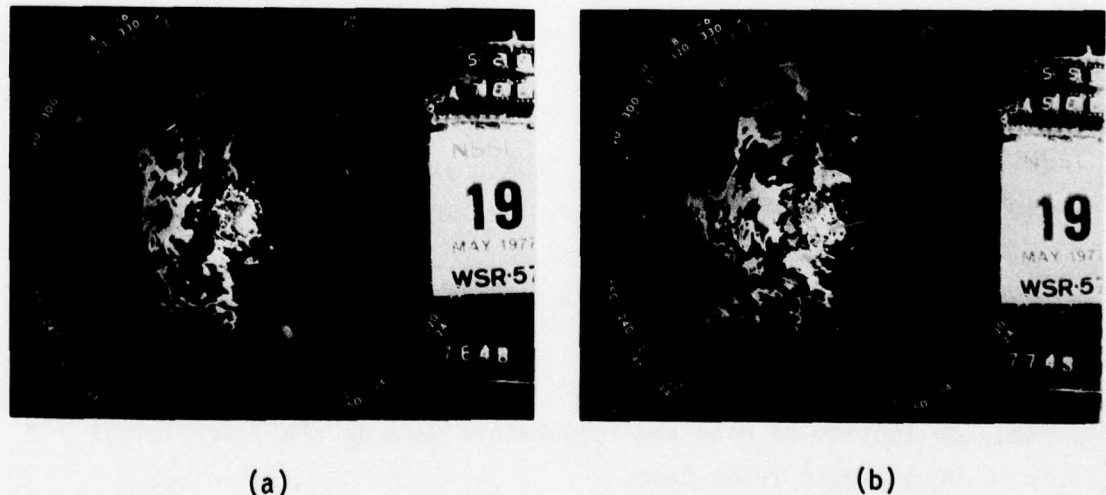


Figure 2-1 WSR-57 weather radar display for (a) 1520:17 CST and (b) 1550:15 CST May 19, 1977. 0° elevation. Radar contours at approximately 10 dBZ intervals. Range marks (circles) are at 40 km intervals.

2.1 May 19, 1977

On this date a large squall line extending more than 300 km (162 nm) in a north-south orientation passed through Central Oklahoma (Figures 2-1a and b); its gust front embedded in light precipitation reached the tower at 1557 CST. Figure 2-2 is a section from the objective analysis of the tower data covering the time of this event. Tower data were filtered before plotting the time-height sections (Goff, 1975).

The gust frontal zone is characterized by moderate shear in the wind speed component normal to the front. A sharp temperature discontinuity is also evident. An updraft larger than 4 m s^{-1} at 1557 CST is followed by a downdraft exceeding 2 m s^{-1} , thus creating a somewhat turbulent zone just behind the gust front. Little surface pressure discontinuity was associated

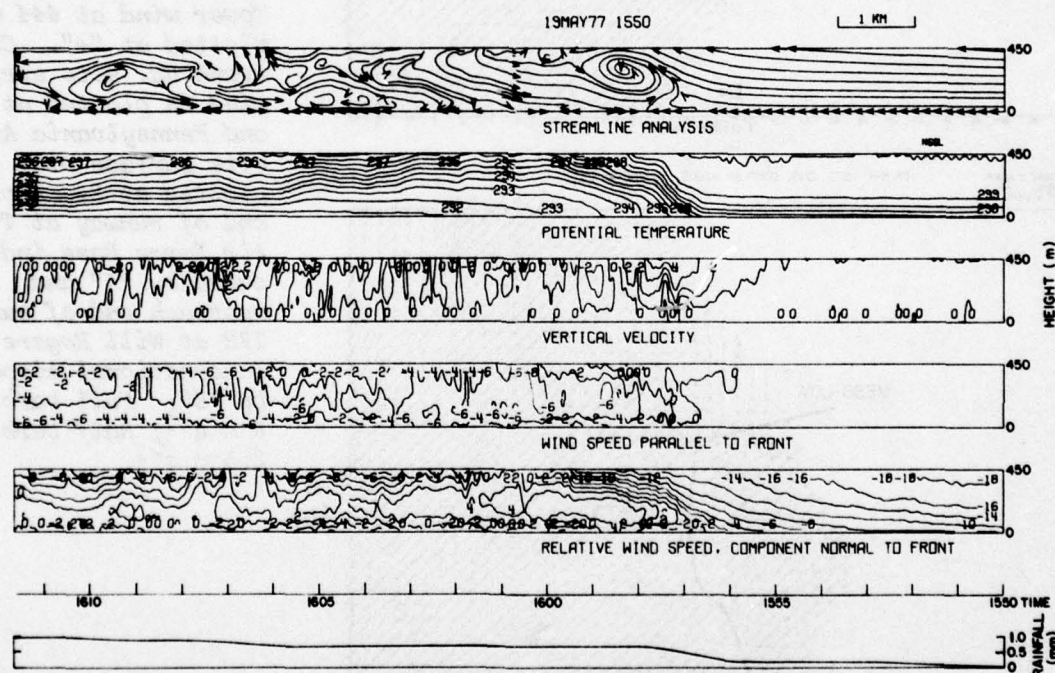
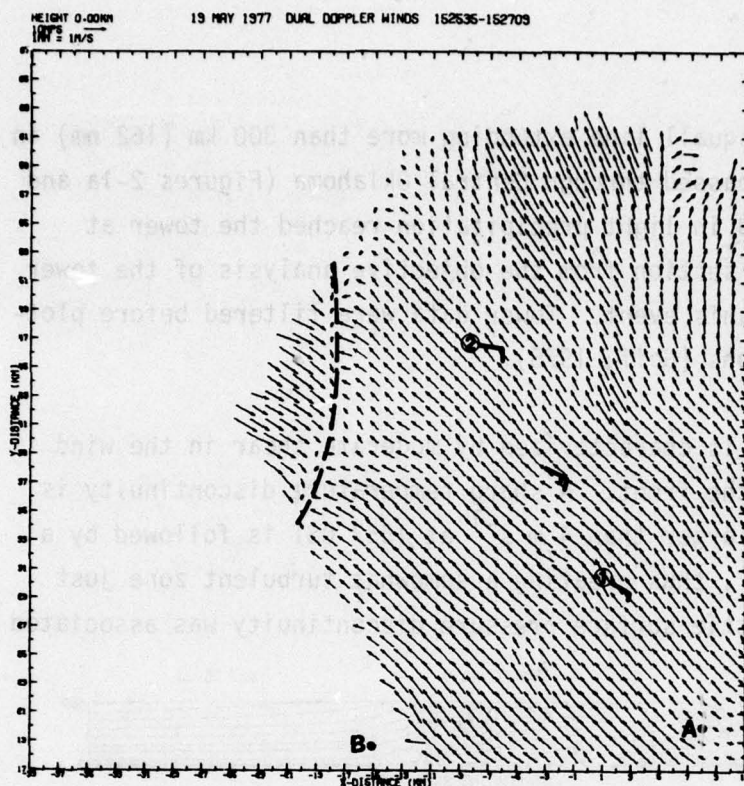
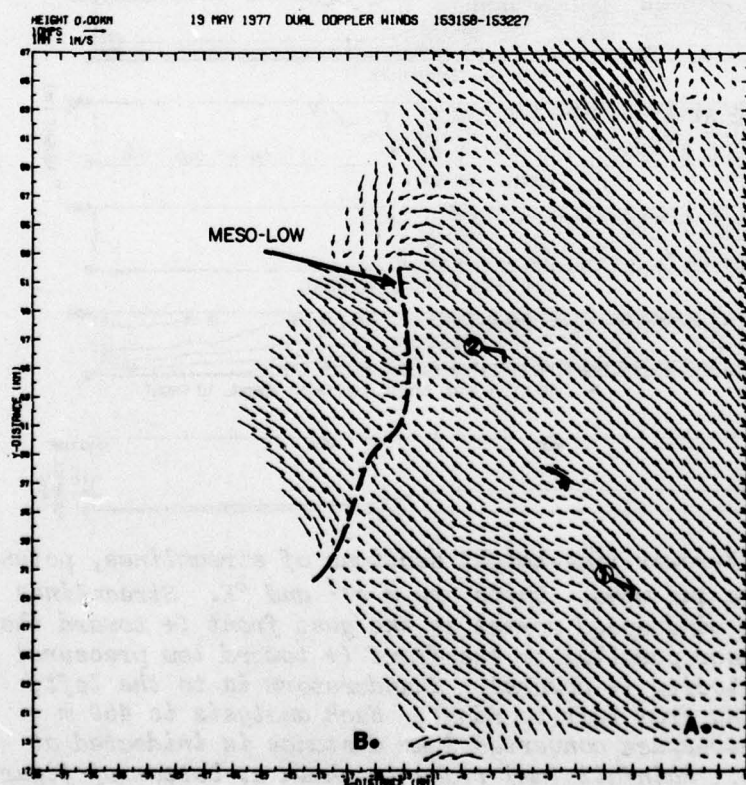


Figure 2-2 19 May 1977 KTVY-tower time-height sections of streamlines, potential temperature and wind. Units are m s^{-1} and $^{\circ}\text{K}$. Streamlines are drawn using wind speed normal to the gust front (+ toward the right), wind shear parallel to the front (+ toward low pressure) and vertical velocity (+ upward). Thunderstorm is to the left; outflow is moving from left to right. Each analysis is 450 m thick. A time-to-space converted 1 km distance is indicated at the upper right. Rainfall (mm) trace is shown at bottom of figure.



(a)

Figure 2-3 Dual-Doppler wind field of a gust front 19 May 1977, for (a) 1526 CST and (b) 1532 CST. Wind speeds are indicated by length of arrow. Dashed line indicates gust front. Tower wind at 444 m plotted at "+". Coltrane Rd. site surface wind is plotted at 1 and Pennsylvania Ave. site surface wind is plotted at 2. Approach end of runway at Tinker Air Force Base indicated by "A" and approach end of runway 17R at Will Rogers International Airport by "B". Full barb = 5 m s^{-1} ; half barb = 2.5 m s^{-1} .



(b)

with the gust front. Light precipitation began a few minutes ahead of the front. Figures 2-3a and b show the low level (center of beam is 250 m above ground) dual-Doppler derived winds at 1526 and 1532 CST. Superimposed are the tower winds at the 444 m level and the surface winds at the Pennsylvania Avenue (10 km NW of tower) and Coltrane Road (9 km SE of tower) sites. Note how well defined is the small meso-low at the north end of the gust front in Figure 2-3b. This characteristic pattern is similar to that shown by Goff et al. (1977).

The F-4-C flying at 460 m (1500 ft) above ground level (AGL) just north of the tower on east-west flight paths measured horizontal and vertical winds and turbulence.

Horizontal winds (\vec{V}) are calculated using the true airspeed and heading (plus wind vane correction) (\vec{V}_{ag}) and the ground speed and track (V_{ga}) as determined by the onboard inertial navigation system (INS) or

$$\vec{V} = \vec{V}_{ga} - \vec{V}_{ag}$$

Vertical winds (w) are computed using

$$w = V_{Ta} \alpha + V_{Ta} \beta_a - V_{Ta} \theta + \int_0^t a_z dt + w_{p,g}(0) + L_v \dot{\theta}$$

where V_{Ta} = true air speed

α = angle of attack

θ = pitch angle

β_a = yaw angle

a_z = vertical acceleration of aircraft

$w_{p,g}(0)$ = vertical motion of the aircraft at time $T = 0$

$\dot{\theta}$ = pitch rate

L_v = distance from accelerometer to angle of attack measurement point.

As a measure of turbulence, the derived gust velocity (U_{de}) is used. This value is computed from aircraft data recorded using the general equation

$$U_{de} = \frac{2w\Delta a_z}{V_e K_g \rho_o C_{L\alpha} S_a}$$

where w = weight of aircraft

Δa_z = measured incremental vertical acceleration for normal

V_e = equivalent air speed at sea level

K_g = gust alleviation factor

ρ_o = air density at sea level

$C_{L\alpha}$ = change in lift coefficient with angle of attack

S_a = wing area

Corresponding subjective turbulence evaluations are (as given by NASA)

light	$U_{de} \leq 6.0 \text{ m s}^{-1} (\leq 19 \text{ ft s}^{-1})$
moderate	$6.1 \leq U_{de} \leq 9.1 \text{ m s}^{-1} (20-29 \text{ ft s}^{-1})$
severe	$9.2 \leq U_{de} \leq 12.1 \text{ m s}^{-1} (30-39 \text{ ft s}^{-1})$
extreme	$U_{de} \geq 12.2 \text{ m s}^{-1} (\geq 40 \text{ ft s}^{-1})$

The horizontal winds for one representative pass made westbound at 1527:21-1528:40 CST are shown in Figure 2-4. Only light turbulence was reported by the pilot which is in agreement with the recorded turbulence and vertical winds as shown in Figure 2-5. At about 1530 CST it was decided to make approaches to Tinker Air Field (TIK) (NE of Norman) (Point A in Figure 2-3a) ahead of the gust front and then to make an approach to Will Rogers International Airport (OKC) (Point B in Figure 2-3a). Figure 2-6 is a plot of the aircraft recorded winds along the flight path during an approach to TIK at 1539-1541 CST. The winds are 10 second mean winds derived from the 0.1 second data and correspond to about 1 km space averaged wind. Only some light turbulence and no precipitation was encountered. The aircraft was then directed toward an approach to OKC. The gust front had

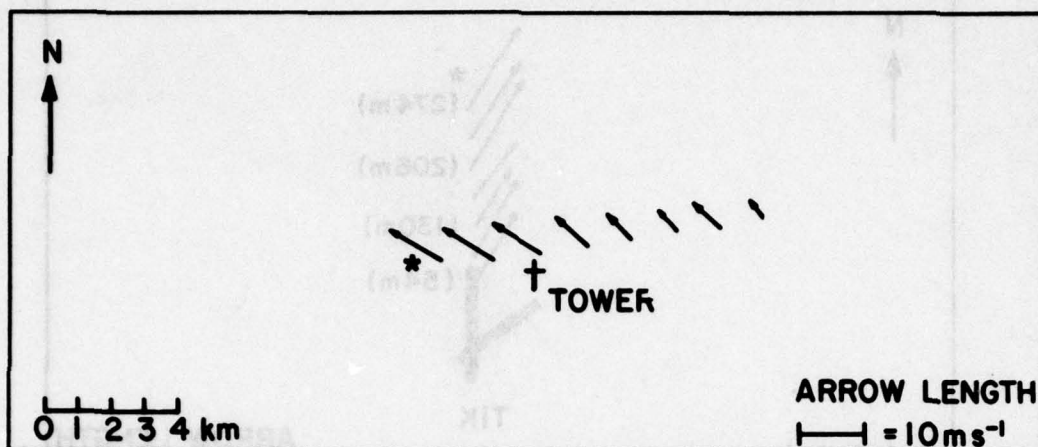


Figure 2-4 Westbound winds recorded by F-4-C aircraft 1527:21-1528:40 CST May 19, 1977 at 460 m (1500 ft) AGL.

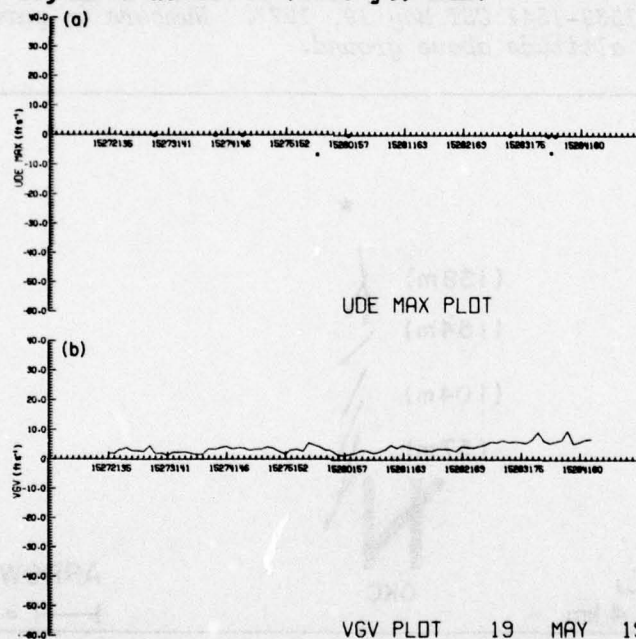


Figure 2-5 Time cross section of F-4-C recorded derived gust velocities (A) and vertical winds (B) for 1527:21-1528:40 CST May 19, 1977.

passed OKC about 1548 CST. The approach was started at 1550 CST and the recorded horizontal winds during the approach are shown in Figure 2-7. Gusty lateral winds, turbulence, lightning and some light precipitation were encountered during the descent.

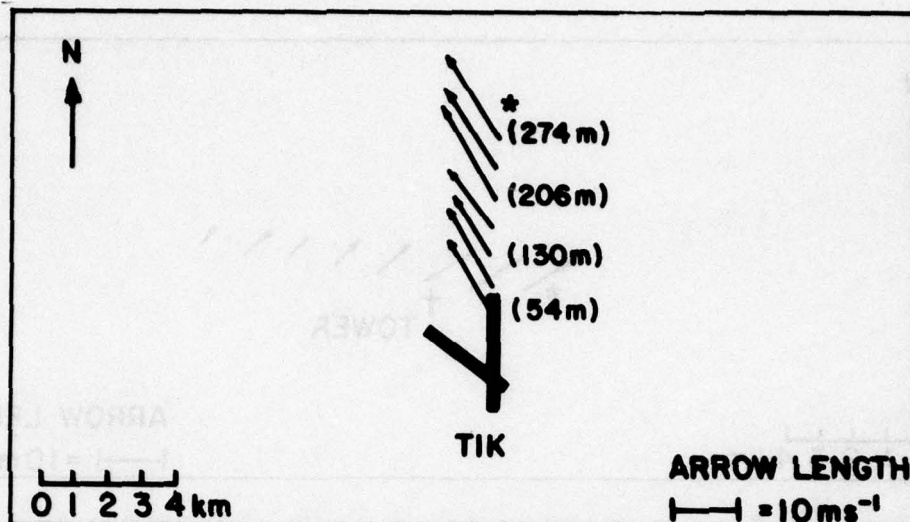


Figure 2-6 Winds recorded by F-4-C aircraft during approach to runway at TIK 1539-1541 CST May 19, 1977. Numbers in parentheses indicate altitude above ground.

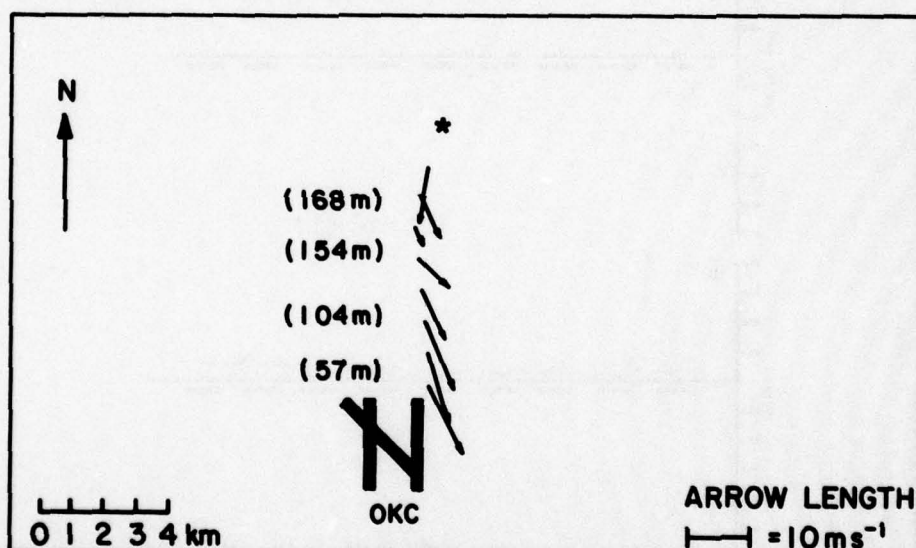


Figure 2-7 Winds recorded by F-4-C during approach to runway 17R at OKC 1550-1552 CST. May 19, 1977. Numbers in parentheses indicate altitude above ground.

Several additional approaches were made to TIK ahead of the gust front. These approaches were terminated just before heavy rain crossed the airport and as fuel became critical. The approaches encountered conditions similar to the first one--no turbulence, no precipitation. This gust front can thus



Figure 2-8 WSR-57 weather radar scope presentation for 1733 CST June 12, 1977. Radar contours at approximately 10 dBZ intervals. Range marks (circles) are at 40 km intervals.

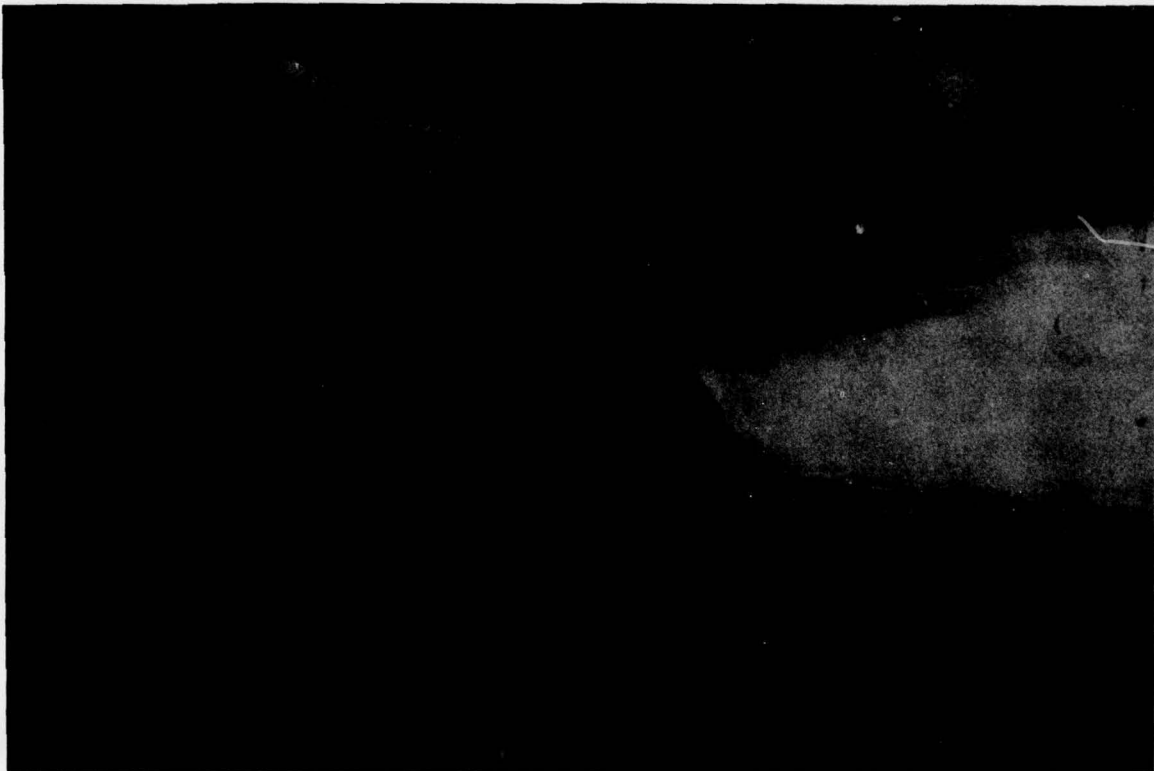


Figure 2-9 Thunderstorm's northeastern edge taken from the ASD F-4-C on June 12, 1977 1733 CST flying at 1520 m (5000 ft) MSL showing sharp leading edge of storm marking separation of warm air inflow and lower cold air outflow.

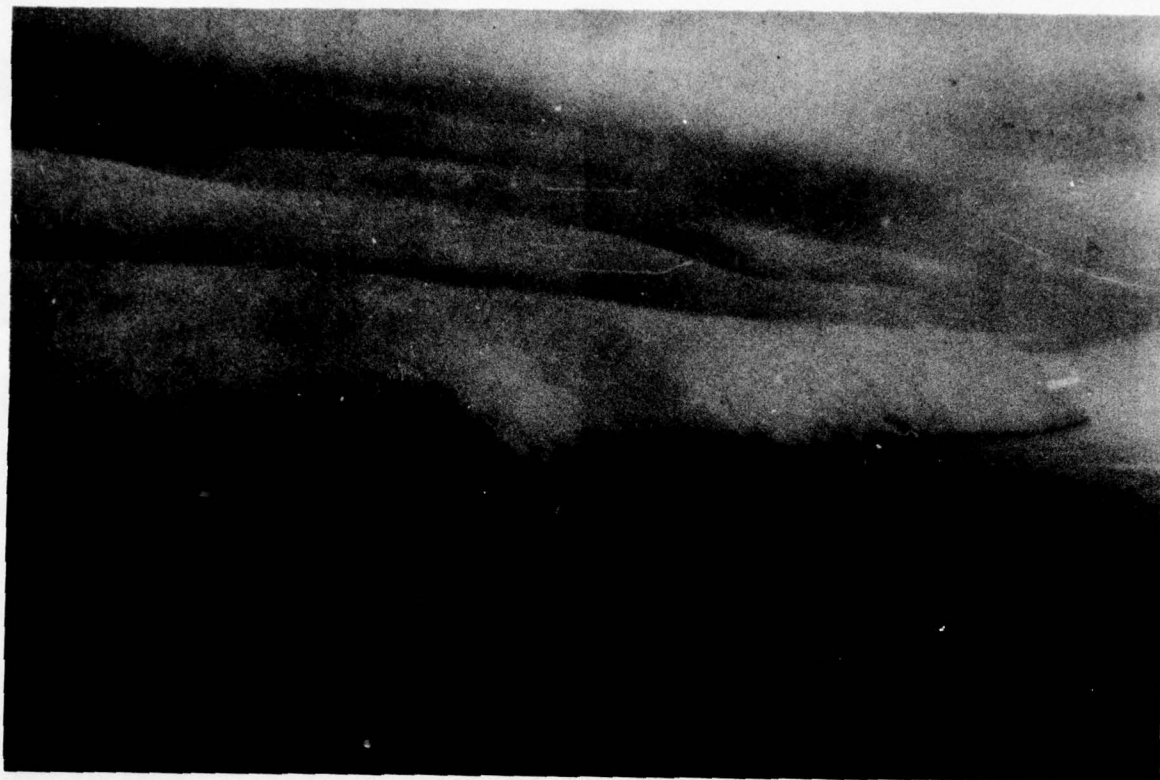


Figure 2-10 Same storm as Figure 2-9 except central portion.

be characterized as having strong low-level southeasterly wind with slight turbulence prior to the wind shift and northerly flow behind the front. This northerly flow is turbulent and gusty. Satellite photographs covering this event showed a large cirrus cloud shield over most of Oklahoma which obscured all low level cloudiness or any other possible identification of the gust front or gust frontal activity.

2.2 June 12, 1977

An extremely unstable air mass prevailed over Oklahoma and a low pressure center was located near Altus, Oklahoma (LTS) in the southwestern part of the state. Around noon (1228 and at 1250 CST) two small tornadoes were reported near Clinton-Sherman AFB [158 km (85 nm) west of NSSL]. These particular storms weakened and then later in the afternoon formed, along with

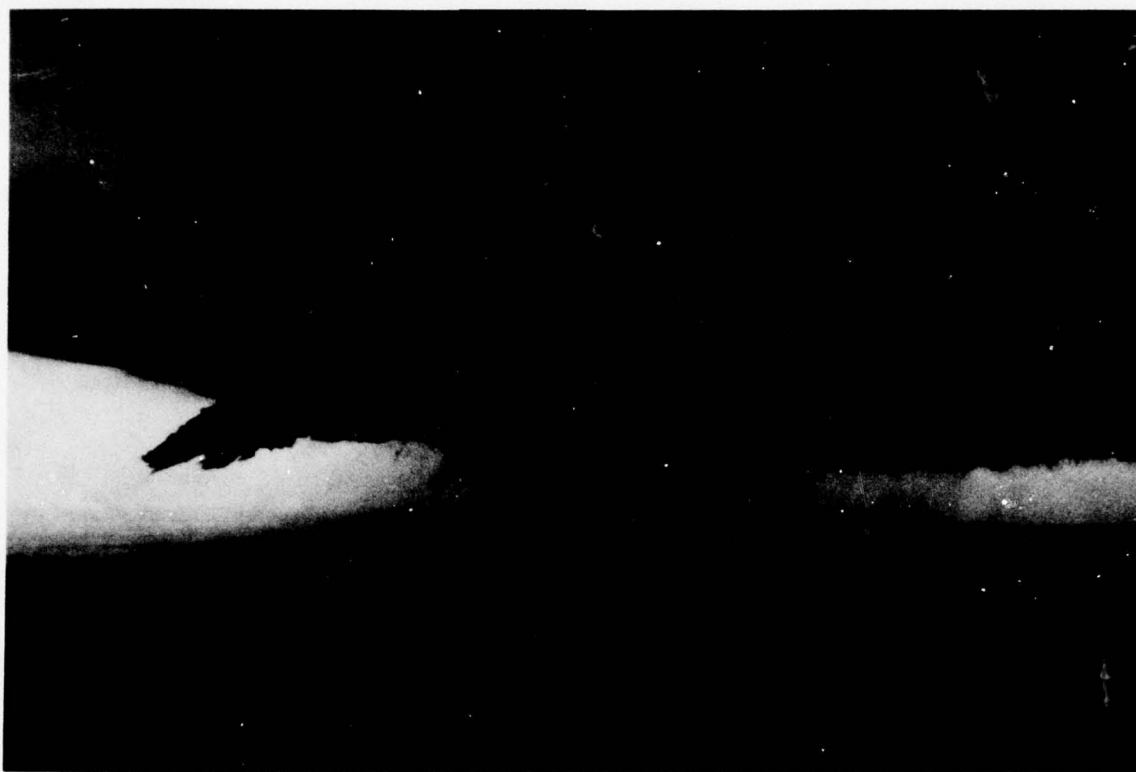


Figure 2-11 Same storm as Figure 2-10 except southern portion.

new cells, a north-south squall line in Central Oklahoma (Figure 2-8). From near 1615 to 1800 CST the F-4-C flew a number of passes just above the gust front. The gust front's surface position was visible to the pilot as a line of dust. This dust was not sufficient to be visible in the photographs. Figure 2-9 to 2-11 are representative photographs. Figure 2-12 shows the turbulence and vertical winds encountered while Figure 2-13 has a plot of the horizontal winds. The corresponding dual-Doppler winds are also shown in Figure 2-13. The heavy line AB is the aircraft track with point A corresponding to the time 1739:42 and point B the aircraft location at 1744:30. The line A'B', showing the aircraft measured horizontal winds, should be superimposed upon AB but for clarity in illustration has been displaced to the right. The satellite photo (Figure 2-14) taken at 1600 CST shows the storm with some indication of the cold air outflow (shown by arrow in Figure 2-14).

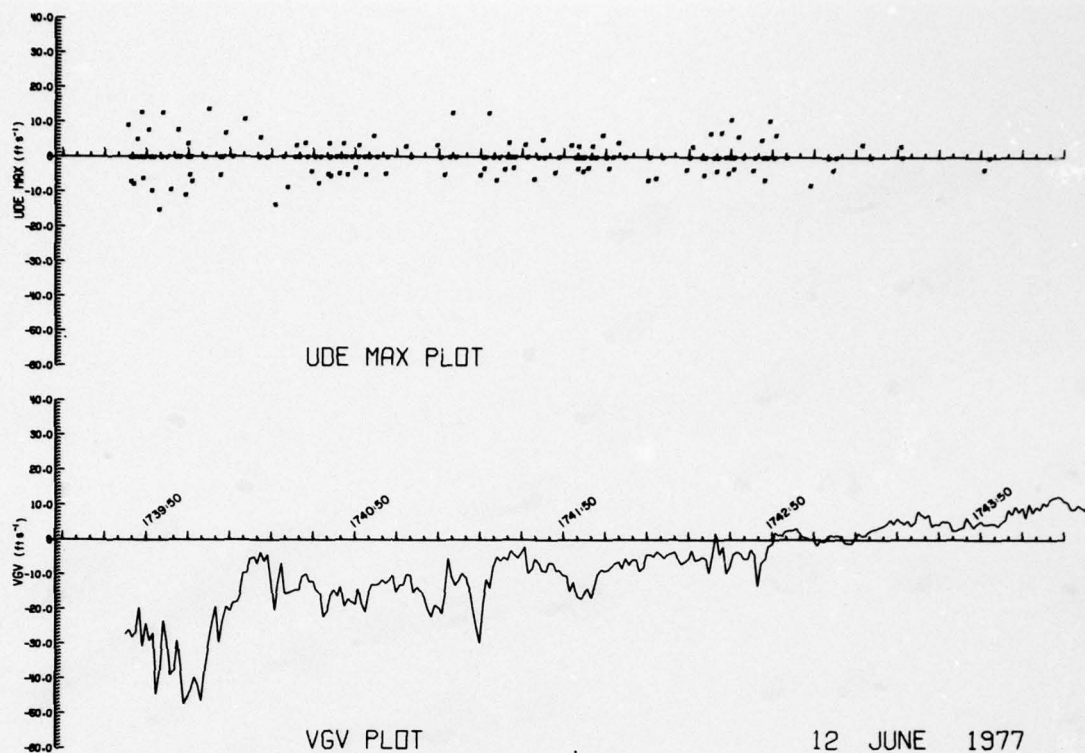


Figure 2-12 Derived gust velocities and vertical wind cross sections for flight above gust front. June 12, 1977 1739-1745 CST at 1520 m (5000 ft) MSL.

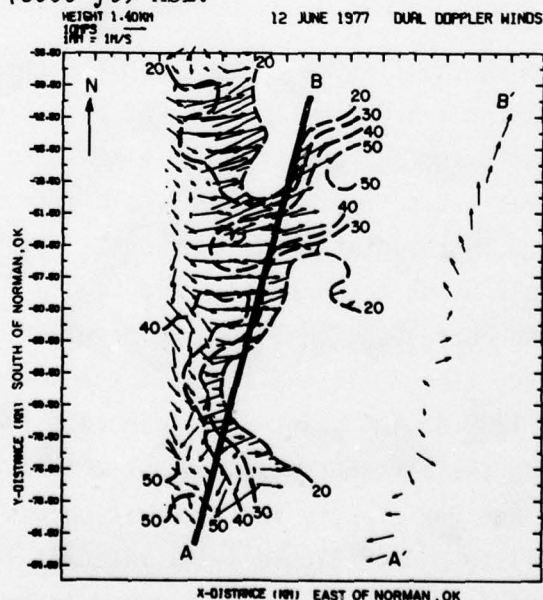


Figure 2-13 Aircraft observed winds and dual-Doppler winds for June 12, 1977. Contour lines are at 10 dBZ radar reflectivity factor intervals.

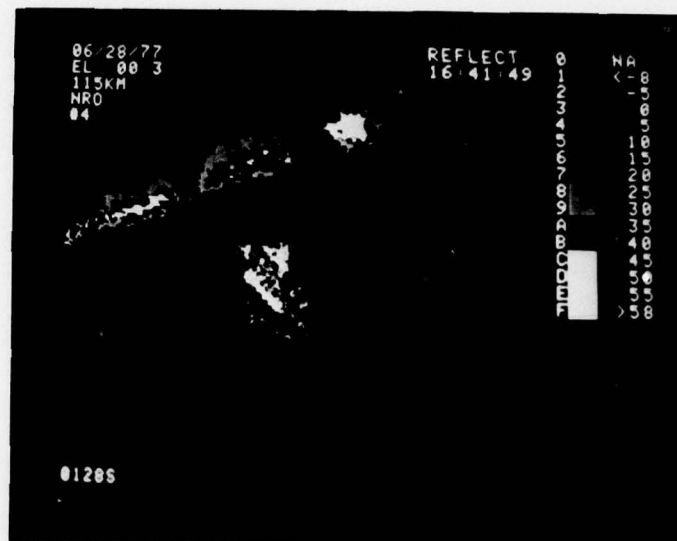


Figure 2-14 Satellite photograph taken at 1600 CST June 12, 1977. Arrow indicates entrance of cold air outflow.

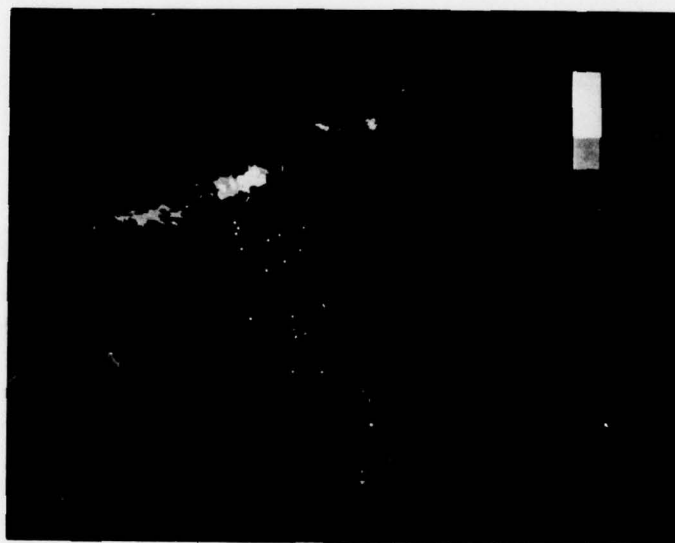
2.3 June 28, 1977

On June 28, 1977 strong cold air outflow associated with a squall line reached the tower at 1704 CST. The tower analysis covering this event is presented in Appendix A, Case I. Surface gusts at the tower reached 28.0 m s^{-1} after the passage of the gust frontal boundary. A sharp temperature discontinuity is evident across the front as the temperature dropped about 6°C in 5 min. Pre-gust front updrafts are greater than 6 m s^{-1} .

The Norman Doppler real-time display of the velocity and reflectivity fields at 1642 CST are shown in Figure 2-15. At this time the leading edge of the squall line was about 10 km away from the tower. The reflectivity pattern (Figure 2-15a) is typical with weaker values along the edges of the



(a)



(b)

Figure 2-15 June 28, 1977 real-time Doppler radar display of (a) radar reflectivity pattern with reflectivity factor (dBZ) scale given at right and (b) Doppler radial velocity with velocity scale (m s^{-1}) at right. Range marks for (a) and (b) 40 km. Elevation angle is zero degrees.

squall line and with numerous embedded cores. The central core values are greater than 40 dBZ. The velocity display (Figure 2-15b) shows clear evidence of strong outflow winds ($\geq 32 \text{ m s}^{-1}$ toward the radar) along the forward edge of the line displaced from the cores by an appreciable amount. From the reflectivity display alone one may have judged the center portion of the squall line to be weaker than the extremities. The Doppler velocity display, however, shows this area having strong winds (gust front). This is an example of how Doppler radar can detect outflow winds.

Damage from this squall line was confined to electric power outages caused by wind and lightning in the northeast Oklahoma City area about 1730 CST. The recording system at the tower lost power at 1712 CST. Between 1930 and 2000 CST hail up to 3.8 cm in diameter fell in a rural area 62 km south of the tower.

3.0 Mean Gust Front Analysis

To examine the general characteristics of the gust front as observed from tower measurements, eight of the 1976 gust front cases and four of the 1977 cases were averaged to give a mean analysis. Only gust front cases when the faster recording data rate (1.3 s and 1.7 s intervals in 1976 and 1.5 s interval in 1977) was in operation were used to determine this mean structure (see Table 1).

The time-to-space conversion,

$$\Delta x = -c\Delta t \quad (3.1)$$

was used to calculate distance relative to gust frontal passage. Here Δx is the distance traveled by the frontal boundary during a time interval Δt at a speed of c . A 50 x 10 array was determined for each case at 250 m intervals in the horizontal and 50 m intervals in the vertical. Each horizontal grid point represents an average over 250 m. The grid points extended from 2.125 km ahead of the gust front to 10.125 km behind the front and from 0 to 450 m in the vertical for each of the twelve cases. To arrive at the

Table 1. Gust Frontal Cases used in Mean Analysis

Date	Time (CST)	Speed (m s^{-1})	Orientation* (deg)
10 May 1976	0144	14.2	65
12 May 1976	0844	6.6	65
22 May 1976	2208	16.3	352
26 May 1976	0014	13.8	355
26 May 1976	0727	13.3	30
29 May 1976	2359	5.0	75
30 May 1976	1828	6.1	240
23 June 1976	2140	13.0	350
5 May 1977	1807	6.0	20
16 May 1977	2154	7.8	65
19 May 1977	1556	9.8	30
26 May 1977	2138	5.6	38

* Orientation refers to azimuthal direction of the storm's left flank with respect to the gust front.

composite diagram (Figure 3-1) the twelve cases were simply averaged point for point.

As seen in Figure 3-1 the mean analysis, extending from 2.125 km ahead of the front to 5.125 km behind the front, is just a smoothed version of the individual cases. Note that no portion of the zero contour of the relative wind speed component is coincident with the zero on the distance scale as one expects. This discrepancy is probably due to displacement of the gust front boundary during the averaging process and due to errors in the speeds of the individual gust fronts.

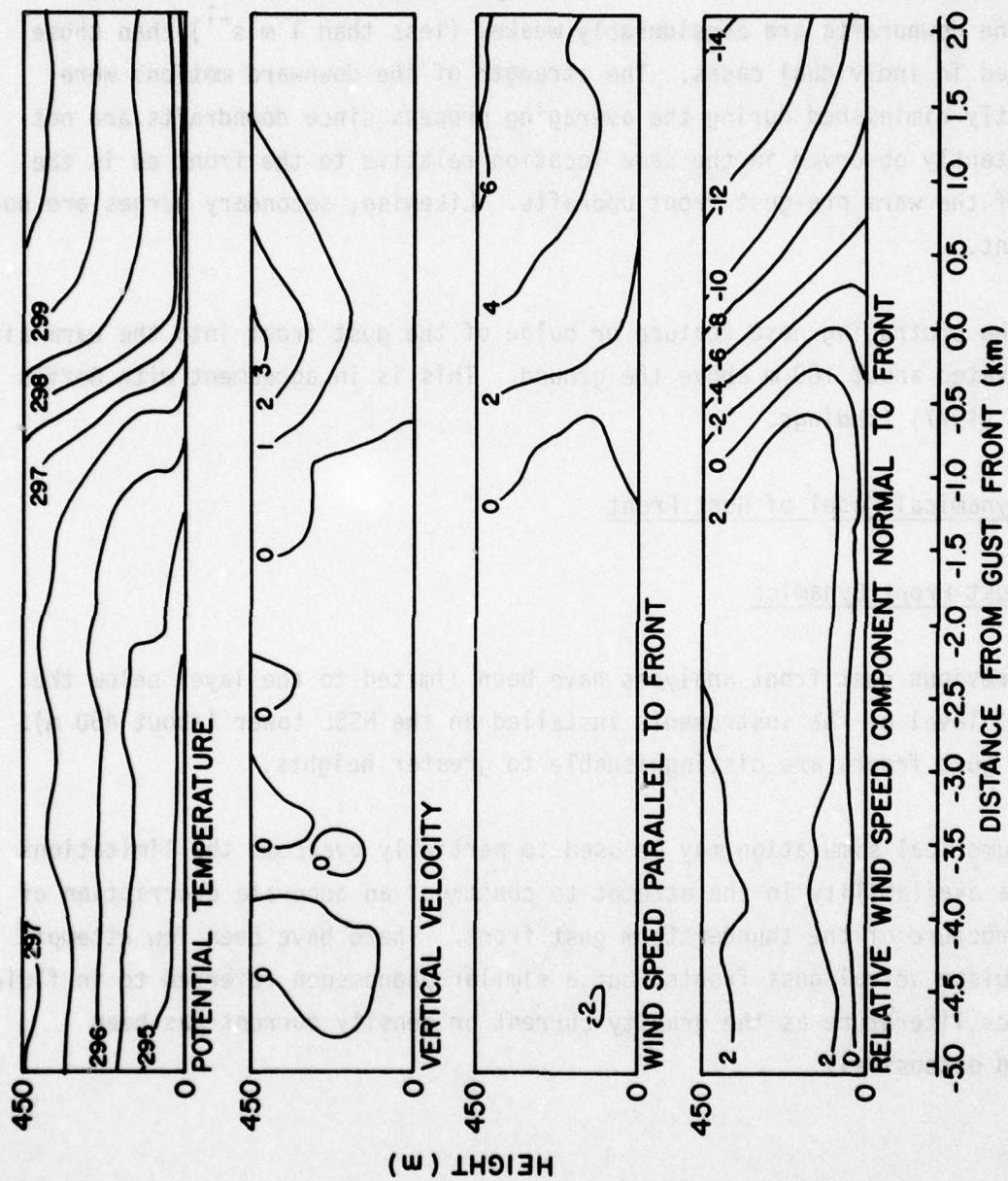


Figure 3-1. Average thunderstorm outflow determined from gust frontal cases listed in Table 1. Units are m s⁻¹ and °K.

Since all of the cases used in this composite analysis were of the squall line-type some of the features of the frontal zone for the squall line as discussed by Goff et al. (1977) are present. Namely, the updraft in the warm air ahead of the front is followed by a downdraft behind the front. Here the downdrafts are considerably weaker (less than 1 m s^{-1}) than those observed in individual cases. The strength of the downward motions were evidently diminished during the averaging process since downdrafts are not consistently observed in the same location relative to the front as is the case of the warm pre-gust front updrafts. Likewise, secondary surges are not apparent.

The protruding nose feature or bulge of the gust front into the warm air is elevated about 100 m above the ground. This is in agreement with Goff's et al. (1977) findings.

4.0 Dynamical Model of Gust Front

4.1 Gust Front Dynamics

Previous gust front analyses have been limited to the layer below the highest level of the instruments installed on the NSSL tower (about 450 m). Actual gust fronts are distinguishable to greater heights.

Numerical simulation may be used to partially overcome the limitations of data availability in the attempt to construct an accurate description of the structure of the thunderstorm gust front. There have been few attempts to simulate actual gust fronts, but a similar phenomenon referred to in fluid dynamics literature as the gravity current or density current has been studied extensively.

The work by Mitchell and Hovermale (1977), referred to hereafter as the M-H simulation, is a simulation of a gust front. To illustrate the evolution of the gust front, we shall discuss this model in some detail. They used a non-hydrostatic, dry, two-dimensional primitive equation model as described by the following equations:

equations of motion

$$\frac{\partial u}{\partial t} + u \frac{\partial u}{\partial x} + w \frac{\partial u}{\partial z} + \frac{1}{\rho} \frac{\partial p}{\partial x} + F_r(u) = 0 \quad (4.1)$$

$$\frac{\partial w}{\partial t} + u \frac{\partial w}{\partial x} + w \frac{\partial w}{\partial z} + \frac{1}{\rho} \frac{\partial p}{\partial z} + g + F_r(w) = 0 \quad (4.2)$$

thermodynamic energy equation

$$\frac{\partial p}{\partial t} + u \frac{\partial p}{\partial x} + w \frac{\partial p}{\partial z} + w \frac{c_p}{c_v} p \left(\frac{\partial u}{\partial x} + \frac{\partial w}{\partial z} \right) + F_r(p) = 0 \quad (4.3)$$

mass continuity

$$\frac{\partial \rho}{\partial t} + u \frac{\partial \rho}{\partial x} + w \frac{\partial \rho}{\partial z} + \rho \left(\frac{\partial u}{\partial x} + \frac{\partial w}{\partial z} \right) + F_r(\rho) = 0 \quad (4.4)$$

where x and z are the horizontal and vertical coordinates, u and w are the velocity components of the x and z coordinates, p and ρ are the pressure and density of dry air, c_p and c_v are specific heat capacities of dry air at constant pressure and constant volume.

The temperature (T) and potential temperature (θ) are obtained from the equation of state for dry air and Poisson's equation:

$$T = \frac{p}{\rho R} \quad (4.5)$$

and

$$\theta = T \left(\frac{1000}{p} \right)^{R/c_p} \quad (4.6)$$

where R is the gas constant for dry air.

The F_r terms in equations (4.1) through (4.4) represent linear diffusion expressed for a given variable μ as follows:

$$F_r(\mu) = K_x \frac{\partial^2 \mu}{\partial x^2} + K_z \frac{\partial^2 \mu}{\partial z^2} \quad (4.7)$$

where K_x and K_z are constant: $K_x = 2.25 \times 10^6 \text{ cm}^2 \text{ s}^{-1}$ and $K_z = 1.25 \times 10^6 \text{ cm}^2 \text{ s}^{-1}$ for interior points and $K_x = K_z = 0$ at the boundaries.

The boundary conditions are: (1) for w, under the condition of flat bottom and top surfaces,

$$w = 0 \text{ at } z = 0, H \quad (4.8)$$

(2) for u , the slip condition is used at the top,

$$\frac{\partial u}{\partial z} = 0 \text{ at } z = H \quad (4.9)$$

and at the bottom surface a "limited slip" formulation is used, that is,

$$\frac{\partial u}{\partial z} = 0 \text{ at } z = 0 \quad (4.10)$$

and

$$\frac{\partial}{\partial z} \left(\frac{\tau}{\rho} \right) = \frac{-C_D |u_1| u_1}{\Delta z} \text{ at } z = 175 \text{ m} \quad (4.11)$$

where τ is the stress and C_D a non-dimensional constant that represents the average drag coefficient over the lowest 175 m and u_1 is u at 175 m.

The boundary conditions for pressure and density are chosen as

$$\frac{\partial p}{\partial z} = -\rho g \text{ and } \frac{\partial}{\partial z} \left(\frac{\partial \rho}{\partial t} \right) = 0 \text{ at } z = 0, H \quad (4.12)$$

The lateral boundary conditions for u , w , p and ρ are,

$$u = 0, \frac{\partial w}{\partial x} = 0, \frac{\partial p}{\partial x} = 0 \text{ and } \frac{\partial \rho}{\partial x} = 0, \text{ at } x = 0, L. \quad (4.13)$$

The initial condition used for the experiment is a horizontally uniform initial vertical temperature profile, $T_0(z)$ as constructed from the National Hail Research Experiment sounding data which were obtained near Fort Morgan, Colorado on a day during which four severe convective storms occurred

locally. The initial pressure $p_0(z)$ and density $\rho_0(z)$ are computed from $T_0(z)$ by using the hydrostatic equation and the equation of state.

$$\frac{\partial \ln p_0}{\partial z} = \frac{-g}{RT_0} \quad (4.14)$$

$$\rho_0 = \frac{p_0}{RT_0} \quad (4.15)$$

and

$$\frac{\partial p_0}{\partial x} = \frac{\partial \rho_0}{\partial x} = \frac{\partial T_0}{\partial x} = 0 \quad (4.16)$$

The atmosphere is assumed to be at rest initially.

4.1.1 Downdraft Simulation

The gust front results from a downdraft developed inside a thunderstorm by evaporation and the drag of raindrops. The evaporation cools the air and increases the density causing a downward acceleration. The drag of falling raindrops also produces a downward acceleration. A complete simulation of a realistic downdraft development has not yet been done. Mitchell and Hovermale assume that a cold downdraft somehow develops and persists. To establish the downdraft, the temperature in the desired downdraft location was reduced each time step by a pre-determined small increment during the first half minute of the prediction period. The artificial cooling was maximum (approximately 0.33°K per time step) at about $z = 1.4$ km and $x = 0$. After the initial cooling during the first half minute, the potential temperature field is shown in Figure 4-1. Within the boxed region in Figure 4-2a, the potential temperature is held constant for the remainder of the forecast.

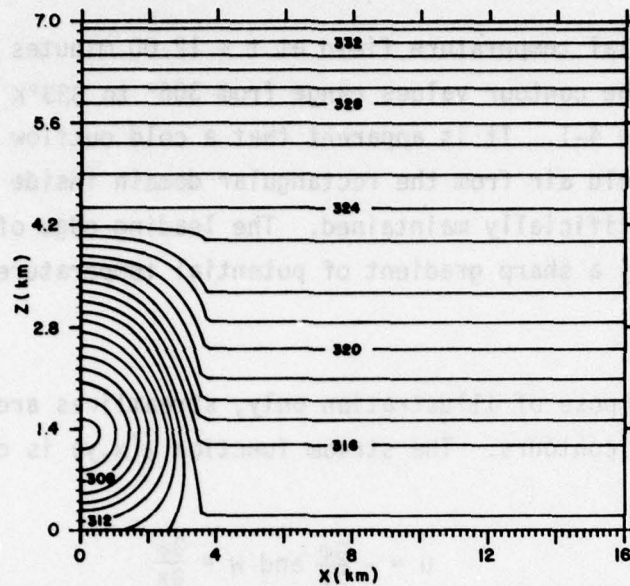


Figure 4-1 Potential temperature field (Θ) at $t = 0.40$ minutes. Contour values range from 306° to 333°K at interval of 1°K . (Courtesy of Mitchell and Hovermale, 1977.)

4.1.2 Numerical Computation

The governing equations (4.1) through (4.4) are numerically integrated over a 70×41 rectangular grid having a horizontal extent of 16 km ($x = 233$ m) and a vertical extent of 7 km ($z = 175$ m). The finite difference formulation of equations (4.1) through (4.4) used in the gust front simulation is identical to that of Shuman and Hovermale (1968). In order to suppress the high-frequency oscillations, mostly computational noise, a temporal filter described by Asselin (1972) was applied at every time step. For any function of time $F(t)$, the filtered function $\overline{F(t)}$ is obtained from

$$\overline{F(t)} = F(t) + \frac{\nu}{2} [F(t-\Delta t) - 2F(t) + F(t+\Delta t)] \quad (4.17)$$

where ν is taken as 0.5 in this simulation. This filter has a good low-pass response characteristic and does an effective job of controlling the computational mode arising from the centered-in-time integration.

The potential temperature field at $t = 12.00$ minutes is shown in Figure 4-2a. The contour values range from 306° to 333°K at the interval of 1°K as in Figure 4-1. It is apparent that a cold outflow is formed by steady subsidence of cold air from the rectangular domain inside which the cold downdraft is artificially maintained. The leading edge of the outflow is characterized by a sharp gradient of potential temperature, nearly discontinuous.

For the purpose of illustration only, streamlines are depicted as stream function contours. The stream function $\psi(x,y)$ is defined by

$$u = -\frac{\partial\psi}{\partial z} \text{ and } w = \frac{\partial\psi}{\partial x} \quad (4.18)$$

and calculated by solving the following equation by a Liebmann method

$$\frac{\partial^2\psi}{\partial x^2} + \frac{\partial^2\psi}{\partial z^2} = \left(\frac{\partial w}{\partial x} - \frac{\partial u}{\partial z}\right) \quad (4.19)$$

The flow at $t = 12$ minutes is depicted by Figure 4-3, 4-4 and 4-5. The wind blows in the direction of the streamlines and is faster where streamlines are closer together. At $t = 12$ minutes, a strong downdraft of 15 m s^{-1} is obtained at $z = 1.4$ to 2.0 km , $x = 0$ within the initially cooled area (Figure 4-1).

The downdraft turns into the horizontal as it approaches the ground, reaching a maximum horizontal speed of 24 m s^{-1} at 0.3 km , $x = 3.5$ and $z = 0.7 \text{ km}$, $x = 8 \text{ km}$. The outflow air displaces the low-level air in its path toward the downwind boundary. As this air approaches the boundary it is artificially forced upward, since the boundary condition allows no flow through the boundary.

This boundary condition and the initial rest (no motion) condition are significant weaknesses of this simulation. Because of the boundary condition, the same air which is forced to ascend near the right lateral boundary

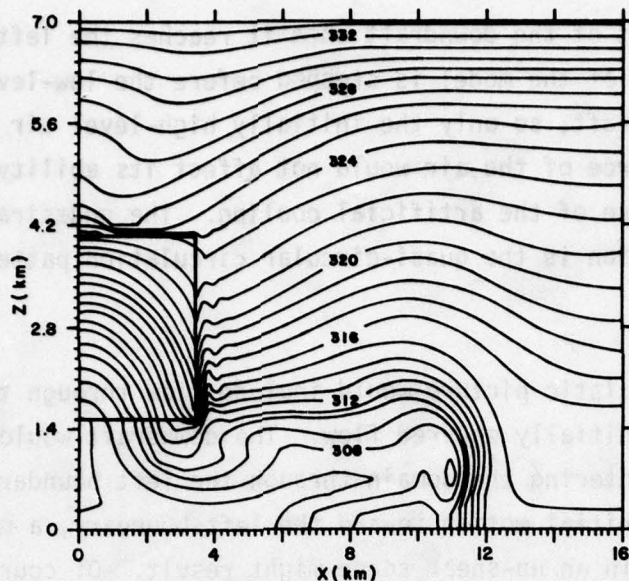


Figure 4-2a Potential temperature field (Θ) at $t = 12.00$ min. Boxed area denotes region of fixed Θ values. Contour range and interval as in Figure 4.1 (Courtesy of Mitchell and Hovermale, 1977).

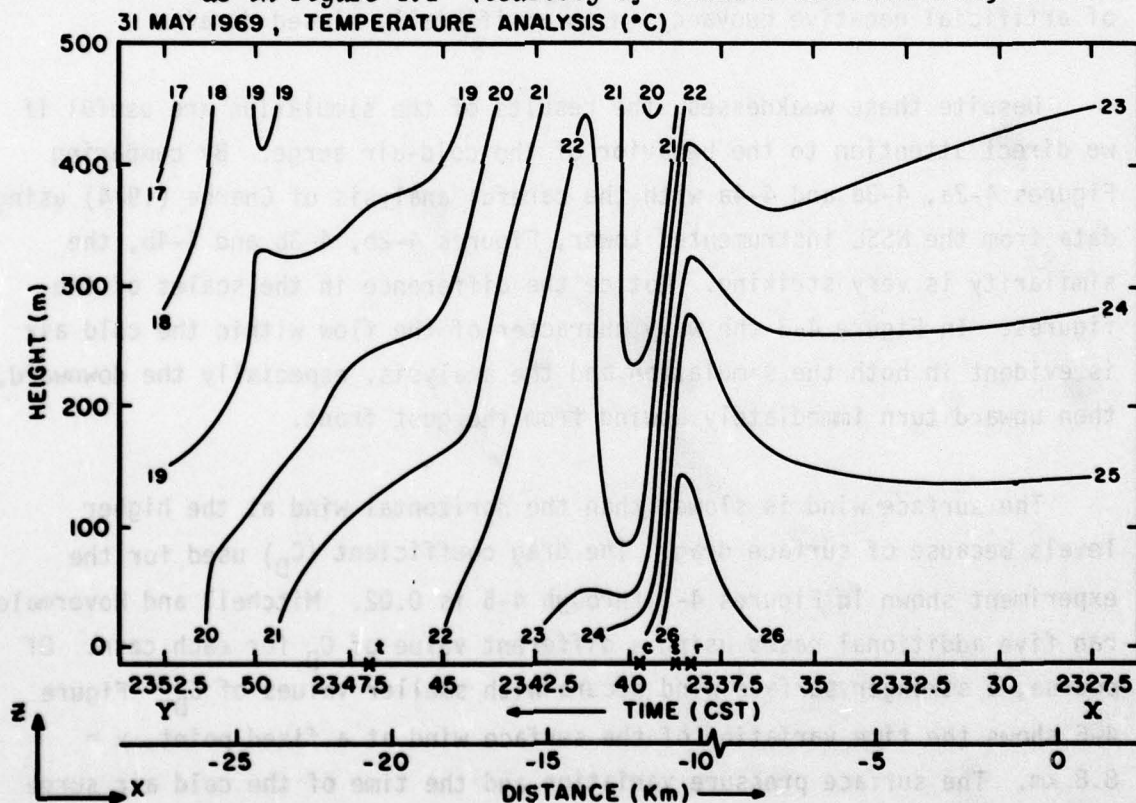


Figure 4-2b Objective analysis of a gust front associated temperature field for May 31, 1969. Cross-section is normal to the gust front. (Courtesy of Charba, 1972.)

must become part of the downdraft when it reaches the left boundary. However, the integration of the model is stopped before the low-level air has time to reach the downdraft, so only the initially high-level air enters the downdraft. The source of the air would not affect its ability to sustain the downdraft because of the artificial cooling. The undesirable result of the boundary condition is the quasi-circular circulation pattern depicted in Figure 4-3a.

A more realistic picture would include flow through the lateral boundaries and an initially sheared flow. The downdraft would then be fed by mid-level air entering the domain through the left boundary. If the low-level air had initial motion toward the left boundary, a more realistic updraft tilted in an up-shear sense might result. Of course cross-boundary flow would introduce computational difficulties. Unfortunately, in this simulation the circulation pattern results completely from the introduction of artificial negative buoyancy in an artificially closed domain.

Despite these weaknesses, the results of the simulation are useful if we direct attention to the behavior of the cold-air surge. By comparing Figures 4-2a, 4-3a and 4-4a with the careful analysis of Charba (1974) using data from the NSSL instrumented tower, Figures 4-2b, 4-3b and 4-4b, the similarity is very striking. Notice the difference in the scales of the figures. In Figure 4-3 the wavy character of the flow within the cold air is evident in both the simulation and the analysis, especially the downward, then upward turn immediately upwind from the gust front.

The surface wind is slower than the horizontal wind at the higher levels because of surface drag. The drag coefficient (C_D) used for the experiment shown in Figures 4-1 through 4-5 is 0.02. Mitchell and Hovermale ran five additional cases using a different value of C_D for each case. Of course, a stronger surface wind occurs with smaller values of C_D . Figure 4-6 shows the time variation of the surface wind at a fixed point, $x = 8.8$ km. The surface pressure variation and the time of the cold air surge are for the case where $C_D = 0.01$. It is interesting to note that the

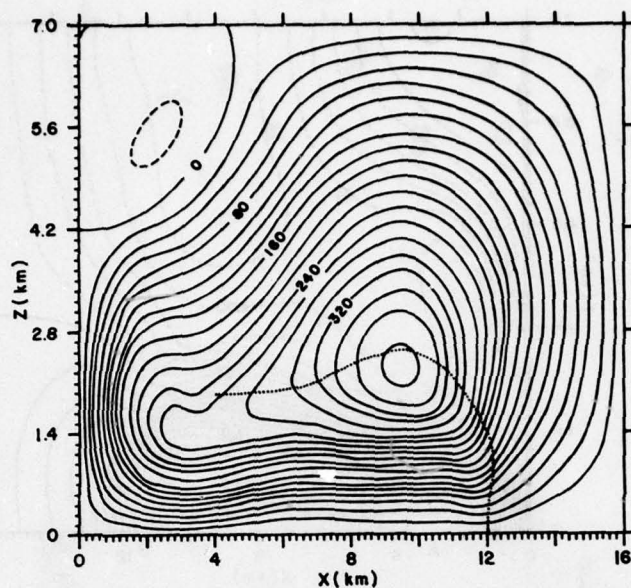


Figure 4-3a Streamfunction (ψ) at $t = 12.00$ min. Contour interval is $2.0 \times 10^3 \text{ m}^2 \text{ s}^{-1}$. (In all streamfunction plots, labels are scaled by -1.0×10^{-2} and solid contours depict counter-clockwise flow.) (Courtesy of Mitchell and Hovermale, 1977.)

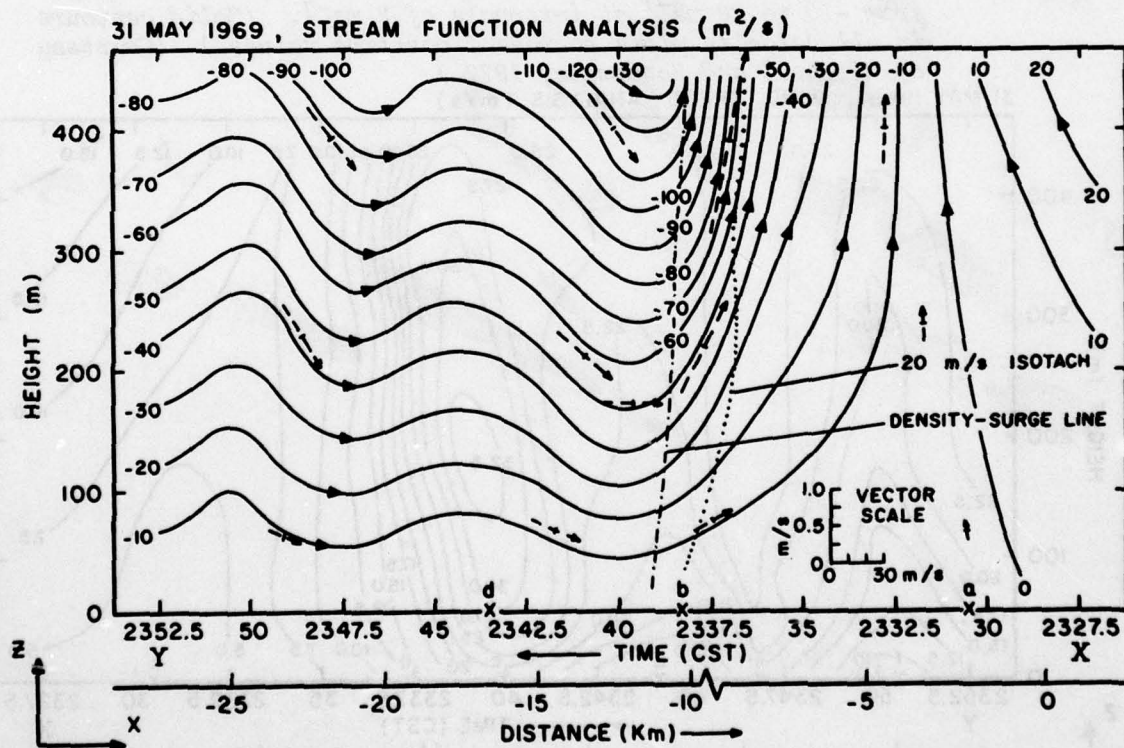


Figure 4-3b Same as Figure 4-2b except stream function analysis. (Courtesy of Charba, 1972.)

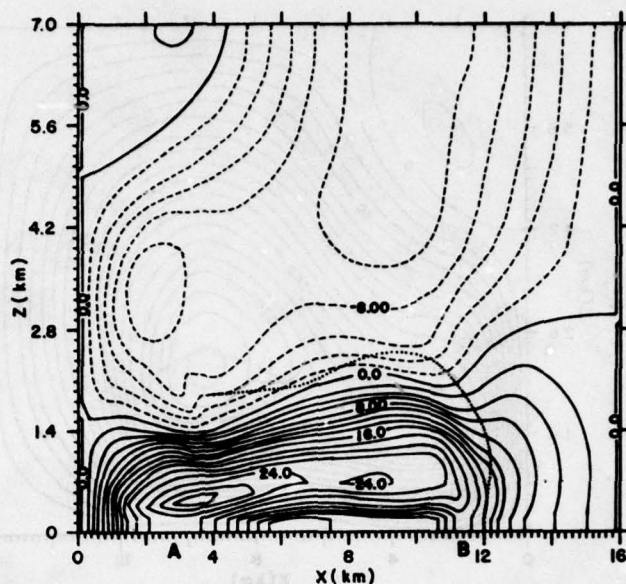


Figure 4-4a Horizontal velocity field (u) at $t = 12.00$ min. The superimposed dashed (or dotted) line, whenever it is given in any figure, represents the 314°K isentrope in the corresponding θ field. A and B denote surface maxima and C denotes the high velocity core above the surface. Contour values range from -10 to 28 ms^{-1} at intervals of 2 ms^{-1} . (Solid contours in all velocity plots represent positive values.) (Courtesy of Mitchell and Hovermale, 1977.)

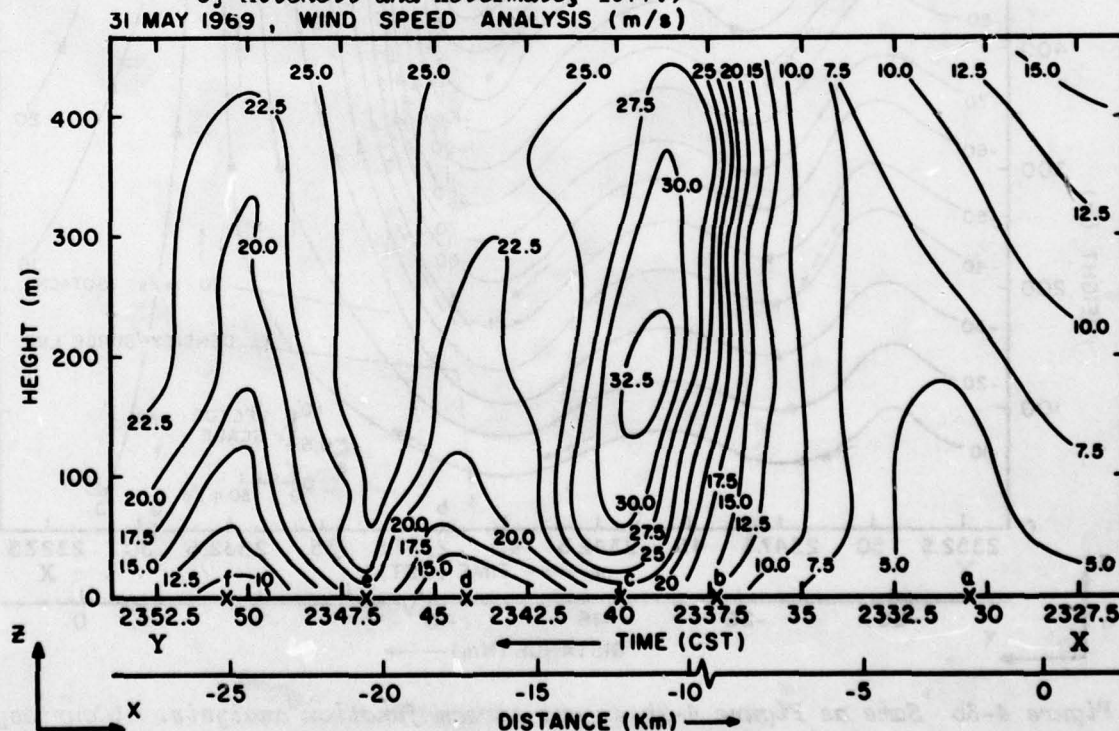


Figure 4-4b Same as Figure 4-2b except wind field analysis. (Courtesy of Charba, 1972.)

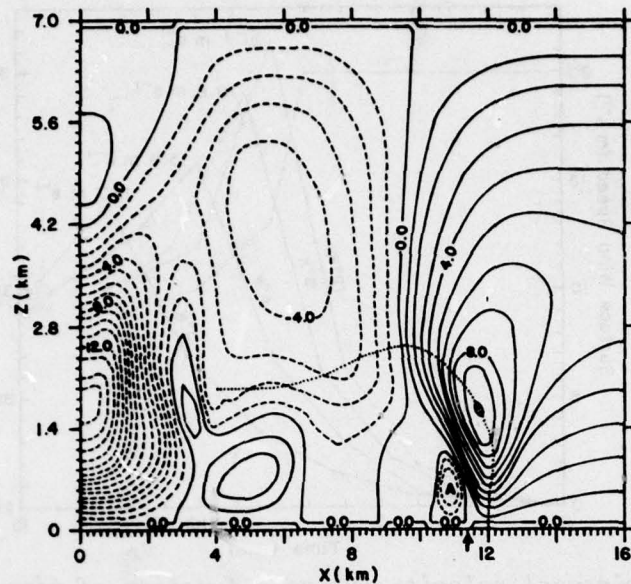


Figure 4-5 Vertical velocity field (w) at $t = 12.00$ min. A denotes the relative maximum of downward motion behind the front. Contour values range from -15 to 10 ms^{-1} at intervals of 1 ms^{-1} . (Courtesy of Mitchell and Hovermale, 1977.)

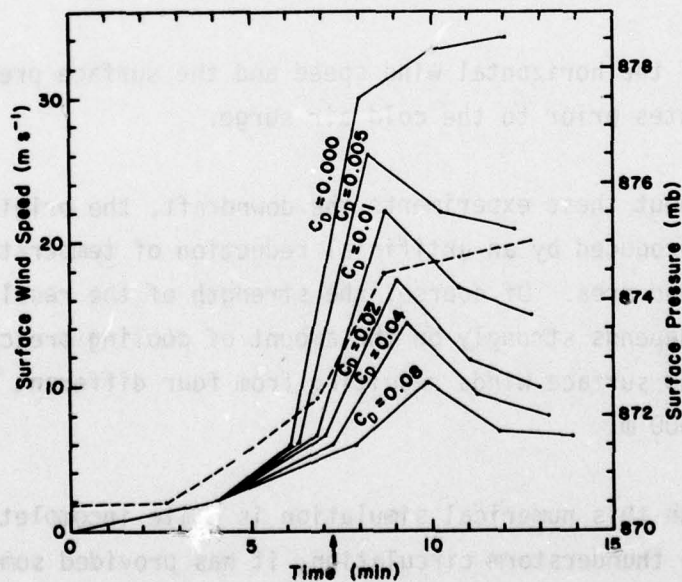


Figure 4-6 Horizontal velocity (u) as a function of time at a fixed point ($x = 8.8$ km) at the surface ($z = 0$) for all six surface drag cases. For the $C_D = 1.01$ case, the arrow denotes the onset of cold air and the dashed line depicts the surface pressure variation. The amplitude of the surface pressure rise in all cases was 4.5 ± 0.3 mb. (Courtesy of Mitchell and Hovermale, 1977.)

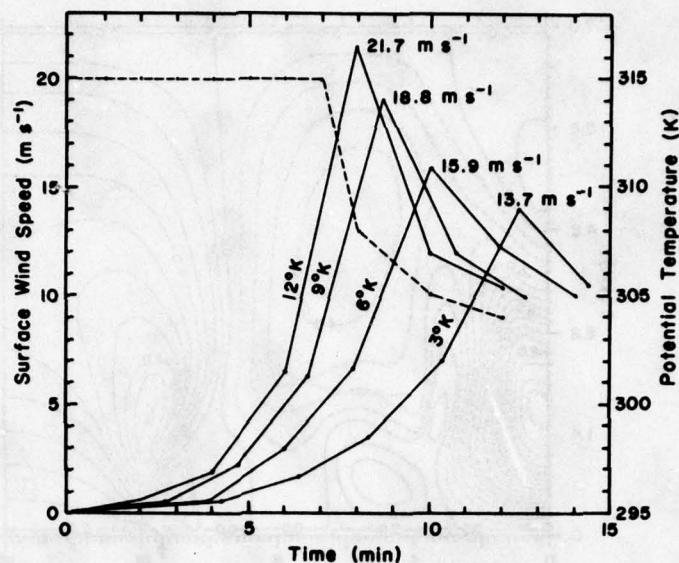


Figure 4-7 Horizontal velocity (u) as a function of time at a fixed point ($x = 9.7$ km) at the surface ($z = 0$) for the four cases given in Table 1. Each profile is labeled with the maximum surface wind speed and the corresponding maximum potential temperature decrease ($\Delta\theta$ at $z \approx 500$ m). The dashed line depicts the surface θ variation in the 12°K case. (Courtesy of Mitchell and Hovermale, 1977.)

increases of the horizontal wind speed and the surface pressure started several minutes prior to the cold air surge.

Throughout these experiments the downdraft, the origin of the gust front, was produced by an artificial reduction of temperature inside the pre-determined area. Of course, the strength of the resulting downdraft and gust front depends strongly on the amount of cooling prescribed. Figure 4-7 shows the surface winds resulting from four different values of total cooling at 500 m.

Although this numerical simulation is quite incomplete from the viewpoint of the thunderstorm circulation, it has provided some useful quantitative insights into the mechanics of thunderstorm gust fronts.

4.2 Origin of the Gust Front

Our knowledge of the gust front structure is fairly complete after extensive analyses of the data from tower-mounted meteorological sensors, special radar and radiosonde observations, and aircraft. The thunderstorm outflow, the leading edge of which forms a gust front, has many characteristics analogous to gravity or density currents from both laboratory and theoretical studies. We have just seen that Mitchell and Hovermale's numerical experiments succeeded in simulating many aspects of the gust fronts by using artificial cooling to generate a downdraft. This mechanism of gust front generation is essentially the Margules Process (1905).

4.2.1 Margules Process

Let us consider as an initial state, two air columns of the same height (h) standing side by side above the ground. One is colder, marked by {1}, and the other is warmer, marked by {2} in Figure 4-8. The fraction of the area {1} to the total area is β . The total horizontal dimension is λ and hence the column {1} occupies the area $\beta\lambda$.

The pressure of the air at the top of each column is p_h . The temperatures at the top of {1} and {2} are T_{h1} and T_{h2} , respectively. Temperatures at the ground are denoted by T_{01} and T_{02} and the pressure by p_{01} and p_{02} , respectively. If we assume that both columns have dry adiabatic lapse rates, Γ_d , T_{01} and T_{02} become

$$T_{01} = T_{h1} + \Gamma_d h \quad (4.20)$$

and

$$T_{02} = T_{h2} + \Gamma_d h, \quad (4.20')$$

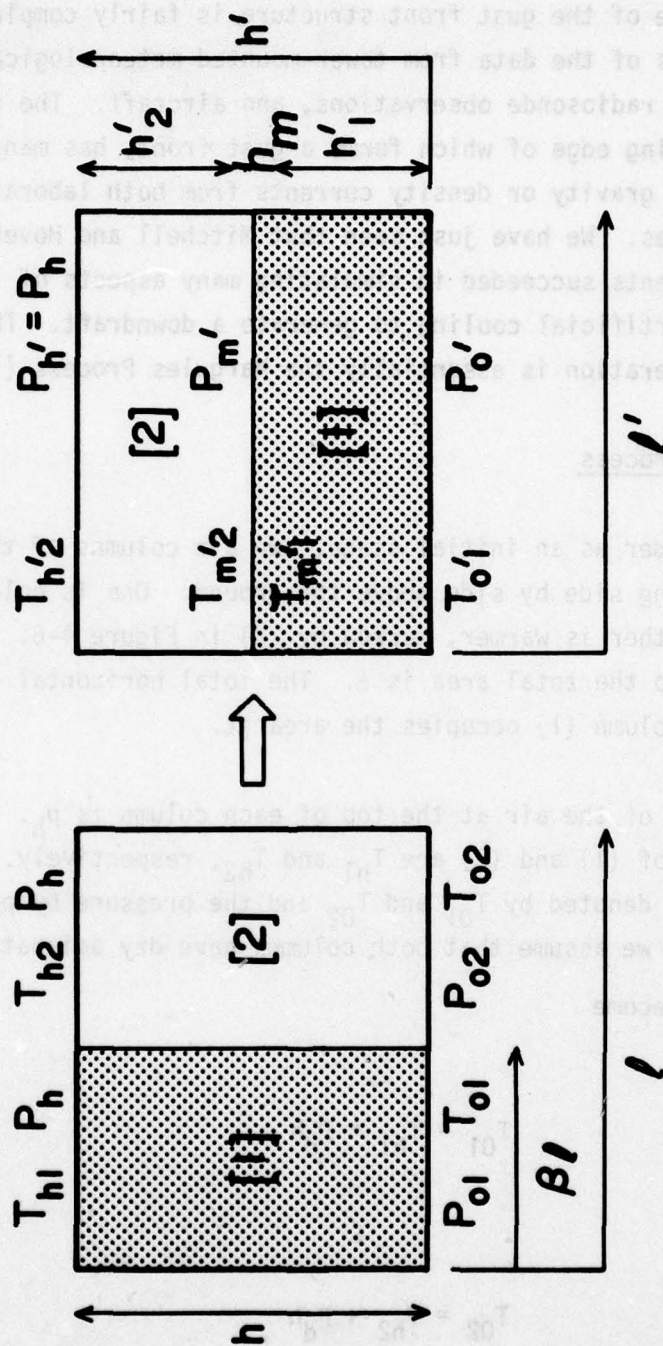


Figure 4-8 Schematic of Margules' Process.

and the surface pressures are

$$P_{01} = P_h \left(\frac{T_{01}}{T_{h1}} \right)^{\frac{\gamma}{\gamma-1}} \quad (4.21)$$

and

$$P_{02} = P_h \left(\frac{T_{02}}{T_{h2}} \right)^{\frac{\gamma}{\gamma-1}} \quad (4.21')$$

where $\gamma = \frac{c_p}{c_v}$.

The potential energy, PE, of a unit cross section of a column is, using the hydrostatic relation,

$$PE = \int_0^h g \rho z dz = \int_0^h \rho dz - p_h h \quad (4.22)$$

and the internal energy IE, using the equation of state, is

$$IE = c_v \int_0^h \rho T dz = \frac{c_v}{R} \int_0^h p dz = \frac{1}{\gamma-1} \int_0^h p dz. \quad (4.23)$$

Adding (4.22) and (4.23), the total energy, E, per unit cross section of a column becomes

$$E = PE + IE = \frac{\gamma}{\gamma-1} \int_0^h p dz - p_h h. \quad (4.24)$$

Substituting $p = p_0 \left(\frac{T_{01} - \Gamma_d z}{T} \right)^{\frac{\gamma}{\gamma-1}}$ into (4.24) and carrying out the integration, the total static energy per unit cross section becomes

$$E = - \frac{K}{1+K} \frac{p_0 T_0 c_p}{g} \left[\left(\frac{T_h}{T_0} \right)^{K+1} - 1 \right] - p_h h. \quad (4.25)$$

where $K = \frac{\gamma}{\gamma-1}$ and Γ_d has been replaced by $\frac{g}{c_p}$. Writing E for each of the two columns and summing, the total static energy of the system is

$$TE = - \frac{K}{1+K} \frac{c_p}{g} \left\{ \beta \ell p_{01} T_{01} \left[\left(\frac{T_{h1}}{T_{01}} \right)^{K+1} - 1 \right] + \right. \\ \left. (1-\beta) \ell p_{02} T_{02} \left[\left(\frac{T_{h2}}{T_{02}} \right)^{K+1} - 1 \right] \right\} - \ell p_h h \quad (4.26)$$

The dimension of the columns perpendicular to the page in Figure 4-8 is taken to be unity.

Now since air column {1} is denser than column {2}, it may be presumed that, lacking any restraining mechanism, column {1} will seek a position underneath column {2}, reducing the static energy and resulting in the configuration pictured in the right half of Figure 4-8. If we compare Equation 4.26 to a similar equation describing the total static energy of the system after the rearrangement, the difference will represent the kinetic energy generated by reducing the potential energy of the system.

$$TE' = - \frac{K}{1+K} \frac{c_p}{g} \ell' \left\{ p_0' T_0' \left[\left(\frac{T_{m1}'}{T_0'} \right)^{K+1} - 1 \right] + p_m' T_m' \left[\left(\frac{T_{h2}'}{T_m'} \right)^{K+1} - 1 \right] \right\} - \ell' p_h h \quad (4.27)$$

where the primes represent the final state.

The unknown temperatures and pressures of the final state, as well as ℓ' and p_m' may be determined from the conservation of the masses of the two columns. Assuming that

$$p_h' = p_h$$

and therefore

$$h' = h ,$$

the masses of the two columns at initial and final times are obtained by integrating the hydrostatic equation:

$$m_1 = \beta \ell \frac{p_{01} - p_h}{g}$$

$$m_1' = \ell' \frac{p_0' - p_m'}{g}$$

$$m_2 = (1-\beta) \ell \frac{p_{02} - p_h}{g}$$

$$m_2' = \ell' \frac{p_m' - p_h}{g} .$$

Since $m_1 = m_1'$

$$\beta \ell (p_{01} - p_h) = \ell' (p_0' - p_m') \quad (4.28)$$

and because $m_2 = m_2'$

$$(1-\beta) \ell (p_{02} - p_h) = \ell' (p_m' - p_h) . \quad (4.29)$$

Solving (4.28) and (4.29) for ℓ' and p_m' ,

$$\ell' = \frac{\beta(p_{01} - p_h) + (1-\beta)(p_{02} - p_h)}{(p_0' - p_h)} \ell \quad (4.30)$$

$$p'_m = p'_0 - \frac{\beta(p_{01} - p_h)(p'_0 - p_h)}{\beta(p_{01} - p_h) + (1-\beta)(p_{02} - p_h)} \quad (4.31)$$

If the redistribution of the air columns is simply adiabatic, then

$$T'_{h2} = T_{h2} \quad (4.32)$$

$$T'_{01} = T_{h1} \left(\frac{p'_0}{p_h} \right)^{\frac{1}{\gamma}} \quad (4.33)$$

$$T'_{m2} = T_{h2} \left(\frac{p'_m}{p_h} \right)^{\frac{1}{\gamma}} \quad (4.34)$$

$$T'_{m1} = T_{h1} \left(\frac{p'_m}{p_h} \right)^{\frac{1}{\gamma}} \quad (4.35)$$

$$p'_0 = \beta p_{01} + (1-\beta)p_{02} \quad (4.36)$$

If the total energy of the system is conserved during the adiabatic redistribution, and if the system was initially at rest ($KE = 0$), then

$$KE' = TE - TE' \quad (4.37)$$

Since

$$KE = \frac{1}{2} M V^2 \quad (4.38)$$

where M is the mass of the system

$$M = \ell' \frac{p_0' - p_h}{g} \quad (4.39)$$

and V is a representative wind speed. Therefore,

$$V = \left[\frac{2g}{\ell' (p_0' - p_h)} (T_E - T_E') \right]^{1/2} \quad (4.40)$$

In order to make a sample calculation of the wind speeds which might result from such a process, let us take the following initial conditions:

$$h = 5568.15 \text{ m}$$

$$p_{01} = 1000 \text{ mb}$$

$$T_{01} = 302.51^\circ \text{ K}$$

$$T_{h1} = 248.16^\circ \text{ K}$$

$$p_h = 500 \text{ mb}$$

$$p_{02} = 987.63 \text{ mb}$$

$$T_{02} = 307.51^\circ \text{ K}$$

$$T_{h2} = 253.16^\circ \text{ K}$$

After the rearrangement,

$$p_0' = 990.10 \text{ mb}$$

$$\ell' = \ell$$

$$p_m' = 890.10 \text{ mb}$$

$$T_{h2}' = 253.16^\circ \text{ K}$$

$$T_{01}' = 301.65^\circ \text{ K}$$

$$T_{m2}' = 298.51^\circ \text{ K}$$

$$T_{m1}' = 292.61^\circ \text{ K}$$

If the remaining calculations are carried out, we see that for this hypothetical situation, which we might view as a typical case of evaporative cooling in a thunderstorm, if all the energy was converted to horizontal motion, then a typical wind speed of 12 m s^{-1} could result.

This procedure might be refined to produce an estimate of the maximum surface winds to be expected with thunderstorms if the thunderstorms produced a gust front. The temperature of the colder air mass could be taken to be the wet-bulb temperature of the middle-level air. The warmer air mass could be assigned the wet-bulb temperature of the low-level air. The role of vertical momentum transport also has to be included.

4.2.2 Far-reaching Gust Fronts

Gust fronts frequently propagate as far as 30-50 km away from the thunderstorm center without losing much of their kinetic energy (Figures 4-9 and 4-10). In the M-H simulation this distance was typically about 10 km (Figure 4-2a). The simulated gust front leads the thunderstorm by a shorter distance than was typical in the case study of Charba, despite the fact that the maximum horizontal wind speed was also smaller in the simulation (28 m s^{-1} compared to 32.5 m s^{-1} in the Charba analysis), and also despite the fact that the temperature difference between the downdraft and its environment has about the same magnitude in both the simulation and the analysis (compare Charba's vertical temperature profiles in Figure 4-11 to Figure 4-2a). This weakness of the simulation has not been adequately explained.

4.3 Microphysical Processes (One Dimensional Thunderstorm Simulation)

We will now examine the microphysical processes which cool the air and create thunderstorm downdrafts. The cooling is mainly due to evaporation, and the downward acceleration of the air is generated by the negative buoyancy of the colder air and by the drag of falling rain drops.

Figure 4-12 shows the scheme of cloud microphysical processes used by Ogura and Takahashi (1971) for their one dimensional (vertical) simulation of a thunderstorm. The microphysical processes considered to be responsible for changes among the water phases (vapor, liquid and ice) are condensation, evaporation, conversion, sublimation, glaciation and melting. These microphysical processes will be described here in some detail and their effect on the gust front will be considered.

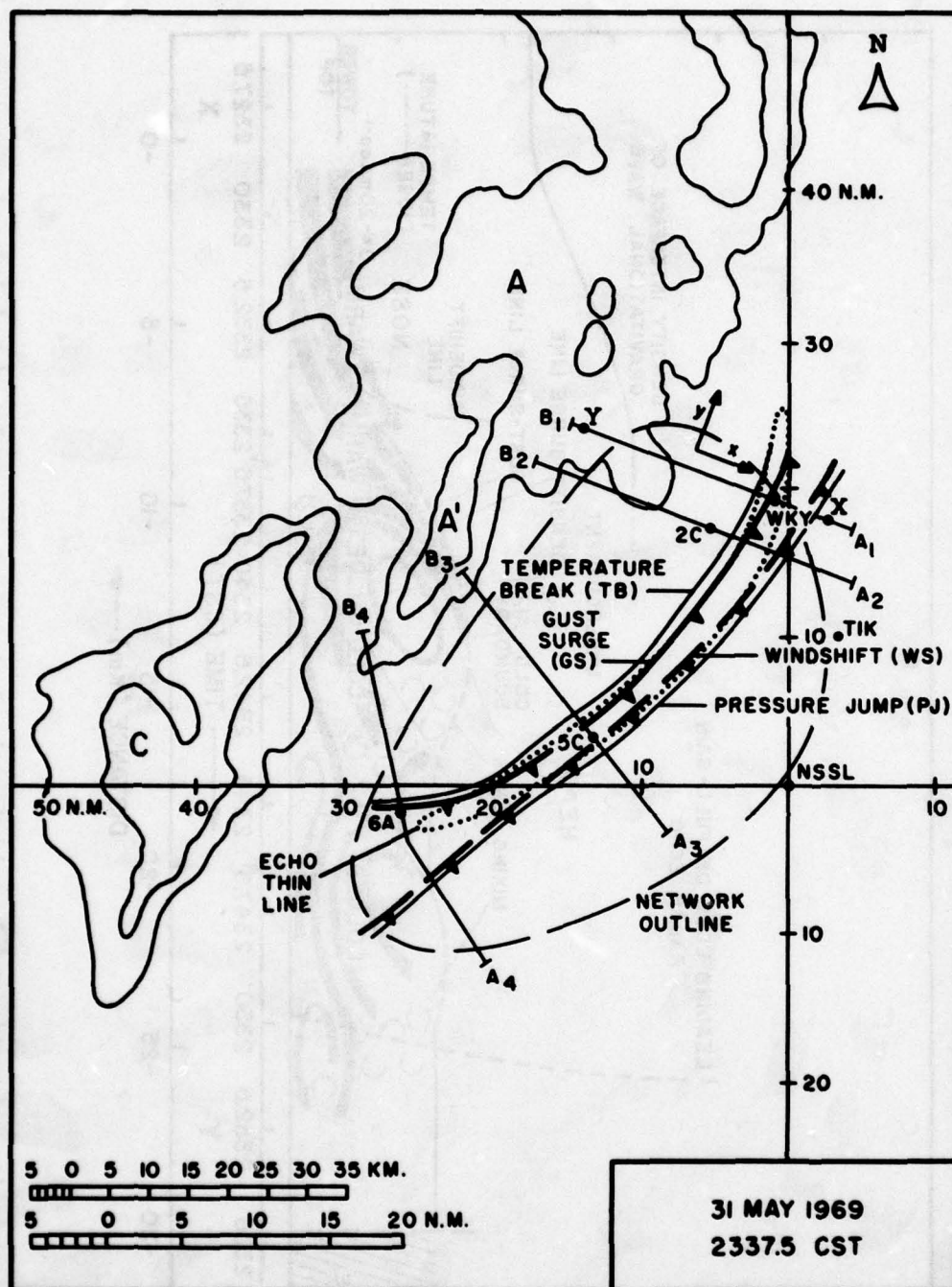


Figure 4-9 Major squall line features at 2337 CST May 31, 1969. The PPI radar echo tracing is of the 2×10 and $2 \times 10^4 \text{ mm}^6 \text{ m}^{-3}$ reflectivity factor contours. XY is the section line for the plane of vertical cross section analysis of the WKY tower data shown in Figure 4-10. A_1B_1 , A_2B_2 , etc. are section lines used by Charba (1968) for the time-to-space converted surface network data traces of the stations indicated. (Courtesy of Charba.)

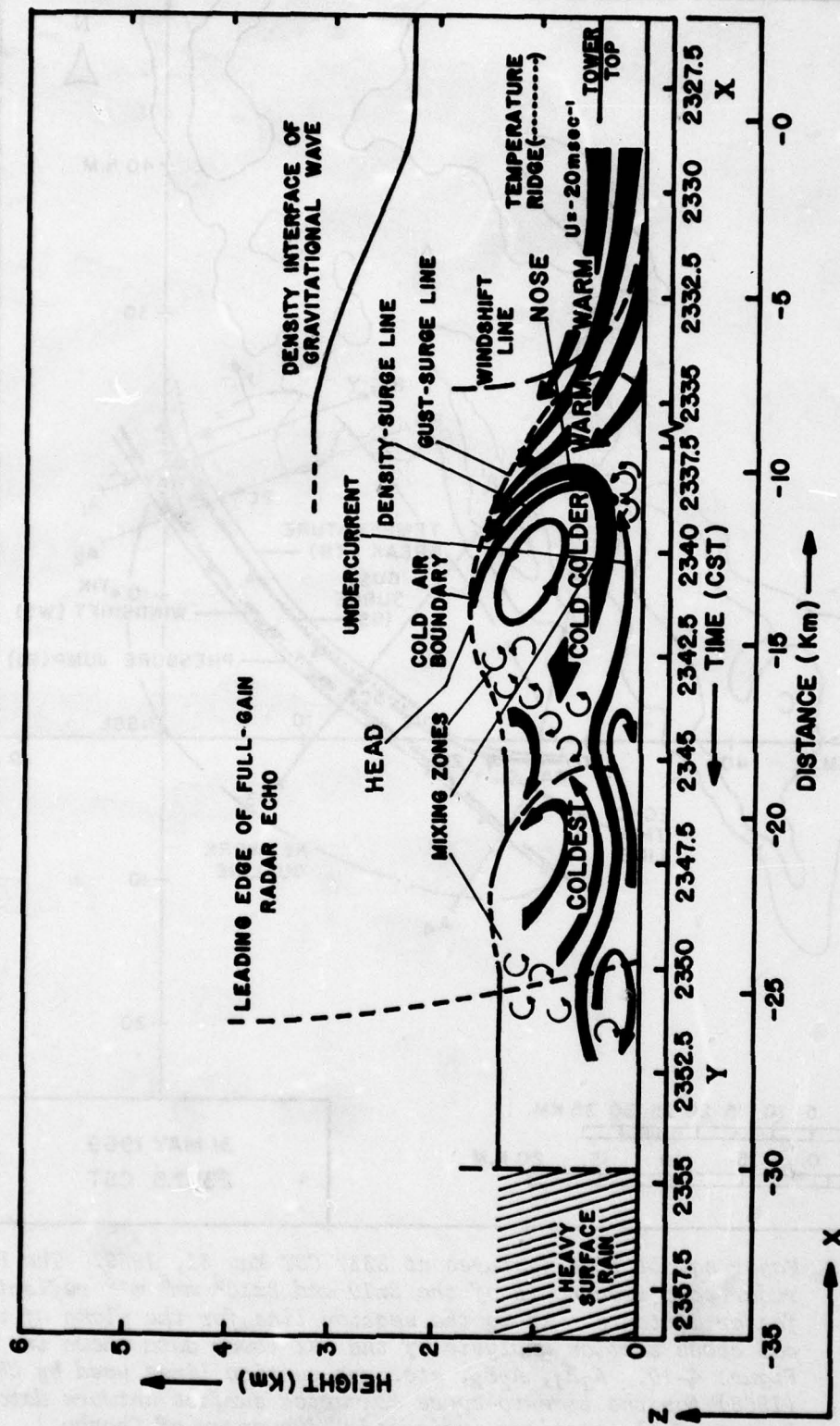


Figure 4-10 A composite schematic model combining the features of the analyzed and deduced structure of the windshift and gust front leading the squall line of May 31, 1969. (Courtesy Charba).

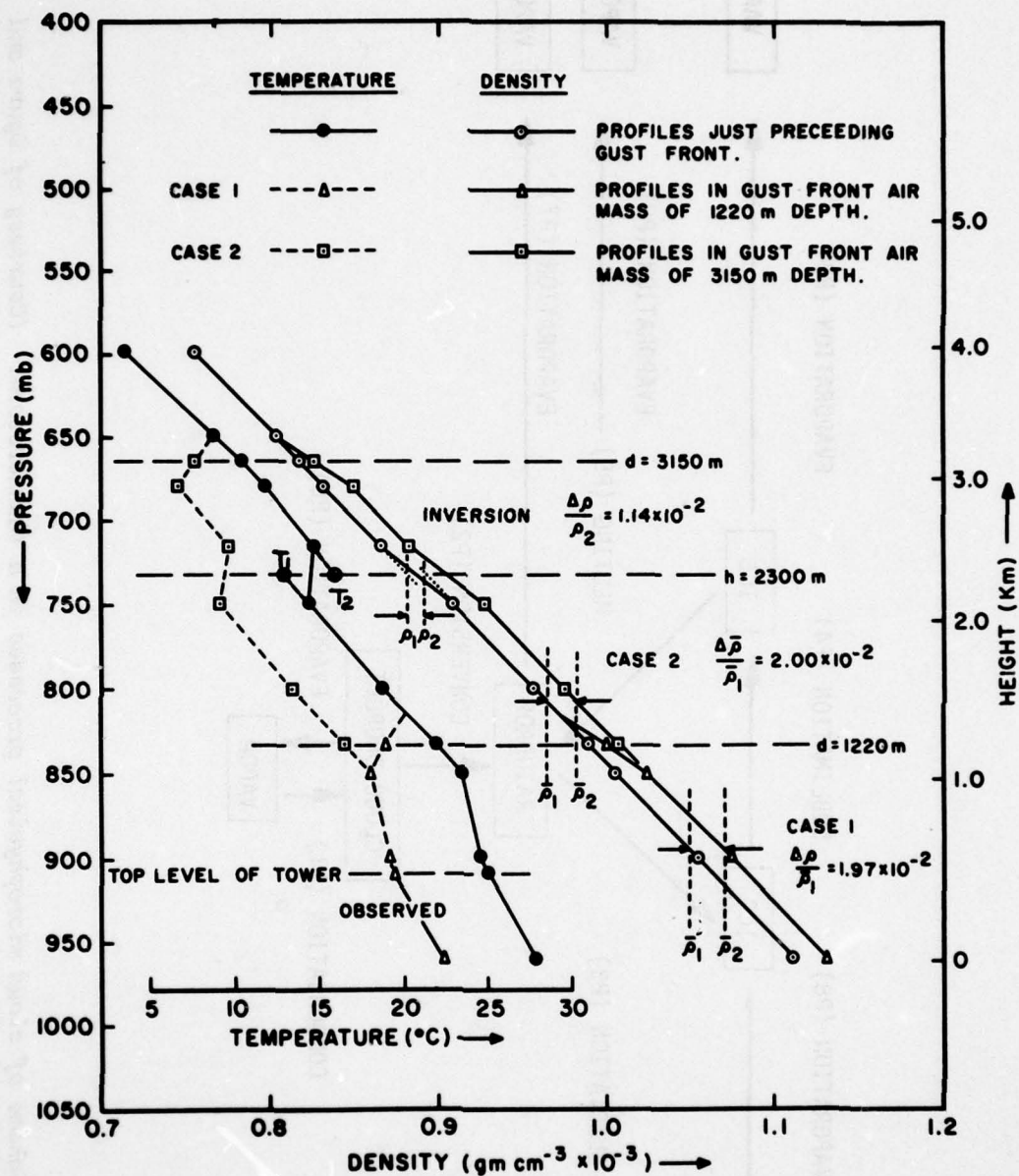


Figure 4-11 Vertical profiles of temperature and density at WKY just before and just after the gust surge passed, 2300 and 2345 CST, respectively. (Courtesy Charba).

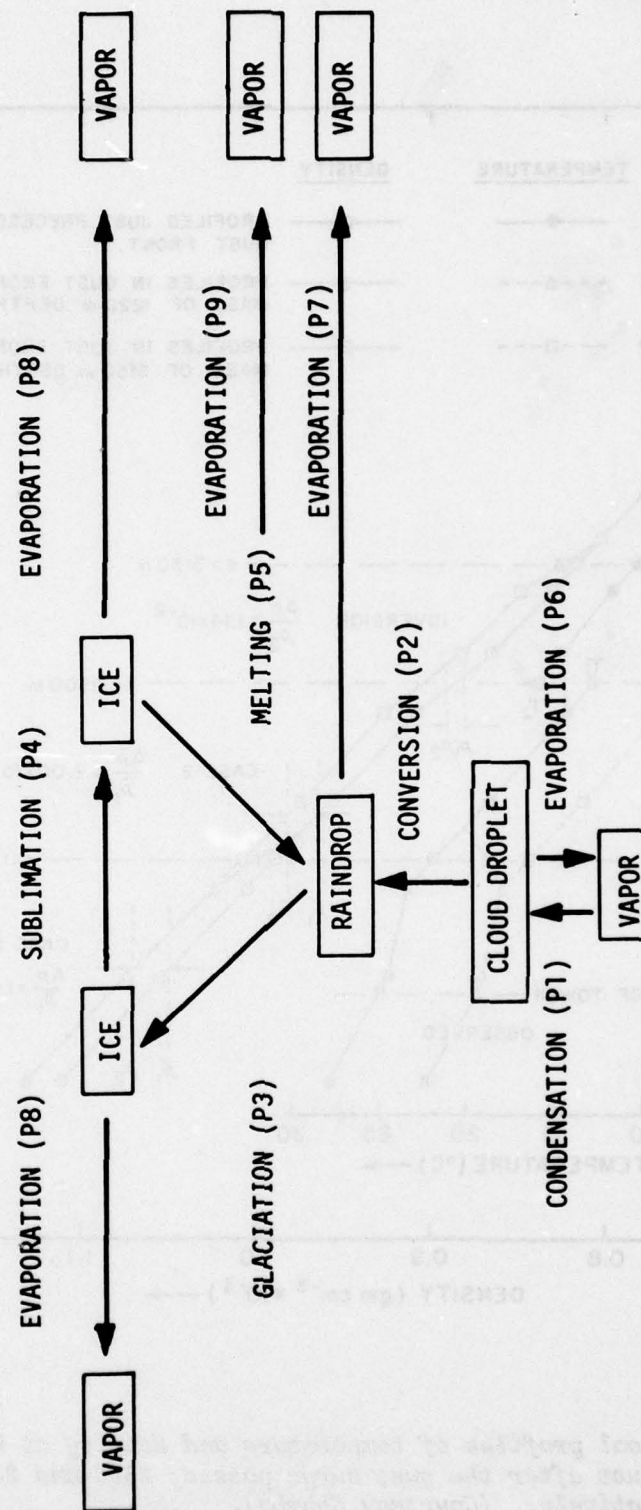


Figure 4-12 Scheme of cloud microphysical processes in a thunderstorm. (Courtesy of Ogura and Takahashi, 1971.)

Ogura and Takahashi parameterized the various microphysical processes in an attempt to evaluate their relative importance. The condensation rate,

$$P1 \equiv \frac{dq_v}{dt} = \frac{dq_{vs}}{dt} \quad \text{for } q_v \geq q_{vs} \quad (4.41)$$

$$= 0 \quad \text{for } q_v < q_{vs},$$

where q_v and q_{vs} are the mixing ratio of water vapor and its saturated value, respectively. The rate of conversion from cloud droplets to raindrops,

$$P2 \equiv \left(\frac{dq_r}{dt} \right)_{\text{CONV}} = C_0 q_c \quad (4.42)$$

where q_c and q_r are the mixing ratios of cloud droplets and of raindrops, respectively, and the parameter C_0 is the reciprocal of the conversion time, taking values in the range of 0 to 0.2 s^{-1} . The glaciation rate

$$P3 \equiv \left(\frac{dq_i}{dt} \right)_{\text{glac}} = G q_r \quad (4.43)$$

where q_i is the mixing ratio of ice crystals and G is the reciprocal of the glaciation time from 0 to 0.05 s^{-1} . The rate of sublimation used is

$$P4 = \frac{1}{\rho_a} \frac{\left(\frac{q_v}{q_{is}} - 1 \right) (\rho_a q_i)^{0.525} f_0^{-0.42}}{7 \times 10^5 + \frac{0.41 \times 10^7}{e_{is}}} \quad (4.44)$$

where q_{is} and e_{is} are the saturation mixing ratio of water vapor and saturation vapor pressure measured in mb over a plane ice surface, respectively. The constant f_0 is used in the computation of the terminal velocity of ice particles and takes the value 0.75 here. The rate of melting is

$$P5 = 2.27 \times 10^{-6} C (T-273) (\rho_a q_i)^{0.525} \rho_a^{-1} f_0^{-0.42} \quad (4.45)$$

C represents the ventilation constant given by

$$C = 1.6 + 0.57 \times 10^{-3} (v_i)^{1.5} f_o^{-1}$$

The rate of evaporation from cloud droplets to water vapor

$$P6 \equiv -\left(\frac{dq_c}{dt}\right)_{\text{evap}} = \left(\frac{dq_v}{dt}\right)_{\text{evap}} \quad (4.46)$$

and evaporation was assumed to be instantaneous as long as the air was not saturated with water vapor. The rate of evaporation of raindrops

$$P7 = 5.8 \times 10^{-4} (q_v - q_{vs}) \quad (4.47)$$

where the units are $\text{gm gm}^{-1} \text{s}^{-1}$. This equation is a simplified form of

$$P7 = -\frac{1}{\rho_a} \frac{\left(\frac{q_v}{q_{vs}} - 1\right) C (\rho_a q_r)^{0.525}}{5.4 \times 10^5 + \frac{0.41 \times 10^7}{e_{ws}}} \quad (4.48)$$

where e_{ws} is the saturation vapor pressure over a water surface. The rate of evaporation of ice crystals is

$$P8 = -\frac{1}{\rho_a} \frac{\left(\frac{q_v}{q_{is}} - 1\right) C (\rho_a q_i)^{0.525} f_o^{-0.42}}{7 \times 10^5 + \frac{0.41 \times 10^7}{e_{is}}} \quad (4.49)$$

which is similar to that for raindrops except for different values of the latent heat of sublimation and vapor pressure. The rate of evaporation of melting ice crystals

$$p_g = - \frac{1}{\rho_a} \frac{\left(\frac{q_v}{q_{vs}} - 1\right) C(\rho_a q_i)^{0.525} f_o^{-0.42}}{5.4 \times 10^5 + \frac{0.41 \times 10^7}{e_{ws}}} \quad (4.50)$$

These parameterizations are applied within the framework of a one dimensional model describing a right circular cylinder, with radial symmetry and coordinates (r, λ, z) . The pressure distribution is not considered but is assumed identical to the environmental conditions. The equation of vertical motion is simplified to

$$\frac{\partial w}{\partial t} = -w \frac{\partial w}{\partial z} - \frac{2\alpha^2}{a} w |w| + \frac{2}{a} (w - \tilde{w}_a) \tilde{u}_a + g \frac{T_v - T_{vo}}{T_{vo}} - g(q_c + q_r + q_i) \quad (4.51)$$

where for any variable A,

$$\tilde{A}_a = \frac{1}{2\pi} \int_0^{2\pi} A \, d\lambda \text{ at } r = a,$$

T_v is the virtual temperature and the added subscript zero refers to environmental conditions. The first term of the right hand side represents the vertical advection, the second term the lateral eddy exchange, the third term the dynamical entrainment which is required to satisfy mass continuity between the cloud and the environment,

$$\frac{2}{a} \tilde{u}_a + \frac{1}{\rho_{ao}} \frac{\partial}{\partial z} (\rho_{ao} \tilde{w}) = 0 \quad (4.52)$$

where

$$\tilde{w} = \frac{1}{\pi a^2} \int_0^{2\pi} \int_0^a w r \, dr \, d\lambda \quad (4.53)$$

The fourth term is the buoyancy and the last term the drag force, assumed to be proportional to the weight of cloud droplets, raindrops and ice crystals.

Similarly, the thermodynamic equation is given by

$$\frac{\partial T}{\partial t} = -w \left(\frac{\partial T}{\partial z} + r_d \right) + \frac{2\alpha^2}{a} |w| (T_o - T) + \frac{2}{a} \tilde{u}_a (T - \tilde{T}_a) + \left[\frac{L_s}{c_p} (P1 - P6 - P7 - P9) + \frac{L_s}{c_p} (P4 - P8) + \frac{L_f}{c_p} (P3 - P5) \right] \quad (4.54)$$

where L_v , L_s , L_f are the latent heats of evaporation (600 cal gm^{-1}), sublimation (680 cal gm^{-1}) and fusion (80 cal gm^{-1}), respectively. The continuity equations for water vapor, cloud droplets, raindrops and ice crystals are

$$\frac{\partial q_v}{\partial t} = -w \frac{\partial q_v}{\partial z} + \frac{2\alpha^2}{a} |w| (q_{vo} - q_v) + \frac{2}{a} \tilde{u}_a (q_v - \tilde{q}_{va}) - P1 + P6 + P7 + P8 - P4 + P9 \quad (4.55)$$

$$\frac{\partial q_c}{\partial t} = -w \frac{\partial q_c}{\partial z} + \frac{2\alpha^2}{a} |w| (q_{co} - q_c) + \frac{2}{a} \tilde{u}_a (q_c - \tilde{q}_{ca}) + P1 - P2 - P6 \quad (4.56)$$

$$\frac{\partial q_r}{\partial t} = -(w - V_w) \frac{\partial q_r}{\partial z} + \frac{q_r}{\rho_{ao}} \frac{\partial (\rho_{ao} V_w)}{\partial z} + \frac{2\alpha^2}{a} |w| (q_{ro} - q_r) + \frac{2}{a} \tilde{u}_a (q_r - \tilde{q}_{ra}) + P2 - P3 - P7 + P5 \quad (4.57)$$

and

$$\frac{\partial q_i}{\partial t} = -(w - V_i) \frac{\partial q_i}{\partial z} + \frac{q_i}{\rho_{ao}} \frac{\partial (\rho_{ao} V_i)}{\partial z} + \frac{2\alpha^2}{a} |w| (q_{io} - q_i) + \frac{2}{a} \tilde{u}_a (q_i - \tilde{q}_{ia}) + P3 + P4 - P5 - P8 - P9 \quad (4.58)$$

where V_w is the terminal velocity of raindrops

$$V_w = 3.12 \times 10^3 (\rho_a q_r)^{0.125} \text{ cm s}^{-1} \quad (4.59)$$

and V_i is the terminal velocity of ice particles

$$V_i = 3.12 \times 10^3 (\rho_a q_i)^{0.125} f_o \text{ cm s}^{-1} \quad (4.60)$$

Ogura and Takahashi conducted an initial experiment without any micro-physical processes. Figure 4-13 shows the time-height cross sections of vertical velocity, excess temperature and liquid water content. A strong updraft forms and reaches a steady state after about 45 minutes. No downdraft and no middle-level temperature deficit occurs. The strong temperature deficit appearing at 11 km is apparently caused by adiabatic cooling in the upper stable layer while the updraft air is losing its momentum.

A much more realistic simulation was achieved when the microphysics were added, as shown by Figure 4-14, which is similar to Figure 4-13 but the concentrations of cloud droplets, raindrops and ice crystals are also depicted. The maximum downdraft of 4 m s^{-1} developed at about 4 km after about 65 min, but the accompanying temperature is hardly significant. The downdraft starts developing first in the lower part of the cloud at 40 min and spreads to the higher altitudes. At approximately 60 min, the downdraft replaces the updraft throughout the domain. In particular, a strong downdraft appears at the melting zone. After the downdraft reaches the ground, it decreases and soon dies at about 70 min. The maximum updraft and downdraft throughout the life cycle is 17 m s^{-1} and 5 m s^{-1} , respectively.

The excess temperature increases during the initial 40 min in a way similar to the case without the microphysical processes. After that time

the temperature starts decreasing and at 55 min, a negative temperature anomaly developed near the melting level. Figure 4-15 reveals that the maximum downward velocity is observed very close to the time and level where four processes are occurring: evaporation of ice crystals (P8) and of melting of ice crystals (P9), evaporation of raindrops (P7), and melting of ice crystals (P5). All of these processes appear during the decaying stage of the cumulus. The evaporation processes P7, P8, and P9 have the same order of magnitude while the melting of ice crystals (P5) cools the air at a rate about one order larger. The total cooling is very small compared to observations in real thunderstorms, largely because the experiment was one-dimensional, precluding the possibility of considering the evaporation of cloud water by invading middle level dry air.

4.4 Dry Air Intrusion (Two Dimensional Thunderstorm Simulation)

Perhaps the weakest feature of the one dimensional simulation is its failure to portray a strong downdraft with accompanying strong evaporative cooling. The evaporation process was hindered by the absence of a source of dry air into which water could easily evaporate.

Figure 4-16 is a schematic representation of a typical vertical circulation pattern within a cumulonimbus in an environment with vertical shear (Ludlam, 1961). Dry middle level air enters the storm from the upwind side and is cooled by evaporating precipitation (indicated by dashed lines) which falls from the tilted updraft. The resulting intense cooling causes a downdraft of sufficient magnitude to prevent the dry air from destroying the updraft.

In order to simulate this schematic, we need at least a two dimensional model. Several two and three dimensional experiments with vertical shear have been performed (Takeda, 1965, 1966, 1971; Orville and Sloan, 1970; Hane, 1972; Schlesinger, 1973, 1974; Wilhelmson, 1974). We will discuss Hane's experiment for the purpose of illustration.

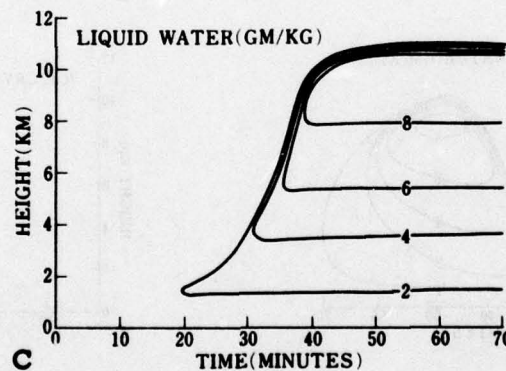
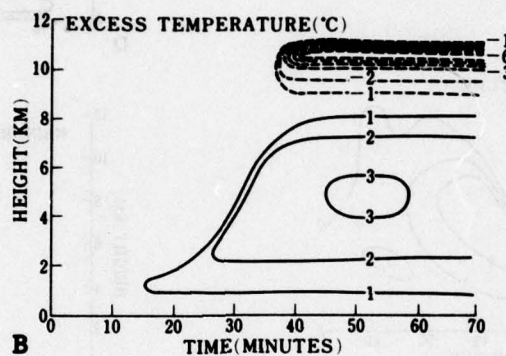
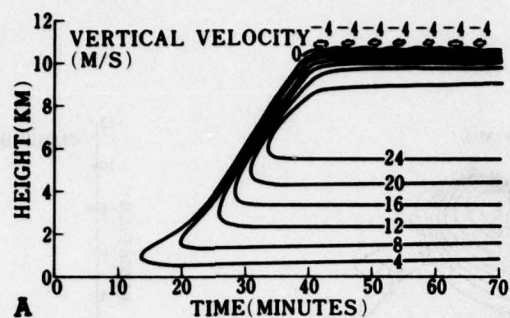


Figure 4-13 Time-height cross sections of (A) vertical velocity, (B) excess temperature, (C) liquid water content for a cloud without microphysical processes. (Courtesy of Ogura and Takahashi, 1971.)

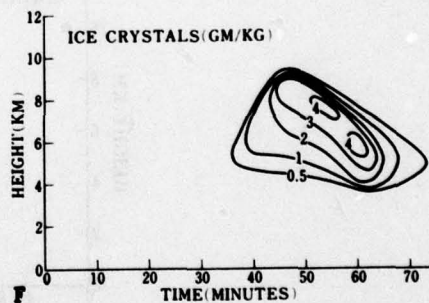
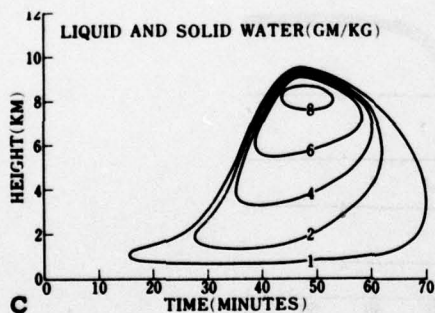
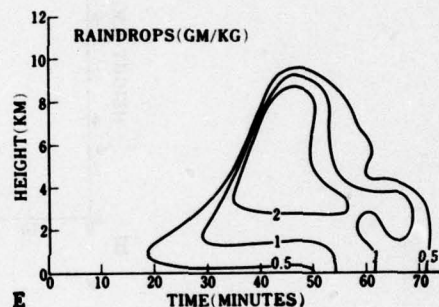
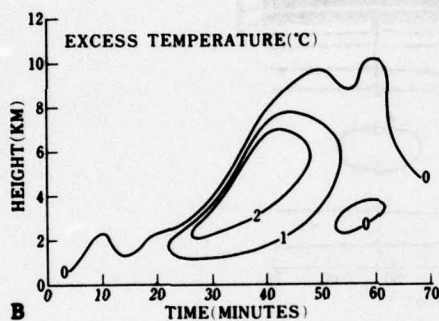
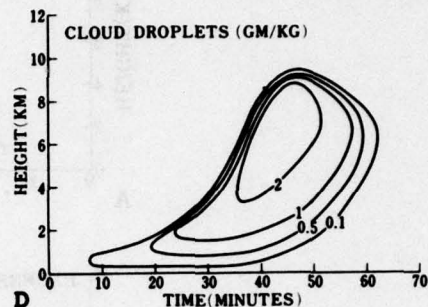
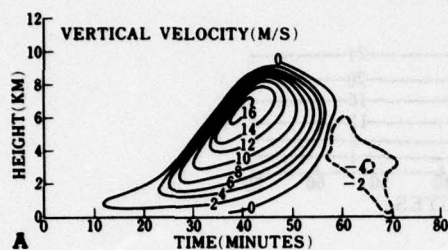


Figure 4-14 Time-height cross sections of (A) vertical velocity, (B) excess temperature, (C) liquid and solid water content, (D) content of cloud droplets (E) content of raindrops and (F) content of ice crystals for a cloud with microphysical processes; $\Gamma_0 = 6.3^\circ\text{C}/\text{km}$, $C_0 = 0.005$. (Courtesy of Ogura and Takahashi, 1971.)

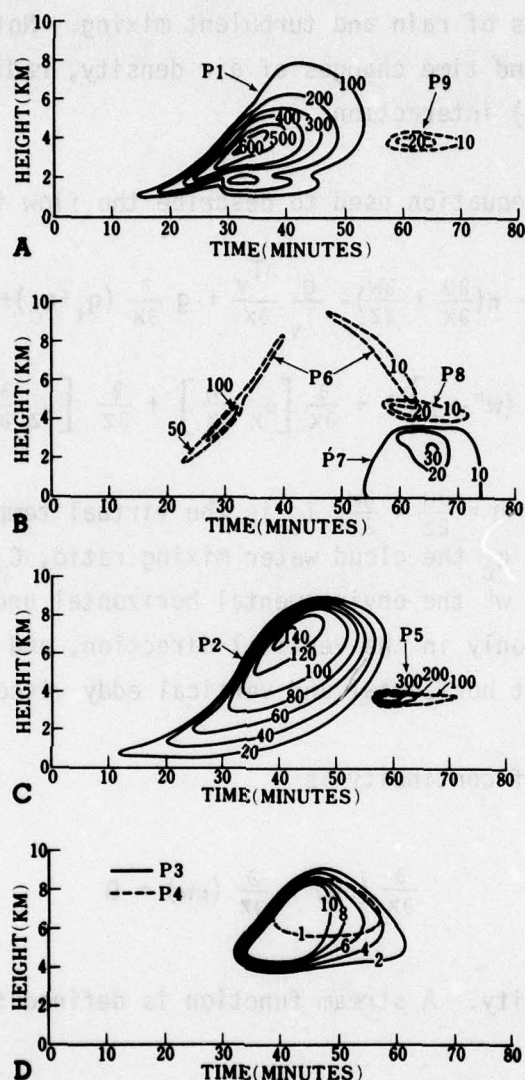


Figure 4-15 Time-height cross sections of the rates of (A) condensation of water vapor into cloud droplets (P1) and evaporation of melting ice crystals (P9); (B) evaporation of cloud droplets (P6), raindrops (P7) and ice crystals (P8); (C) conversion of cloud droplets into raindrops (P2) melting of ice crystals (P5); and (D) glaciation (P3) and growth of ice crystals by sublimation (P4) in units of 10^{-7} s^{-1} . (Courtesy of Ogura and Takahashi, 1971.)

Hane's model includes the condensation and evaporation processes, liquid water "in bulk" assuming the Marshall-Palmer drop-size distribution, variable terminal fall speeds of rain and turbulent mixing. Not included are the ice phase, horizontal and time changes of air density, radiational effects and the air-ground (sea) interaction.

The vorticity equation used to describe the flow is

$$\begin{aligned} \frac{\partial \eta}{\partial t} = & -u \frac{\partial \eta}{\partial x} - w \frac{\partial \eta}{\partial z} - \eta \left(\frac{\partial u}{\partial x} + \frac{\partial w}{\partial z} \right) - \frac{g}{T_v} \frac{\partial T_v}{\partial x} + g \frac{\partial}{\partial x} (q_l + q_c) + C_m \left\{ \frac{\partial}{\partial z} \left[\left| \frac{\partial w}{\partial x} \right| (u'' - u) \right] \right. \\ & \left. - \frac{\partial}{\partial x} \left[\left| \frac{\partial w}{\partial x} \right| (w'' - w) \right] \right\} + \frac{\partial}{\partial x} \left[v_x \frac{\partial \eta}{\partial x} \right] + \frac{\partial}{\partial z} \left[v_z \frac{\partial \eta}{\partial z} \right] \end{aligned} \quad (4.61)$$

where the vorticity $\eta = \frac{\partial u}{\partial z} - \frac{\partial w}{\partial x}$, T_v is the virtual temperature, q_l the rain water mixing ratio, q_c the cloud water mixing ratio, C_m the turbulent mixing coefficient, u'' and w'' the environmental horizontal and vertical wind components which vary only in the vertical direction, and v_x and v_z are the time-space dependent horizontal and vertical eddy viscosity coefficients.

The equation of continuity is

$$\frac{\partial}{\partial x} (\rho u) + \frac{\partial}{\partial z} (\rho w) = 0 \quad (4.62)$$

where ρ is air density. A stream function is defined to satisfy the continuity equation.

$$\rho u = \frac{\partial \psi}{\partial z} \quad \text{and} \quad \rho w = - \frac{\partial \psi}{\partial x} \quad (4.63)$$

The vorticity is expressed by the stream function as

$$\rho \eta = \nabla^2 \psi - \frac{1}{\rho} \frac{\partial \psi}{\partial z} \frac{\partial \rho}{\partial z} \quad (4.64)$$

The first law of thermodynamics is written

$$\frac{\partial T}{\partial t} = -u \frac{\partial T}{\partial x} - w \left[\frac{\partial T}{\partial z} + \Gamma_d \right] + \frac{1}{c_p} \frac{dQ}{dt} + c_m \left| \frac{\partial w}{\partial x} \right| (T'' - T) + \nu_\theta \nabla^2 T \quad (4.65)$$

where T is the absolute temperature, Γ_d the dry adiabatic lapse rate, $\left(\frac{1}{c_p}\right)\left(\frac{dQ}{dt}\right)$ the latent heating or cooling rate, T'' the environmental temperature, a function of z only, and ν_θ the constant thermal diffusivity ($500 \text{ m}^2 \text{ s}^{-1}$).

The prediction equations for the three forms of moisture are

$$\begin{aligned} \frac{\partial q_v}{\partial t} = & -u \frac{\partial q_v}{\partial x} - w \frac{\partial q_v}{\partial z} + c_m \left| \frac{\partial w}{\partial x} \right| (q''_v - q_v) + \nu_\theta \nabla^2 q_v \\ & + \text{evaporation} - \text{condensation} \end{aligned} \quad (4.66)$$

$$\begin{aligned} \frac{\partial q_c}{\partial t} = & -u \frac{\partial q_c}{\partial x} - w \frac{\partial q_c}{\partial z} + c_m \left| \frac{\partial w}{\partial x} \right| (q''_c - q_c) + \nu_\theta \nabla^2 q_c \\ & - \text{autoconversion} - \text{accretion} - \text{evaporation} + \text{condensation} \end{aligned} \quad (4.67)$$

$$\begin{aligned} \frac{\partial q_r}{\partial t} = & -u \frac{\partial q_r}{\partial x} - w \frac{\partial q_r}{\partial z} + \frac{\partial}{\partial z} (q_r V_T) + \frac{q_r V_T}{\rho} + \frac{\partial \rho}{\partial z} \\ & + \text{autoconversion} + \text{accretion} - \text{evaporation} \end{aligned} \quad (4.68)$$

In these equations q_v is the water vapor mixing ratio, q_c the mixing ratio of cloud droplets, q_r the mixing ratio of rain, q''_v and q''_c are environmental quantities that vary only in the vertical direction, and V_T is the effective terminal velocity of the raindrop distribution.

The autoconversion, accretion, evaporation, condensation and terminal velocity of raindrops are evaluated based on Kessler's parameterization (Kessler *et al.* 1961-64) which is similar to that used by Ogura and Takahashi (1971).

Hane simulated storm development for various vertical wind shear cases. Figure 4-17 shows the result of the moderate shear case with the system speed of 10 m s^{-1} at $t = 5.6 \text{ min}$, which includes the two dimensional stream function, ($10^3 \text{ kg m}^{-1} \text{ s}^{-1}$), rain water mixing ratio (gm kg^{-1}) and cloud water mixing ratio (solid lines, dashed lines, scalloped lines respectively) in the top section, temperature anomaly ($^{\circ}\text{K}$) in the middle section and vertical wind speed (m s^{-1}) in the lower section. The negative temperature anomaly (in the middle section of the figure) shows a cold dome-like shape, with the coldest air at the ground. The flow pattern shows that the downdraft originated in the middle levels at the left-hand side of the storm, comparing well with the dry intrusion depicted in Figure 4-16.

The downdraft spreads both forward (to the right) and to the rear (left) near the ground. There is an inflow from the right to left near the ground that sharply slides upward, precipitating and producing rain (top section of Figure 4-17).

The outflow, spreading forward, collides with the low-level inflow underneath the central portion of the storm (as defined by the cloud water area scalloped in Figure 4-17). The energy dissipation caused by the collision may retard the spreading of the cold air. Hane continued the time-integration of experiment R1 up to $t = 16.3 \text{ min}$. The outflow did not move outside the storm area in that time. In experiment R2 (strong shear with the system speed of 19 m s^{-1}), the leading edge of the outflow at $t = 5 \text{ min}$ and 15.7 min never leaves the storm area (Figure 4-18 for $t = 5 \text{ min}$ and 15.7 min).

The right half of Figure 4-18 shows that the typical thunderstorm circulation pattern seen in the left half has been lost by 15.7 min . The two dimensional simulation is a vast improvement over the one dimensional model, but is still unable to capture the persistent features of the mature thunderstorm with a gust front propagating 30 to 50 km ahead of the storm.

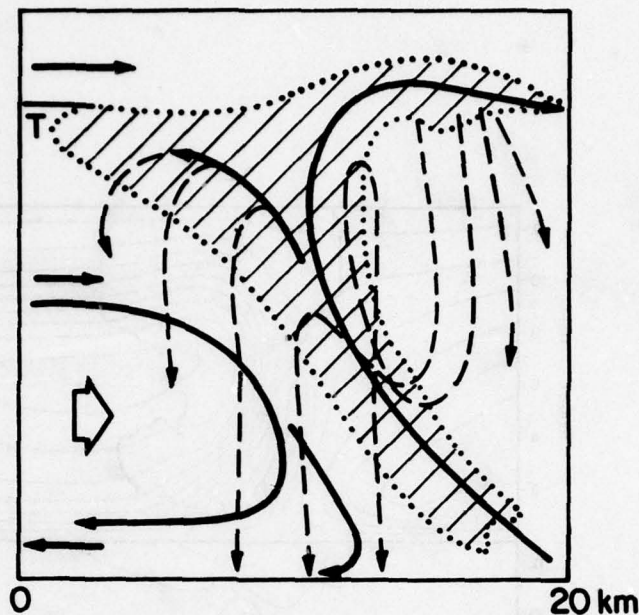


Figure 4-16 Schematic representation of the motion field within a middle latitude cumulonimbus in wind shear. T indicates height of tropopause. The vertical and horizontal scales are the same (after Ludlam, 1961).

4.5 Twisted Storm Circulation (Three Dimensional Model)

One possible reason why the two dimensional simulations fail to produce gust fronts which propagate far away from the storm may be the fact that the shear between the low level flow and the middle level flow is exaggerated. In two dimensions the two flows are exactly opposing each other. Typical thunderstorm environments have somewhat less directional shear between the low and middle levels.

It may well be that a three dimensional simulation with a realistic shear condition would produce a gust front which reaches far ahead of the storm. In recent years, some effort has been directed toward developing three dimensional thunderstorm models, with limited success (Steiner, 1973; Wilhelmson, 1974; Schlesinger, 1975). The new advanced computers should expedite these efforts, resulting in increased understanding of the gust front dynamics.

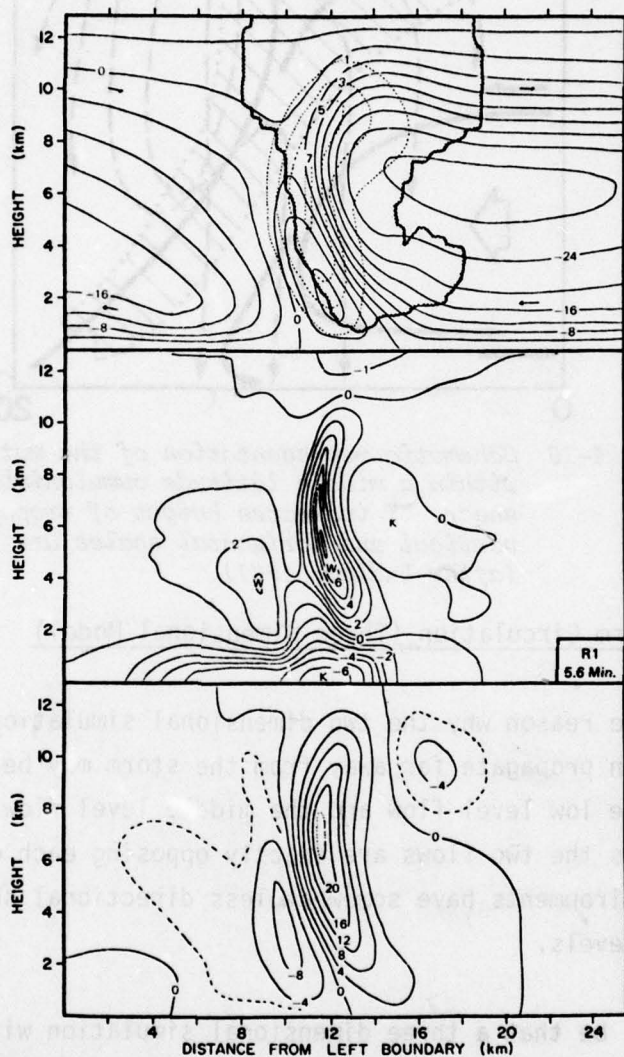


Figure 4-17 Variable fields for Experiment R1 at 5.6 min. Upper: solid lines are streamfunction ($10^3 \text{ kg m}^{-1} \text{ s}^{-1}$); dashed lines rain-water mixing ratio (gm kg^{-1}); scalloped lines cloudwater mixing ratio outline; middle: temperature anomaly ($^{\circ}\text{K}$); lower: vertical wind speed (m s^{-1}).

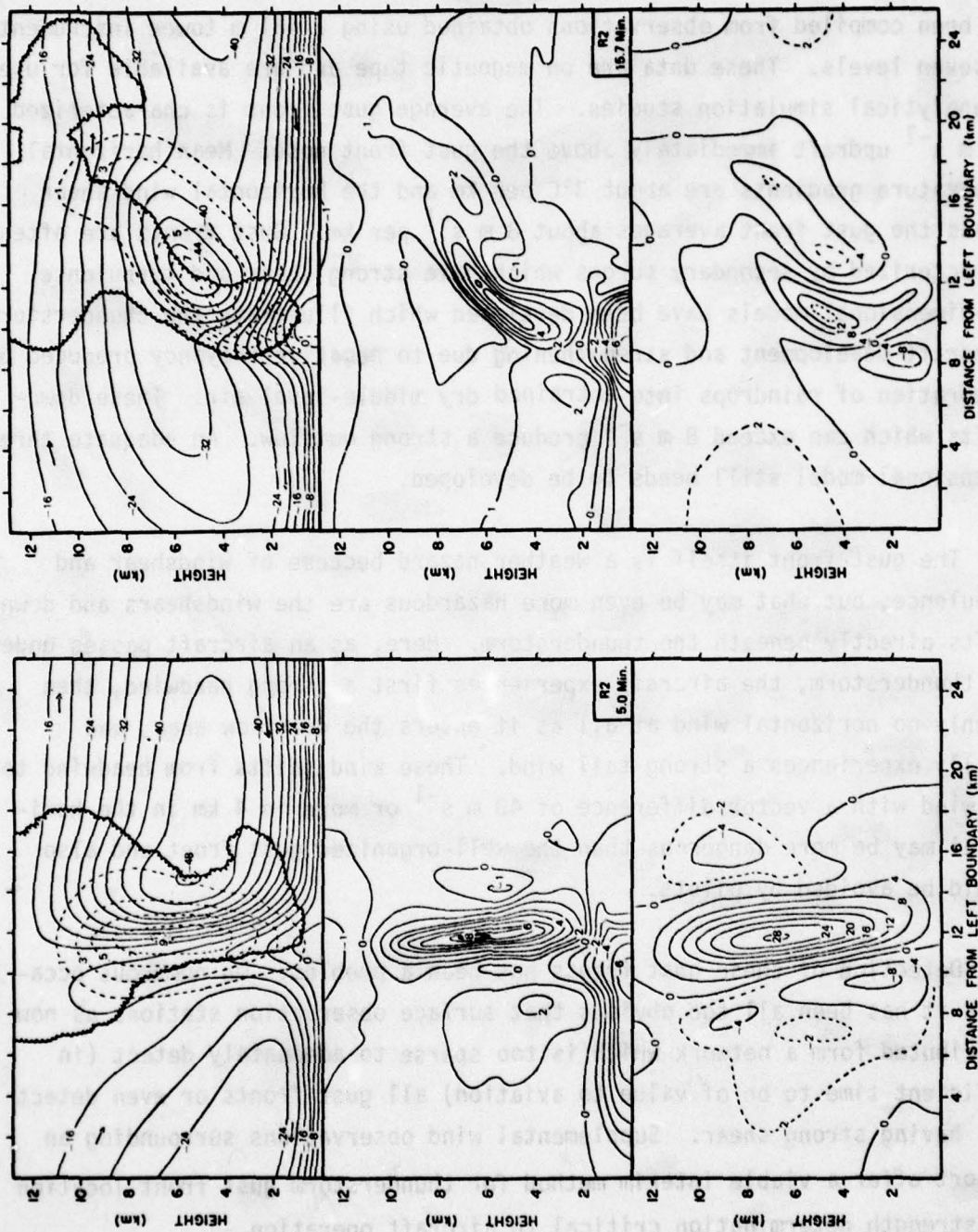


Figure 4-18 As in Figure 4-17 except for R2 at 5.0 min and 15.7 min. Abscissa is distance (km) from left boundary.

5.0 Summary

A large data bank for low level wind shears associated with gust fronts has been compiled from observations obtained using a 461 m tower instrumented at seven levels. These data are on magnetic tape and are available for use in analytical simulation studies. The average gust front is characterized by a 3 m s^{-1} updraft immediately above the gust front nose. Mean horizontal temperature gradients are about 3°C per km and the horizontal wind shear across the gust front averages about 8 m s^{-1} per km. Gust fronts are often characterized by secondary surges which have strong shear and turbulence. Two-dimensional models have been developed which illustrate the thunderstorm downdraft development and strengthening due to negative buoyancy produced by evaporation of raindrops into entrained dry middle-level air. These downdrafts which can exceed 8 m s^{-1} produce a strong outflow. An adequate three-dimensional model still needs to be developed.

The gust front itself is a weather hazard because of windshear and turbulence, but what may be even more hazardous are the windshears and downdrafts directly beneath the thunderstorm. Here, as an aircraft passes under the thunderstorm, the aircraft experiences first a strong headwind, then roughly no horizontal wind at all as it enters the downflow area, and finally experiences a strong tail wind. These wind shifts from headwind to tailwind with a vector difference of 40 m s^{-1} or more in 4 km in the horizontal may be more dangerous than the well-organized gust front and also should be avoided by pilots.

Detection of these gust fronts has been a problem. On numerous occasions it has been all too obvious that surface observation stations as now distributed form a network which is too sparse to adequately detect (in sufficient time to be of value to aviation) all gust fronts or even detect ones having strong shear. Supplemental wind observations surrounding an airport offer a viable interim method for thunderstorm gust front location and strength determination critical to aircraft operation.

Remote detection by satellite is not reliable due to (1) cirrus and other high and middle level clouds which often obscure thunderstorm bases and that volume of space which may contain the gust front; (2) inability of weather satellite to detect "optically clear" gust fronts or those fronts which contain entrained dust particles too small or in insufficient numbers to be resolved by satellite and (3) lack of resolution in the infrared channels used during the night time. These factors, plus the limited observation frequency now available or planned, severely impact satellite usage in gust front detection. The satellite does provide another means besides radar for thunderstorm area determination.

Since a number of gust fronts are in optically clear air, they are most often not observed when conventional weather radar is used. The radar will indicate precipitation intensity but gives no indication of the presence or absence of a gust front. Doppler radar [Goff, et al., 1977] can detect these gust fronts and provides the most promising observation tool.

6.0 Conclusion and Recommendation

Gust fronts and associated thunderstorms are hazardous to aircraft operation. These fronts are extremely variable as to location and strength and are difficult to forecast even though a general life cycle is present consisting of (1) initial downdraft turning into an outward moving cold air mass closely centered near the downdraft to (2) an interface possibly more than ten miles in advance of the storm before dissipating. While low clouds and dust occasionally mark the leading edge of the outflow, usually the gust front is optically invisible and thus rarely detected by conventional weather radar or satellite observation.

Due to the character of gust fronts, surface observations will detect the phenomena and adequate spacing of wind observations in the vicinity of an airport can provide an interim solution. For longer range detection required in air traffic control, microwave Doppler radar offers the highest potential and this option should be actively pursued.

Development of an acceptable forecast procedure appears to be some time off. While simplified techniques can provide an estimate of the maximum intensity based on environmental winds and temperature, they are not adequate for determining which thunderstorms have gust fronts nor where gust fronts are in relationship to the thunderstorm. Therefore observation and tracking of the gust front appears to be the best short range "forecast" option.

It is recommended that continued emphasis and major support be placed on development of both ground and airborne sensors which will alert the pilot and controller to wind shears. Modeling efforts should continue with the realization that it may be some time before an adequate forecasting procedure is developed.

APPENDIX A

Gust Front Cases, 1977

<u>CASE</u>	<u>DATE</u>	<u>TIME (CST)</u>
A	5 May	1807
B	13 May	1346
C	16 May	2154
D	19 May	1556
E	26 May	2138
F	28 May	1035
G	31 May	0746
H	12 Jun	1513
I	28 Jun	1704

Cold Front Cases

J	10 Dec 1976	1021
K	28 Jan 1977	0311

FIGURE LEGEND

Left Pages:

Time-height sections of streamline analysis and vertical velocity (m s^{-1}), potential temperature ($^{\circ}\text{K}$), horizontal wind speed component parallel to the gust front (m s^{-1}) and wind speed component normal and relative to the gust front (m s^{-1}). Each objective analysis is 450 m thick; time increases from right to left. Outflow is moving from left to right. Time-to-space converted 1 km distance is indicated in the upper right. Rainfall and pressure change traces are shown at the bottom of figures when necessary.

Right Pages:

WSR-57 surveillance radar display with echo contouring at 0° elevation. Radar contours are at approximately 10 dBZ intervals. Range marks (circles) are at 40 km intervals. Time clock (CST) is in the upper right. The KTVY-TV tower is located at 358° and 38 km.

Remarks consist of information taken from Storm Data (U.S. Department of Commerce) and personal observations.

1 KM

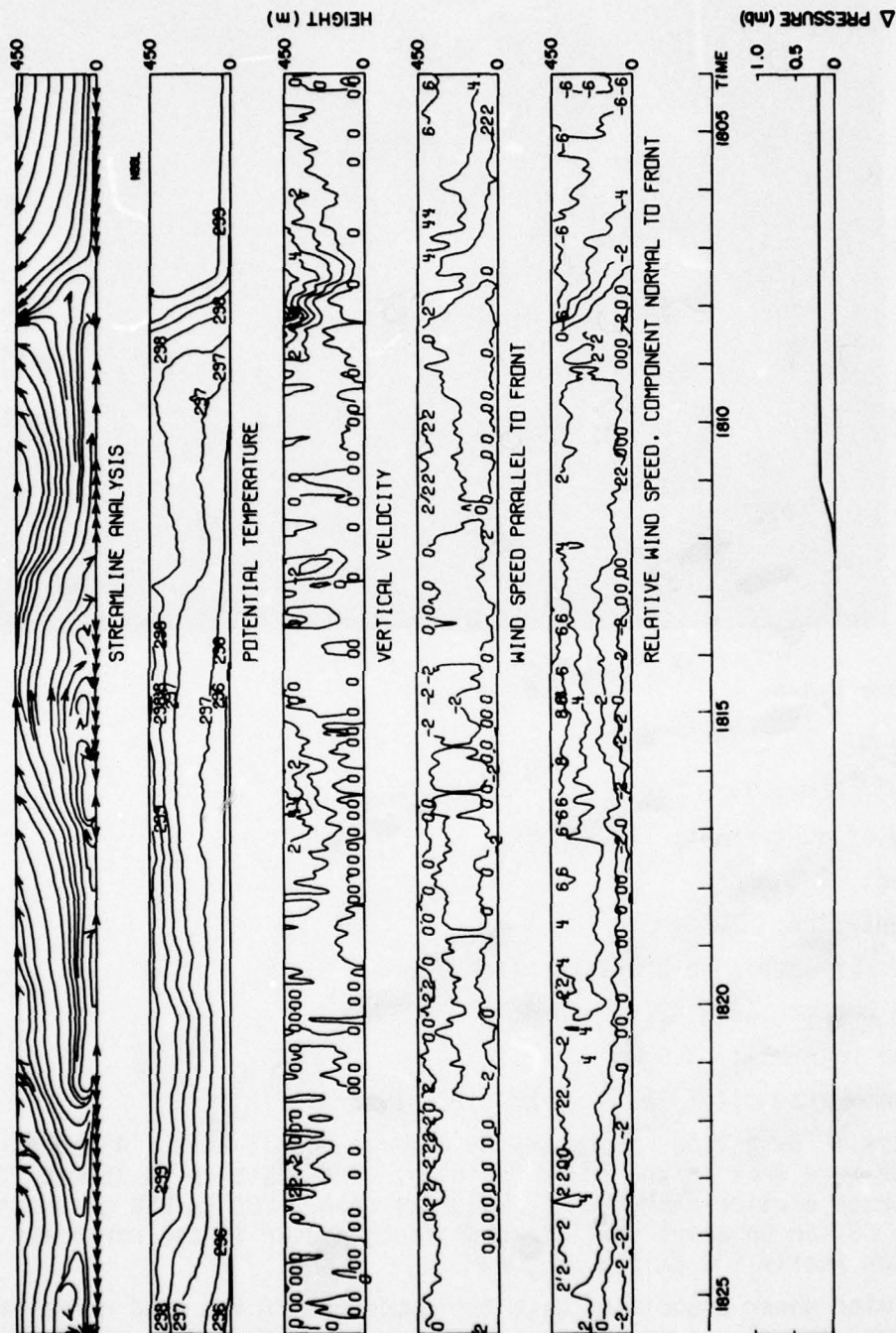


Figure A-A-1.

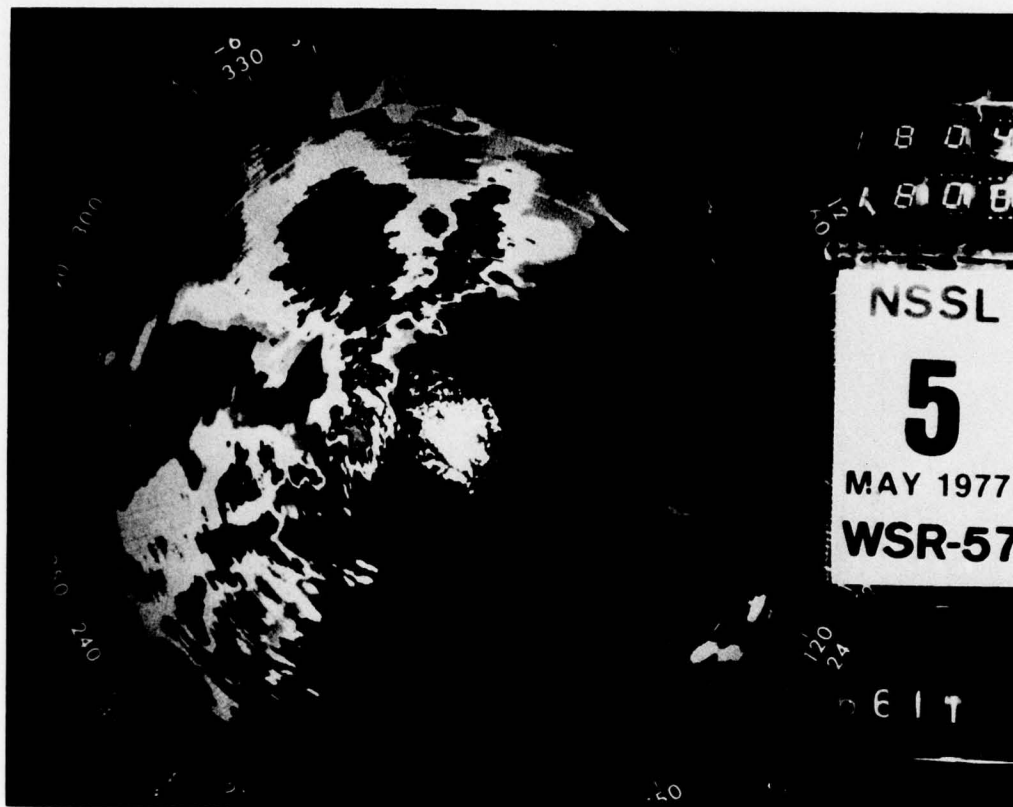


Figure A-A-2

Case A:

Date: 5 May 77

Time of gust front: 1807 CST

Speed: 6.0 m s^{-1}

Orientation: 20°

Pressure jump: no pressure rise

Rain began: 1850 CST ended: 2239 CST

Total rainfall: 8.9 mm

Maximum intensity: 23.9 mm/hr 1921-1929 CST

Remarks: Gust front accompanying a large squall line. Although gust frontal winds were weak in the tower vicinity, wind gusts up to 35 m s^{-1} had been reported earlier near Mangum, Oklahoma (about 200 km WSW of the tower). At 1931 CST an apparent small tornado touched down in the northeast part of Duncan nearly 130 km SSW of tower.

The wind shear associated with the component of the wind normal to the front is weak as well as the temperature discontinuity across the front. Of interest, though, is the strong updraft (greater than 8 m s^{-1} in the top tower layer) prior to frontal passage.

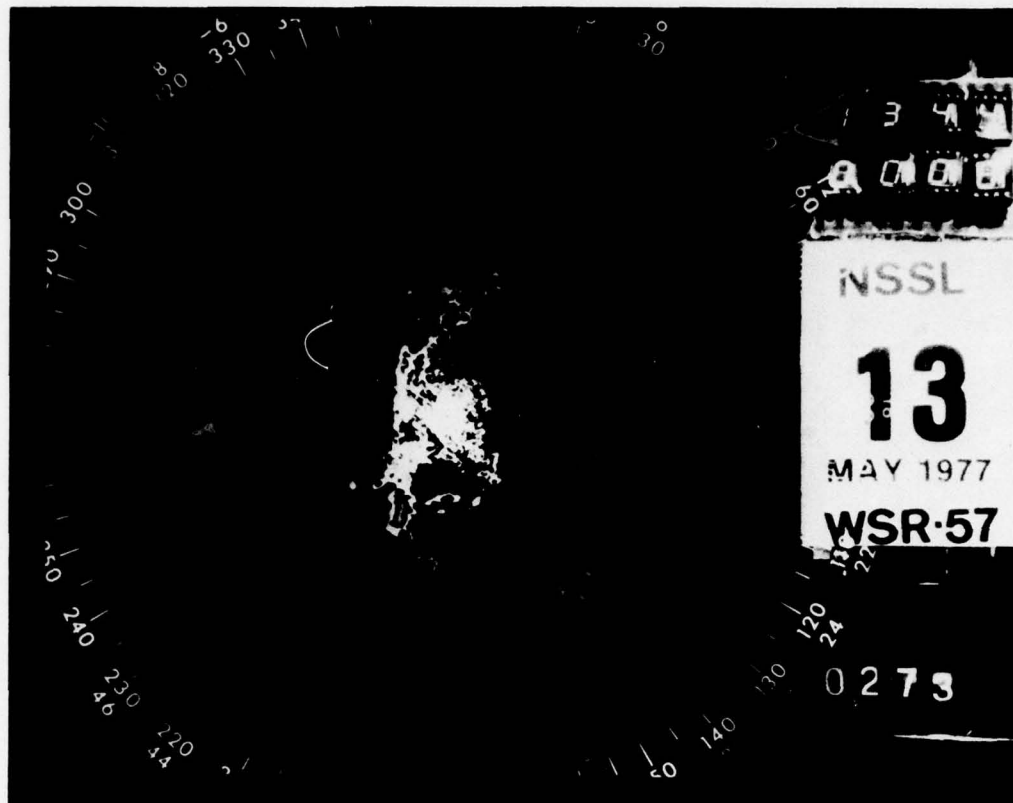


Figure A-B-2

Case B:

Date: 13 May 77

Time of gust front: 1346 CST

Speed: 8.3 m s^{-1}

Orientation: 340°

Pressure jump: no pressure rise

Rain began: 1430 CST **ended:** 1451 CST

Total rainfall: 1.1 mm

Maximum intensity: 2.7 mm/hr 1430-1451 CST

Remarks: Weak outflow accompanying a small line of thunderstorms. Wind shear and temperature discontinuity are not strong across the frontal boundary but an updraft in excess of 4 m s^{-1} occurs just ahead of the front. The strongest shear in the wind component normal to the front began at 1402 CST. A second drop in temperature as well as an increase in upward vertical velocity occurred at this time showing evidence of a secondary surge. No severe weather was associated with this line of storms.

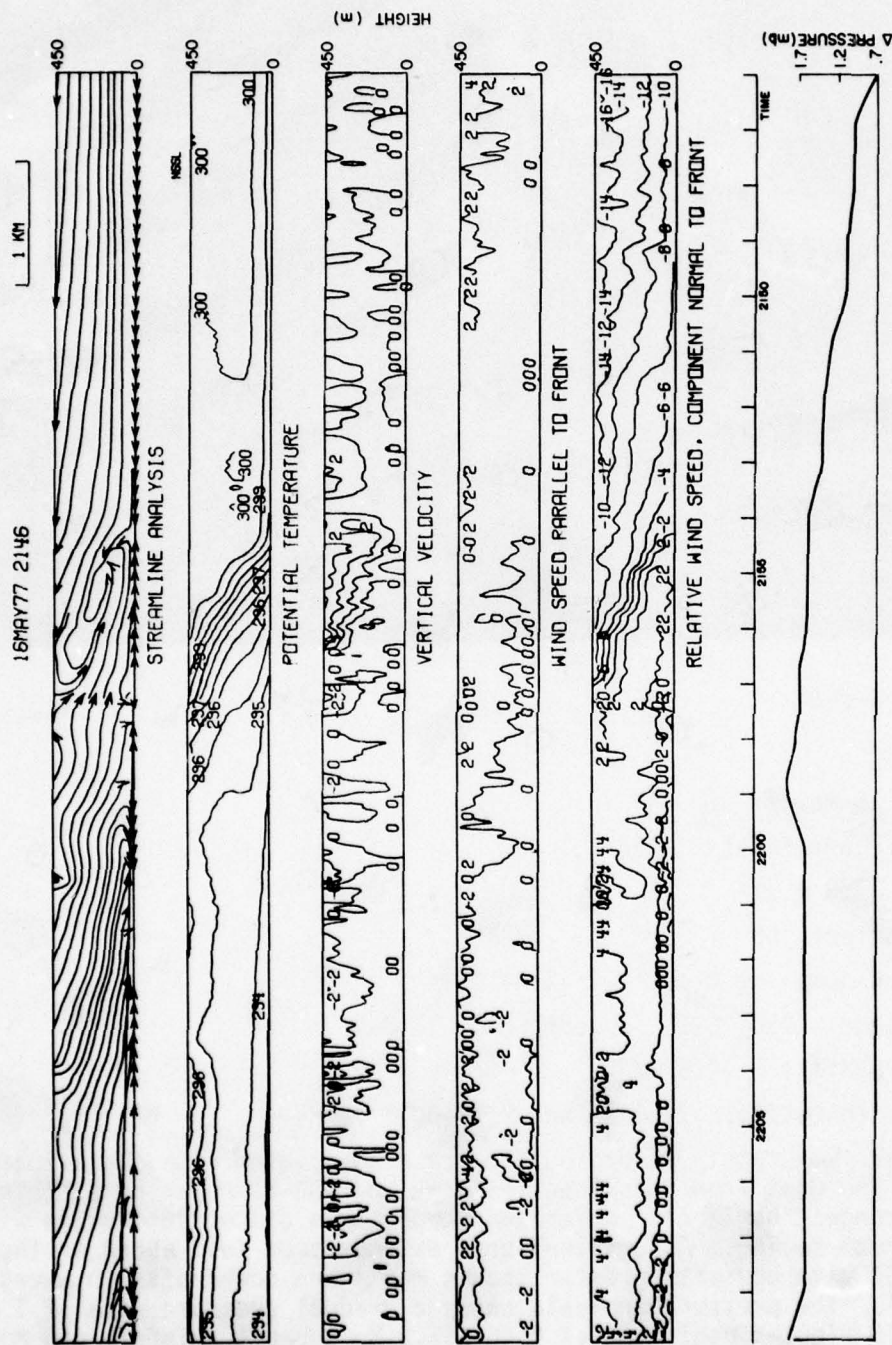


Figure A-C-1.

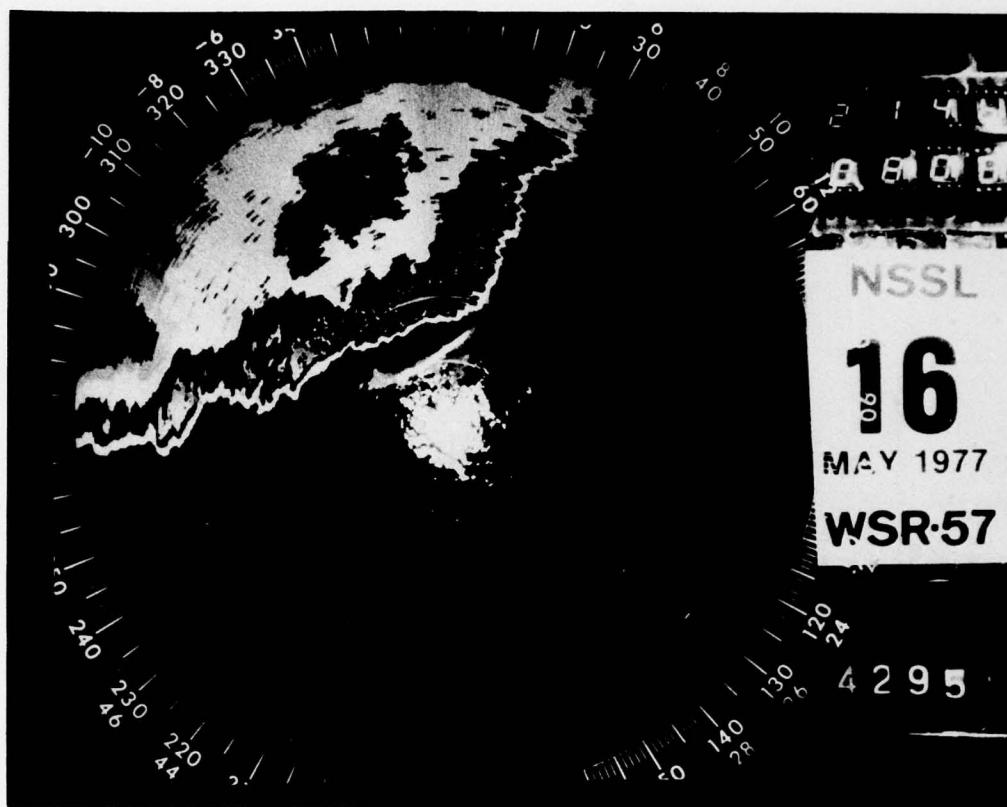


Figure A-C-2

Case C:

Date: 16 May 77

Time of gust front: 2154 CST

Speed: 7.8 m s^{-1}

Orientation: 65°

Pressure jump: 1.8 mb 2115-2159 CST

Rain began: 2347 CST **ended:** 0130 17 May

Total rainfall: 14.5 mm

Maximum intensity: 24.8 mm/hr 2347-0017 17 May

Remarks: Moderately strong outflow case associated with a dissipating squall line. The gust front was identified on the WSR-57 radar by a "thin line." The strongest horizontal shear and temperature discontinuity are within the gust front region. A turbulent zone extends from just ahead of the front to 2157 CST with updrafts greater than 4 m s^{-1} and downdrafts in excess of 3 m s^{-1} . The pressure analysis shows a gradual pressure rise of 1 mb in about 10 minutes beginning at 2146 CST. Measurable rainfall did not begin at the tower until 2347 CST about two hours after the wind shift.

This line had produced tornadoes earlier in extreme western Oklahoma but no severe weather in the vicinity of the tower was reported.

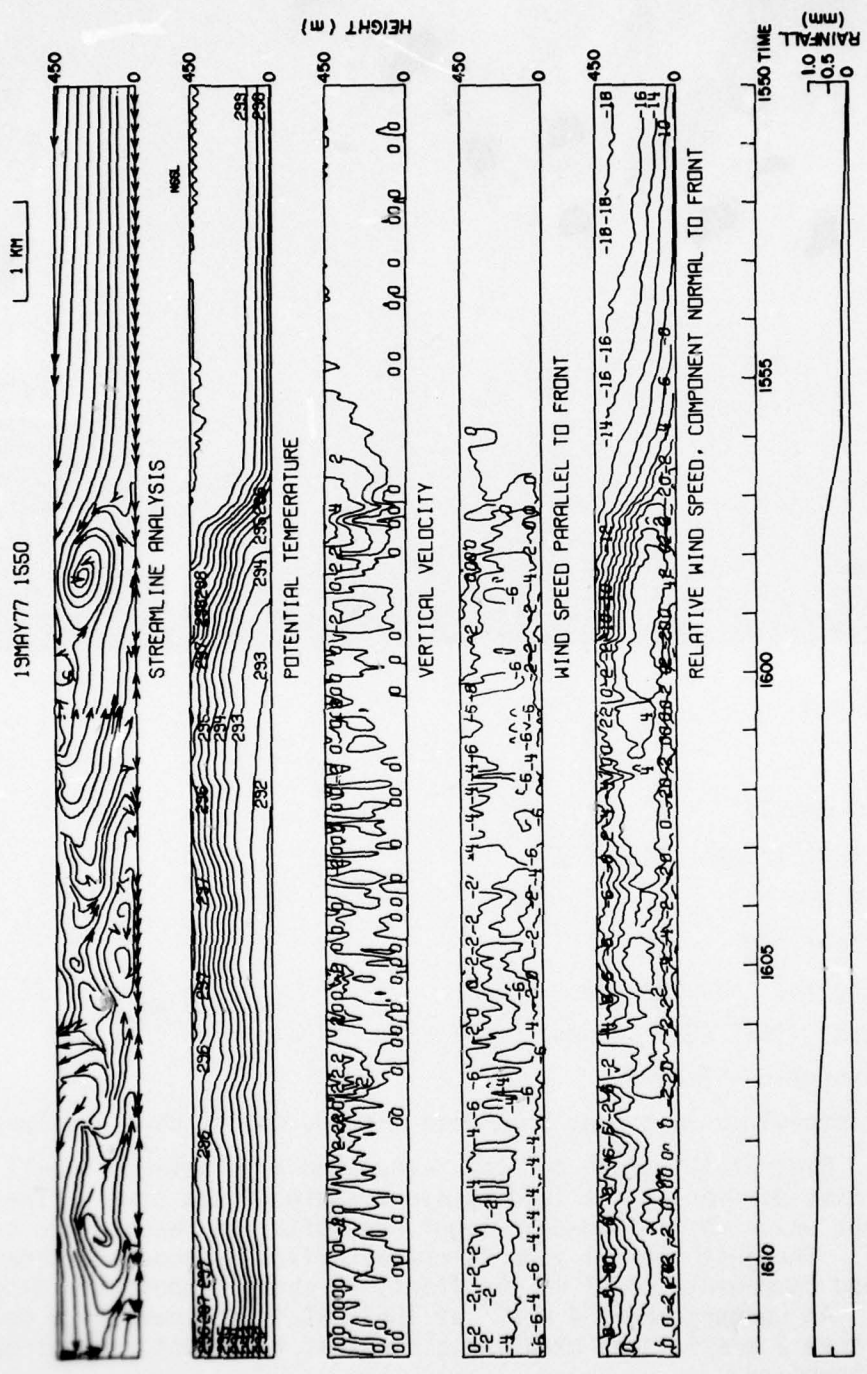


Figure A-D-1.

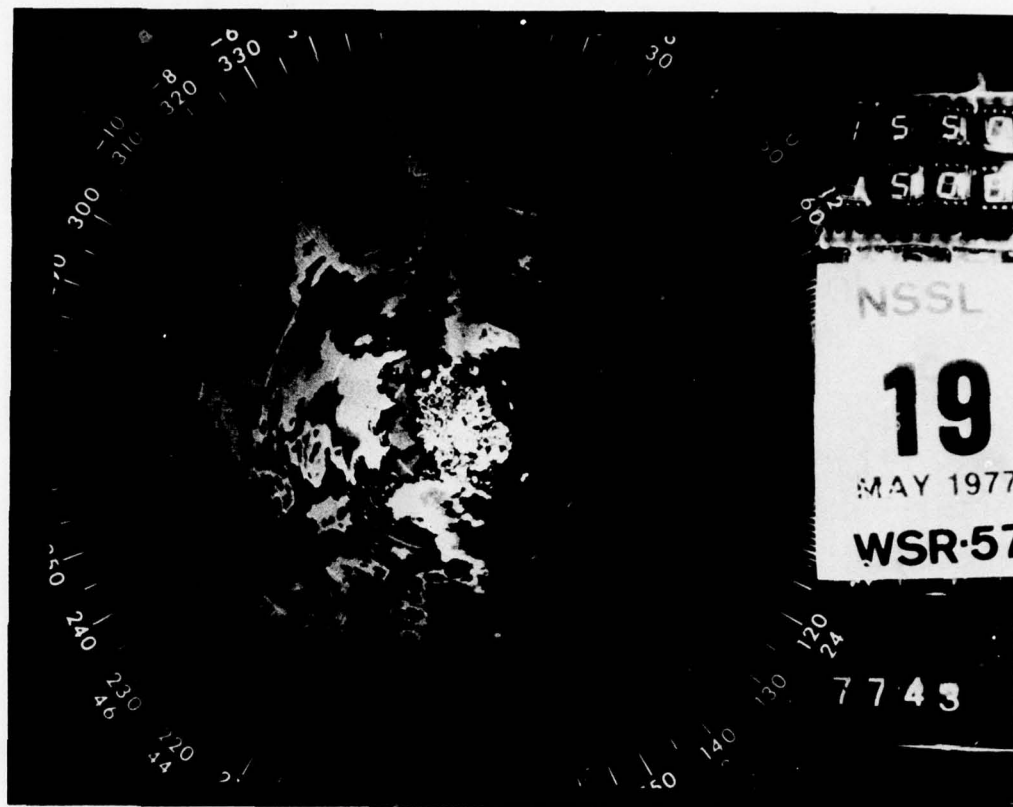


Figure A-D-2

Case D:

Date: 19 May 77

Time of gust front: 1556 CST

Speed: 9.8 m s^{-1}

Orientation: 30°

Pressure jump: no pressure rise

Rain began: 1551 CST ended: 2150 CST

Total rainfall: 52.0 mm

Maximum intensity: unknown, some data missing due to power failure

Remarks: Moderately strong outflow associated with a large squall line. The most intense portion of the line remained south of the tower. The related gust front which was imbedded in light precipitation reached the tower at 1556 CST. The gust frontal zone is characterized by moderate shear in the wind speed component normal to the front. A sharp temperature drop is also evident. An updraft above 4 m s^{-1} at 1557 CST is followed by a downdraft greater than 2 m s^{-1} , thus creating a somewhat turbulent zone along the frontal boundary.

A short narrow tornado occurred north of Foster (112 km S of tower) at 1630 CST. One tornado took place at 1723 CST near White Bead (94 km SSE of tower) and one reported close to Paoli (88 km SSE of tower) at 1736.

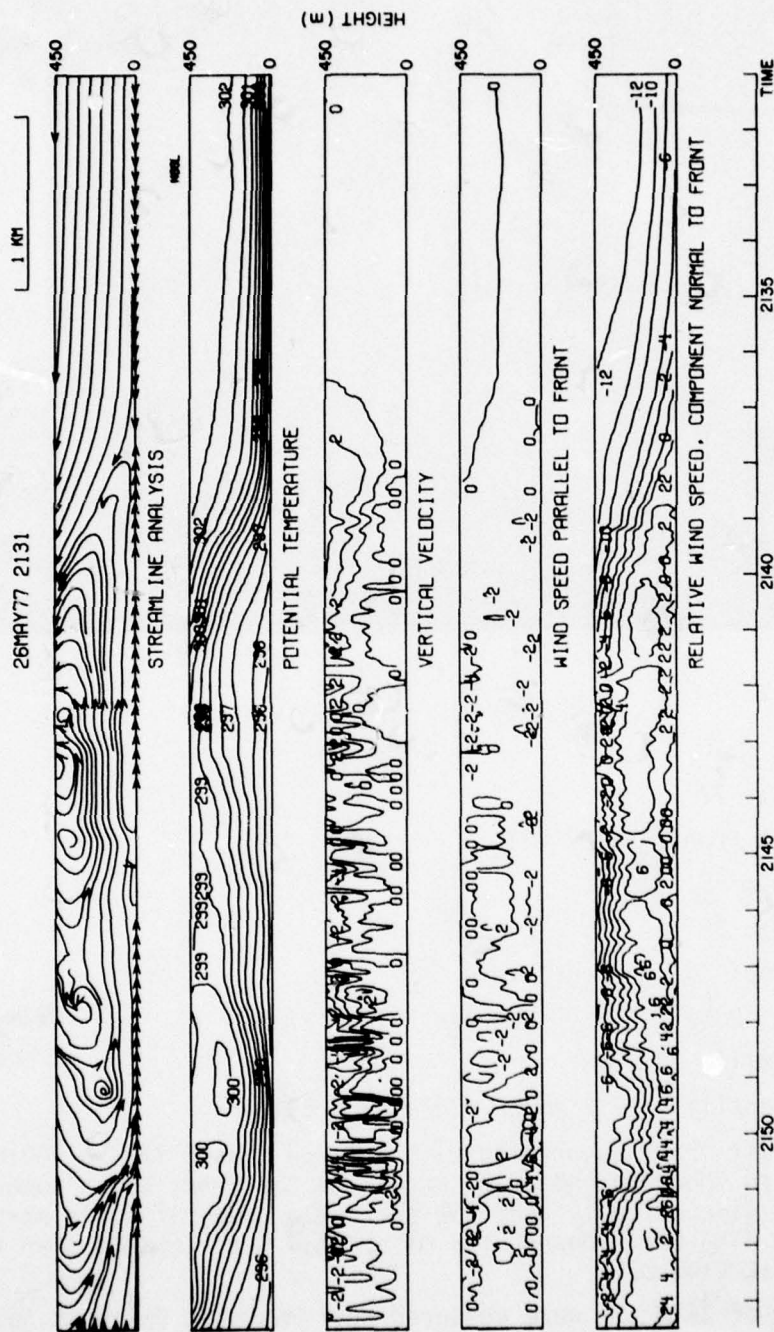


Figure A-E-1.



Figure A-E-2

Case E:

Date: 26 May 77

Time of gust front: 2138 CST

Speed: 5.6 m s^{-1}

Orientation: 38°

Pressure jump: no pressure rise

Rain began: 2309 26 May ended: 0128 27 May

Total rainfall: 28.9 mm

Maximum intensity: 52.2 mm/hr 2309-2332 CST

Remarks: Gust front associated with a large squall line. There is moderate wind shear in the wind component normal to the front but a somewhat weak temperature discontinuity near the surface. Downdrafts are persistent from the 2148 to 2153 CST. Downdrafts of about 4 m s^{-1} extend down to 200 m above the ground at 2149 CST.

Wind speeds of 35 m s^{-1} were measured near Mustang, Oklahoma, at 2135 CST.

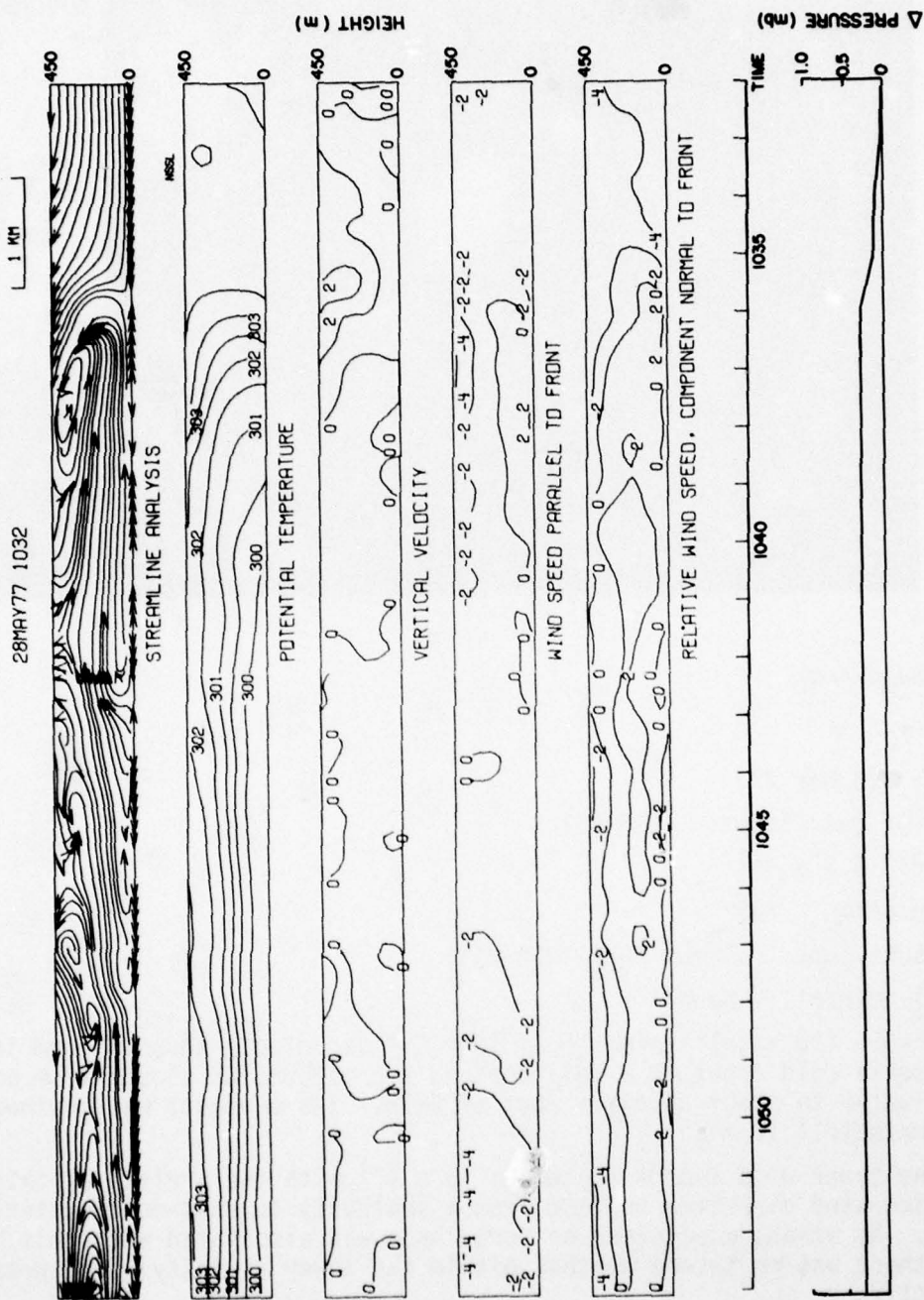


Figure A-F-1.

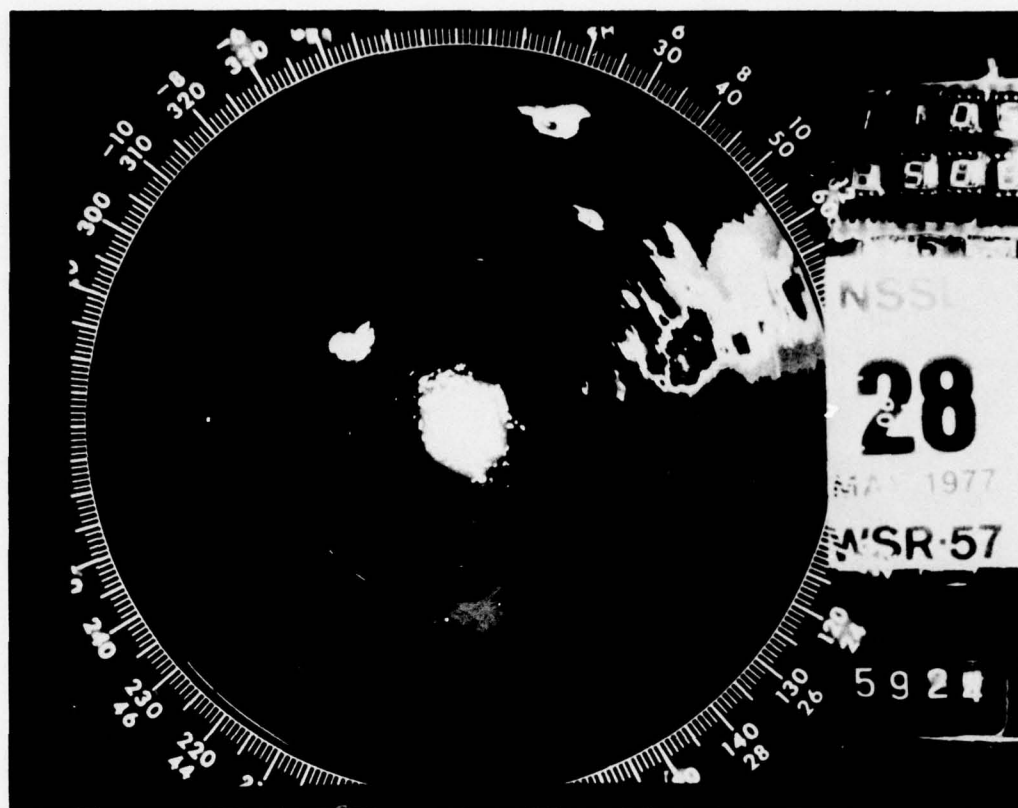


Figure A-F-2

Case F:

Date: 28 May 77

Time of gust front: 1035 CST

Speed: 8.7 m s^{-1}

Orientation: 155°

Pressure jump: .3 mb 1033-1036 CST

Total Rainfall: None

Remarks: The satellite photo at 1000 CST depicted a thunderstorm induced mesoscale cold front as a well-defined arc of cumulus clouds from south of Stillwater to about 50 miles west of Enid. Its movement was southward at approximately 10 m s^{-1} .

At the tower wind speeds gusted to 13 m s^{-1} with the arrival of this boundary and the wind direction shifted from a southerly to east-northeasterly direction. No strong wind shear or turbulence was associated with this boundary and there was no severe weather within the tower vicinity. The pressure rose slightly.

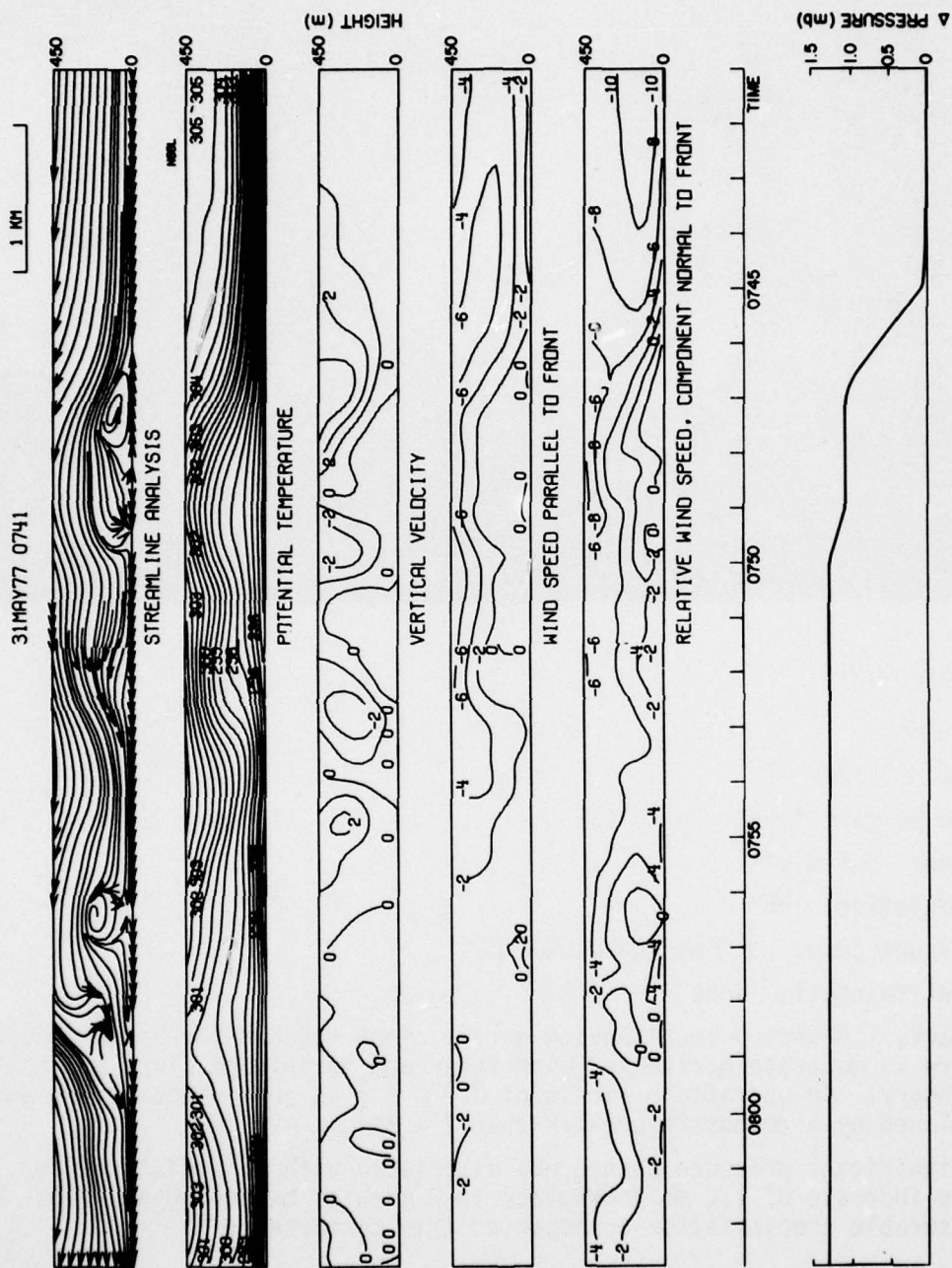


Figure A-G-1.

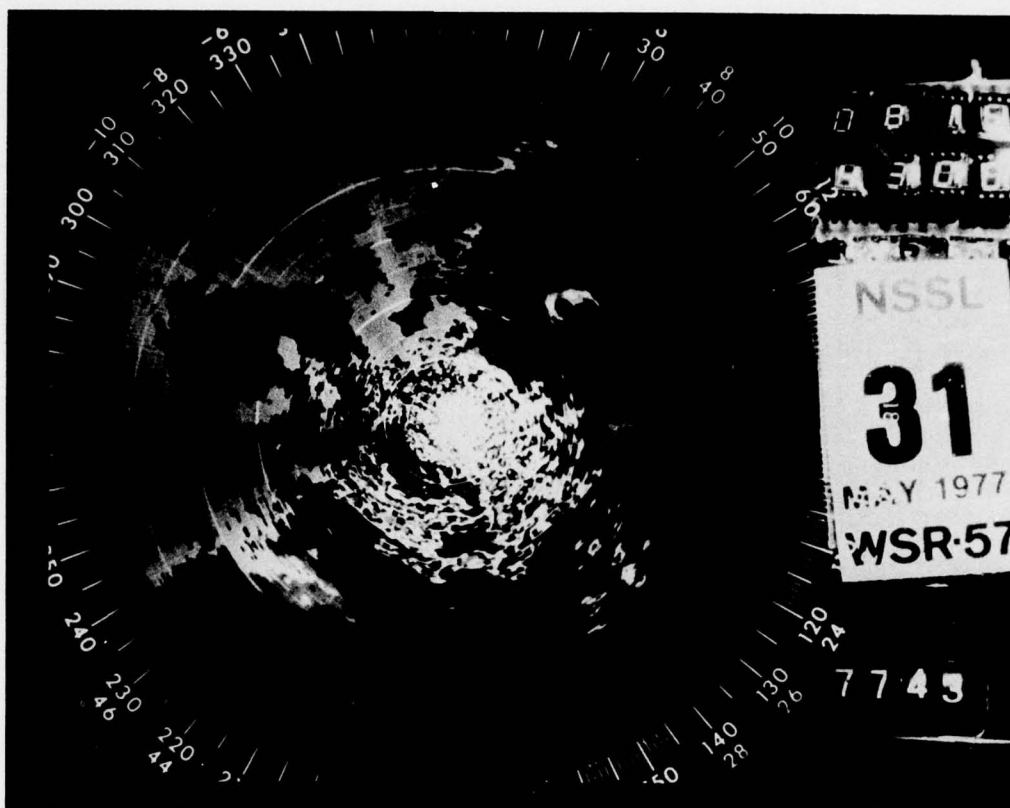


Figure A-G-2

Case G:

Date: 31 May 77

Time of gust front: 0746 CST

Speed: 6.5 m s^{-1}

Orientation: 85°

Pressure jump: 1.3 mb 0744-0750 CST

Total Rainfall: None

Remarks: Boundary accompanying a roll cloud reached the tower at 0746 CST. There is moderate horizontal wind shear and turbulence along and behind this boundary. An updraft in excess of 3.0 m s^{-1} is just ahead of the gust front followed by a downdraft greater than 2 m s^{-1} .

A significant pressure change was associated with this disturbance. A pressure increase of 1.0 mb took place in 3 minutes beginning at 0744. No measurable precipitation accompanied this disturbance.

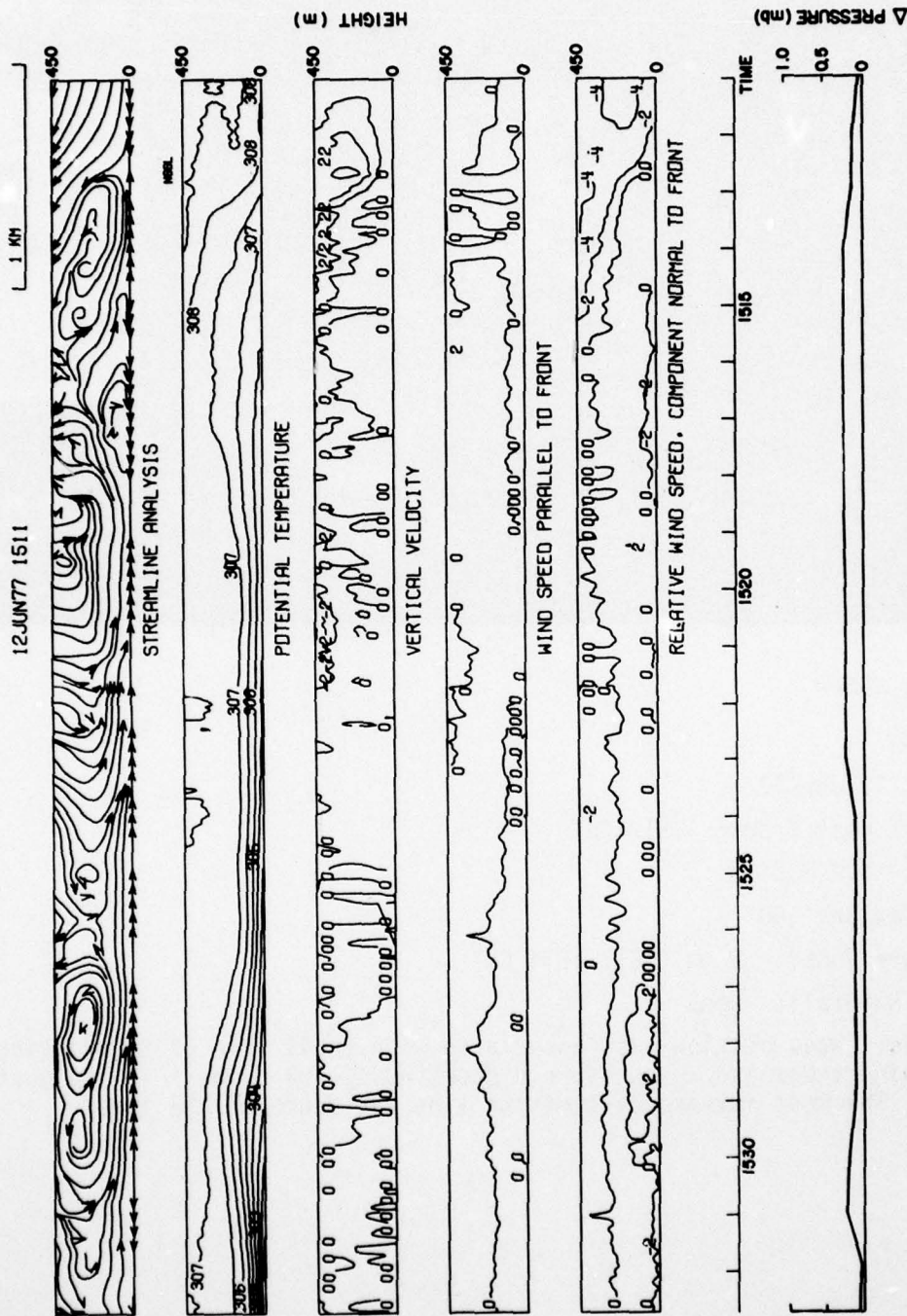


Figure A-H-1.



Figure A-H-2

Case H:

Date: 12 Jun 77

Time of gust front: 1513 CST

Speed: 4.2 m s^{-1}

Orientation: 60°

Pressure jump: .2 mb 1511-1514 CST

Total Rainfall: None

Remarks: Weak outflow case associated with small line of thunderstorms. Weak wind shear and temperature discontinuity are evident in the gust frontal zone. The most intense part of the line was south of the tower.

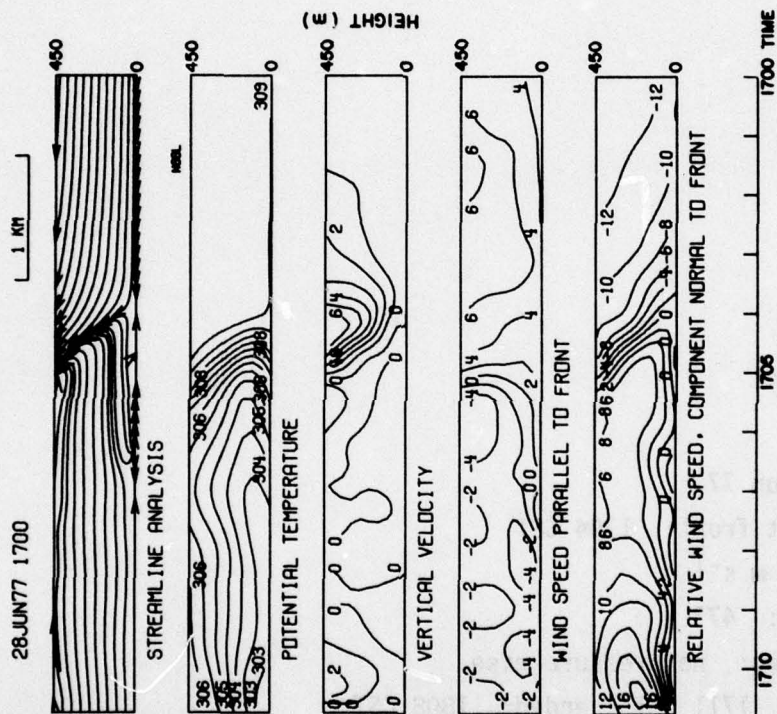


Figure A-I-1:

(WSR-57 photo unavailable)

Figure A-I-2

Case I:

Date: 28 Jun 77

Time of gust front: 1704 CST

Speed: 7.8 m s^{-1}

Orientation: 47°

Pressure jump: no pressure rise

Rain began: 1711 CST ended: 1808 CST

Total rainfall: 5.1 mm

Maximum Intensity: unknown, data loss due to power failure

(See additional remarks in text.)

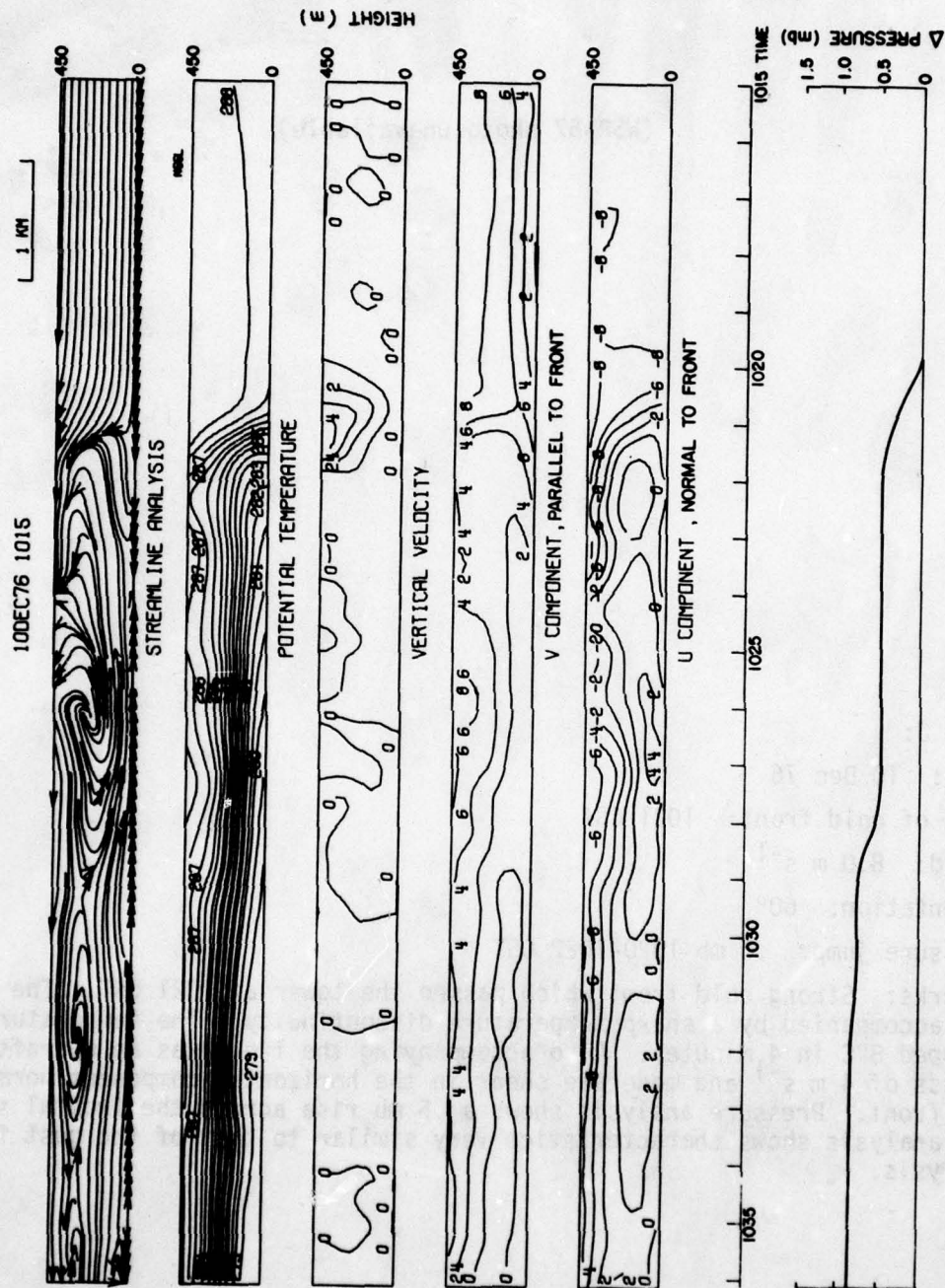


Figure A-J-1.

(WSR-57 photo unavailable)

Case J:

Date: 10 Dec 76

Time of cold front: 1021 CST

Speed: 8.0 m s^{-1}

Orientation: 60°

Pressure jump: .5 mb 1020-1022 CST

Remarks: Strong cold front which passed the tower at 1021 CST. The front was accompanied by a sharp temperature discontinuity. The temperature dropped 8°C in 4 minutes. Also accompanying the front was an updraft in excess of 4 m s^{-1} and moderate shear in the horizontal component normal to the front. Pressure analysis shows a .5 mb rise across the frontal surface. The analysis shows characteristics very similar to that of the gust front analysis.

AD-A068 425

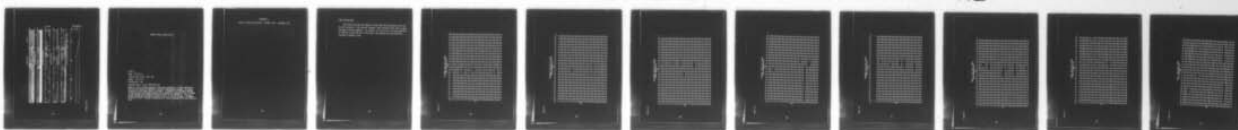
NATIONAL SEVERE STORMS LAB NORMAN OKLA
THUNDERSTORM GUST FONTS--OBSERVATIONS AND MODELING.(U)

F/G 4/2

UNCLASSIFIED

DEC 78 J T LEE, J STOKES, Y SASAKI, T BAXTER DOT-FA76WAI-622
FAA/RD-78/145 NL

2 OF 2
ADA
068425



END
DATE
FILMED

6 79
DDC

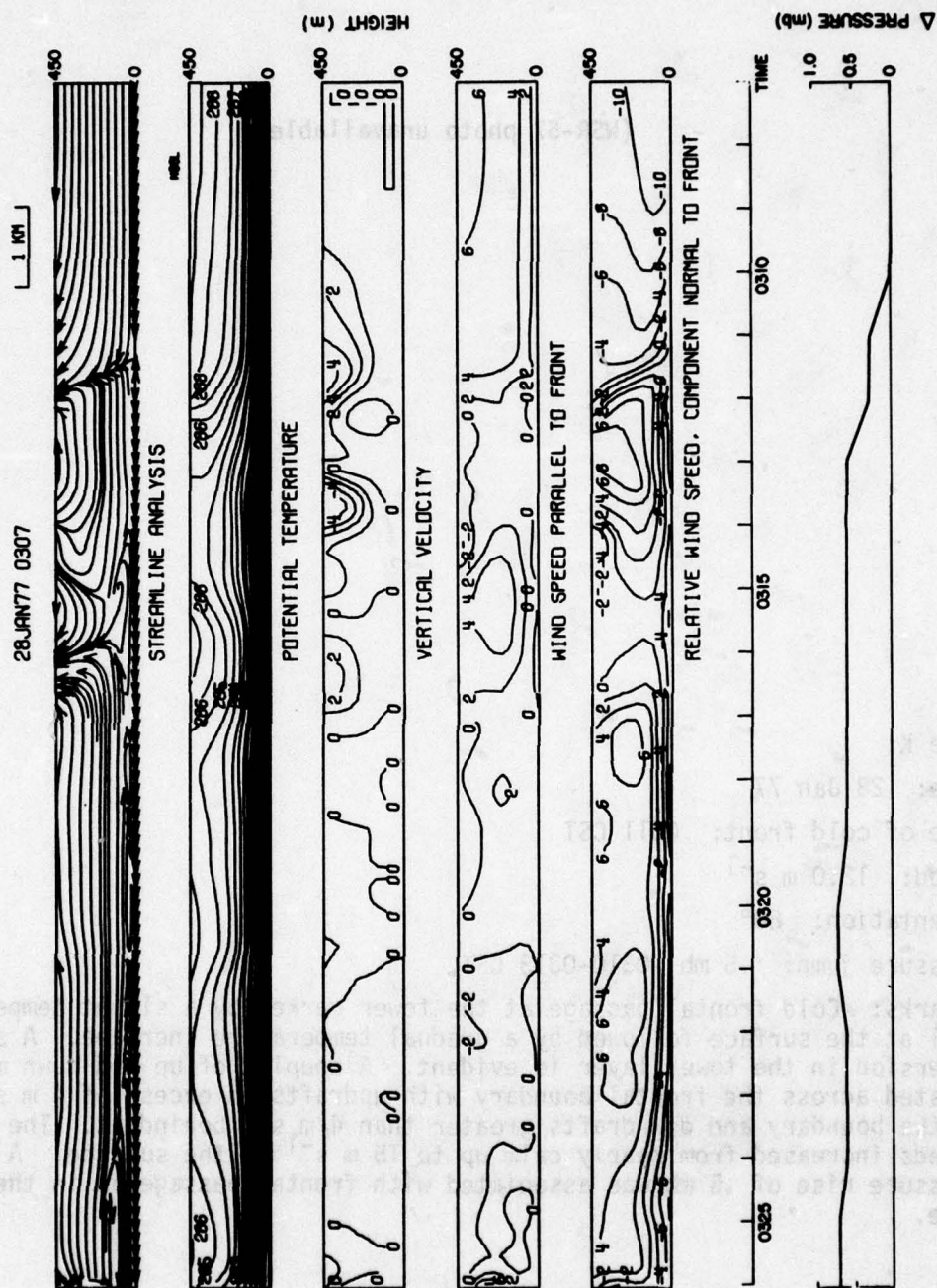


Figure A-K-1.

(WSR-57 photo unavailable)

Case K:

Date: 28 Jan 77

Time of cold front: 0311 CST

Speed: 12.0 m s^{-1}

Orientation: 80°

Pressure jump: .5 mb 0310-0313 CST

Remarks: Cold frontal passage at the tower marked by a slight temperature fall at the surface followed by a gradual temperature increase. A strong inversion in the tower layer is evident. A couplet of up and down motions existed across the frontal boundary with updrafts in excess of 4 m s^{-1} ahead of the boundary and downdrafts greater than 4 m s^{-1} behind it. The wind speeds increased from nearly calm up to 15 m s^{-1} at the surface. A gradual pressure rise of .5 mb was associated with frontal passage as in the 10 Dec 76 case.

APPENDIX B

Index of Tower Observations: October 1976 - September 1977

Each table describes the number of tower observations made per hour per day for one month. Time (Central Standard Time) increases from left to right and dates increase downward. For example, in Table B1 for the hour beginning at 1800 CST on the 18th day of the month, 382 observations were made and recorded on magnetic tape.

TABLE DESCRIPTION

Each table describes the number of tower observations made per hour per day for one month. Time (Central Standard Time) increases from left to right and dates increase downward. For example, in Table B1 for the hour beginning at 1800 CST on the 16th day of the month, 362 observations were made and recorded on magnetic tape.

Table B1.

OCTOBER 1976 KTVY TOWER
NUMBER OF OBSERVATIONS PER HOUR

[illegible]

Table B2.

NOVEMBER 1976 KTVY TOWER
NUMBER OF OBSERVATIONS PER HOUR

[illegible]

DECEMBER 1976 KTVY TOWER
NUMBER OF OBSERVATIONS PER HOUR

89

Table B4.

JANUARY 1977 KTVY TOWER
NUMBER OF OBSERVATIONS PER HOUR

DATE	00	01	02	03	04	05	06	07	08	09	10	11	12	13	14	15	16	17	18	19	20	21	22	23
1	30	30	30	30	30	30	30	30	30	30	30	30	30	30	30	30	30	30	30	30	30	30	30	
2	30	30	30	30	30	30	30	30	30	30	30	30	30	30	30	30	30	30	30	30	30	30	30	
3	30	30	30	30	30	30	30	30	30	30	30	30	30	30	30	30	30	30	30	30	30	30	30	
4	30	30	30	30	30	30	30	30	30	30	30	30	30	30	30	30	30	30	30	30	30	30	30	
5	30	30	30	30	30	30	30	30	30	30	30	30	30	30	30	30	30	30	30	30	30	30	30	
6	30	30	30	30	30	30	30	30	30	30	30	30	30	30	30	30	30	30	30	30	30	30	30	
7	30	30	30	30	30	30	30	30	30	30	30	30	30	30	30	30	30	30	30	30	30	30	30	
8	30	30	30	30	30	30	30	30	30	30	30	30	30	30	30	30	30	30	30	30	30	30	30	
9	30	30	30	30	30	30	30	30	30	30	30	30	30	30	30	30	30	30	30	30	30	30	30	
10	30	30	30	30	30	30	30	30	30	30	30	30	30	30	30	30	30	30	30	30	30	30	30	
11	30	30	30	30	30	30	30	30	30	30	30	30	30	30	30	30	30	30	30	30	30	30	30	
12	30	30	30	30	30	30	30	30	30	30	30	30	30	30	30	30	30	30	30	30	30	30	30	
13	30	30	30	30	30	30	30	30	30	30	30	30	30	30	30	30	30	30	30	30	30	30	30	
14	30	30	30	30	30	30	30	30	30	30	30	30	30	30	30	30	30	30	30	30	30	30	30	
15	30	30	30	30	30	30	30	30	30	30	30	30	30	30	30	30	30	30	30	30	30	30	30	
16	30	30	30	30	30	30	30	30	30	30	30	30	30	30	30	30	30	30	30	30	30	30	30	
17	30	30	30	30	30	30	30	30	30	30	30	30	30	30	30	30	30	30	30	30	30	30	30	
18	30	30	30	30	30	30	30	30	30	30	30	30	30	30	30	30	30	30	30	30	30	30	30	
19	30	30	30	30	30	30	30	30	30	30	30	30	30	30	30	30	30	30	30	30	30	30	30	
20	30	30	30	30	30	30	30	30	30	30	30	30	30	30	30	30	30	30	30	30	30	30	30	
21	30	30	30	30	30	30	30	30	30	30	30	30	30	30	30	30	30	30	30	30	30	30	30	
22	30	30	30	30	30	30	30	30	30	30	30	30	30	30	30	30	30	30	30	30	30	30	30	
23	30	30	30	30	30	30	30	30	30	30	30	30	30	30	30	30	30	30	30	30	30	30	30	
24	30	30	30	30	30	30	30	30	30	30	30	30	30	30	30	30	30	30	30	30	30	30	30	
25	30	30	30	30	30	30	30	30	30	30	30	30	30	30	30	30	30	30	30	30	30	30	30	
26	30	30	30	30	30	30	30	30	30	30	30	30	30	30	30	30	30	30	30	30	30	30	30	
27	30	30	30	30	30	30	30	30	30	30	30	30	30	30	30	30	30	30	30	30	30	30	30	
28	30	30	30	30	30	30	30	30	30	30	30	30	30	30	30	30	30	30	30	30	30	30	30	
29	30	30	30	30	30	30	30	30	30	30	30	30	30	30	30	30	30	30	30	30	30	30	30	
30	30	30	30	30	30	30	30	30	30	30	30	30	30	30	30	30	30	30	30	30	30	30	30	
31	30	30	30	30	30	30	30	30	30	30	30	30	30	30	30	30	30	30	30	30	30	30	30	

FEBRUARY 1977 KTVY TOWER
NUMBER OF OBSERVATIONS PER HOUR

[illegible]

Table B6.

MARCH 1977 KTVY TOWER
NUMBER OF OBSERVATIONS PER HOUR

	00	01	02	03	04	05	06	07	08	09	10	11	12	13	14	15	16	17	18	19	20	21	22	23
1	302	302	303	302	303	303	302	302	303	302	312	273	302	302	303	303	303	303	303	302	303	303	303	302
2	303	303	302	303	302	303	303	303	302	303	302	303	303	302	303	302	303	301	302	303	302	303	302	303
3	303	302	303	303	303	302	303	302	303	302	303	302	303	303	250	242	303	303	302	302	303	302	303	302
4	303	302	303	303	303	302	303	302	303	302	303	302	303	303	311	302	301	302	302	302	303	302	303	303
5	302	303	303	302	303	303	302	303	303	302	303	302	302	302	303	303	301	303	303	302	303	302	303	303
6	303	303	303	303	302	303	303	303	303	301	303	303	303	302	303	302	303	303	302	302	303	302	302	303
7	302	303	303	302	303	303	302	302	303	302	303	302	302	303	302	13	303	302	303	302	303	303	303	303
8	303	303	303	303	303	302	303	303	302	302	302	302	303	302	303	303	302	302	302	302	303	302	303	303
9	303	303	302	303	303	303	302	302	303	302	302	302	302	302	163	301	303	303	302	303	302	303	303	302
10	303	301	303	301	302	302	303	302	302	302	302	303	301	302	303	302	303	303	303	302	306	303	301	303
11	303	303	303	303	302	302	303	302	303	303	303	302	302	303	331	301	302	302	302	302	302	302	302	302
12	302	302	303	302	302	303	302	302	302	302	303	302	302	302	302	302	302	303	301	302	302	302	303	302
13	302	302	303	303	302	303	302	302	302	302	302	302	302	302	302	302	301	302	301	301	302	302	301	302
14	302	302	303	302	303	302	302	302	302	301	302	301	316	302	301	302	302	301	301	302	301	302	301	302
15	302	302	301	303	302	302	301	301	302	302	102	31	301	302	301	301	302	301	301	302	302	301	302	301
16	302	301	302	302	302	302	302	302	301	302	302	301	302	302	27	302	302	302	302	302	302	302	301	302
17	302	302	301	302	301	302	302	302	302	301	302	301	302	301	302	301	301	302	301	302	301	302	301	302
18	302	302	302	302	302	302	302	301	302	302	302	301	302	302	181	302	301	302	302	301	302	302	301	302
19	302	302	301	302	302	302	302	302	302	302	301	301	301	302	302	301	302	301	302	301	302	301	302	302
20	302	302	301	302	302	302	302	302	302	301	302	301	302	302	301	302	302	301	302	302	301	301	301	301
21	302	301	301	302	301	302	301	302	301	301	302	301	303	301	302	301	301	303	302	301	302	301	301	302
22	301	302	302	301	302	302	302	302	302	302	302	301	302	302	301	302	302	302	302	302	302	301	302	301
23	302	301	302	302	301	302	302	302	302	302	151					153	302	303	301	302	303	301	303	302
24	302	302	302	302	302	302	302	302	302	302	301	302	302	303	302	302	302	302	302	302	302	303	302	302
25	302	301	302	302	303	302	302	302	302	302	302	302	302	191	302	302	302	302	302	301	302	301	303	302
26	302	302	302	302	302	302	302	302	302	302	302	302	302	302	302	302	302	301	302	302	302	302	302	302
27	302	302	302	302	302	302	302	302	302	302	302	302	302	301	302	302	302	302	302	302	302	302	302	302
28	302	302	302	302	302	302	302	302	302	302	302	302	302	302	301	301	301	301	301	301	301	302	301	302
29	302	301	302	302	302	301	302	302	302	302	302	301	302	302	301	302	302	301	302	301	302	302	303	302
30	302	302	303	301	301	303	302	302	302	302	302	301	302	301	295	302	302	301	302	302	302	302	302	302
31	302	302	302	302	302	302	302	302	302	302	302	302	302	301	302	302	302	302	301	302	302	302	302	302

Table B7.

APRIL 1977 KTVY TOWER
NUMBER OF OBSERVATIONS PER HOUR

	00	01	02	03	04	05	06	07	08	09	10	11	12	13	14	15	16	17	18	19	20	21	22	23
1	302	302	361	302	302	302	302	302	302	302	302	302	302	302	302	361	302	302	302	302	302	361	302	302
2	361	302	302	302	302	302	302	302	302	302	302	302	302	302	302	302	302	302	302	302	302	302	302	302
3	302	302	302	302	361	302	302	361	302	302	302	302	302	302	302	361	302	302	302	302	302	302	302	302
4	302	302	361	302	302	302	302	302	302	302	302	361	302	302	302	302	302	302	302	302	302	302	302	302
5	302	302	302	302	302	302	302	302	302	302	302	302	302	302	302	302	302	302	302	302	302	302	302	302
6	302	302	361	302	302	302	302	302	302	302	302	302	302	302	302	302	302	302	302	302	302	302	302	302
7	302	302	302	302	302	302	302	302	302	302	302	302	302	302	302	302	302	302	302	302	302	302	302	302
8	302	302	302	302	302	302	302	302	302	302	302	302	302	302	302	302	302	302	302	302	302	302	302	302
9	302	302	302	302	302	302	302	302	302	302	302	302	302	302	302	302	302	302	302	302	302	302	302	302
10	361	302	302	302	302	302	302	302	302	302	302	302	302	302	302	302	302	302	302	302	302	302	302	302
11	302	302	302	302	302	302	302	302	302	302	302	302	302	302	302	302	302	302	302	302	302	302	302	302
12	361	302	302	302	302	302	302	302	302	302	302	302	302	302	302	302	302	302	302	302	302	302	302	302
13	302	302	361	302	302	302	302	302	302	302	302	302	302	302	302	302	302	302	302	302	302	302	302	302
14	302	302	302	302	302	302	302	302	302	302	302	302	302	302	302	302	302	302	302	302	302	302	302	302
15	302	302	302	302	302	302	302	302	302	302	302	302	302	302	302	302	302	302	302	302	302	302	302	302
16	361	302	302	302	302	302	302	302	302	302	302	302	302	302	302	302	302	302	302	302	302	302	302	302
17	302	361	302	302	302	302	302	302	302	302	302	302	302	302	302	302	302	302	302	302	302	302	302	302
18	302	302	302	302	302	302	302	302	302	302	302	302	302	302	302	302	302	302	302	302	302	302	302	302
19	361	302	302	302	302	302	302	302	302	302	302	302	302	302	302	302	302	302	302	302	302	302	302	302
20	302	302	302																					

MAY 1977 KTVY TOWER
NUMBER OF OBSERVATIONS PER HOUR

[illegible]

Table B9.

JUNE 1977 KTVY TOWER
NUMBER OF OBSERVATIONS PER HOUR

	00	01	02	03	04	05	06	07	08	09	10	11	12	13	14	15	16	17	18	19	20	21	22	23
DATE	30	30	30	30	30	30	30	30	30	30	30	30	30	30	30	30	30	30	30	30	30	30	30	30
1	30	30	30	30	30	30	30	30	30	30	30	30	30	30	30	30	30	30	30	30	30	30	30	30
2	30	30	30	30	30	30	30	30	30	30	30	30	30	30	30	30	30	30	30	30	30	30	30	30
3	30	30	30	30	30	30	30	30	30	30	30	30	30	30	30	30	30	30	30	30	30	30	30	30
4	30	30	30	30	30	30	30	30	30	30	30	30	30	30	30	30	30	30	30	30	30	30	30	30
5	30	30	30	30	30	30	30	30	30	30	30	30	30	30	30	30	30	30	30	30	30	30	30	30
6	30	30	30	30	30	30	30	30	30	30	30	30	30	30	30	30	30	30	30	30	30	30	30	30
7	30	30	30	30	30	30	30	30	30	30	30	30	30	30	30	30	30	30	30	30	30	30	30	30
8	30	30	30	30	30	30	30	30	30	30	30	30	30	30	30	30	30	30	30	30	30	30	30	30
9	30	30	30	30	30	30	30	30	30	30	30	30	30	30	30	30	30	30	30	30	30	30	30	30
10	30	30	30	30	30	30	30	30	30	30	30	30	30	30	30	30	30	30	30	30	30	30	30	30
11	30	30	30	30	30	30	30	30	30	30	30	30	30	30	30	30	30	30	30	30	30	30	30	30
12	30	30	30	30	30	30	30	30	30	30	30	30	30	30	30	30	30	30	30	30	30	30	30	30
13	30	30	30	30	30	30	30	30	30	30	30	30	30	30	30	30	30	30	30	30	30	30	30	30
14	30	30	30	30	30	30	30	30	30	30	30	30	30	30	30	30	30	30	30	30	30	30	30	30
15	30	30	30	30	30	30	30	30	30	30	30	30	30	30	30	30	30	30	30	30	30	30	30	30
16	30	30	30	30	30	30	30	30	30	30	30	30	30	30	30	30	30	30	30	30	30	30	30	30
17	30	30	30	30	30	30	30	30	30	30	30	30	30	30	30	30	30	30	30	30	30	30	30	30
18	30	30	30	30	30	30	30	30	30	30	30	30	30	30	30	30	30	30	30	30	30	30	30	30
19	30	30	30	30	30	30	30	30	30	30	30	30	30	30	30	30	30	30	30	30	30	30	30	30
20	30	30	30	30	30	30	30	30	30	30	30	30	30	30	30	30	30	30	30	30	30	30	30	30
21	30	30	30	30	30	30	30	30	30	30	30	30	30	30	30	30	30	30	30	30	30	30	30	30
22	30	30	30	30	30	30	30	30	30	30	30	30	30	30	30	30	30	30	30	30	30	30	30	30
23	30	30	30	30	30	30	30	30	30	30	30	30	30	30	30	30	30	30	30	30	30	30	30	30
24	30	30	30	30	30	30	30	30	30	30	30	30	30	30	30	30	30	30	30	30	30	30	30	30
25	30	30	30	30	30	30	30	30	30	30	30	30	30	30	30	30	30	30	30	30	30	30	30	30
26	30	30	30	30	30	30	30	30	30	30	30	30	30	30	30	30	30	30	30	30	30	30	30	30
27	30	30	30	30	30	30	30	30	30	30	30	30	30	30	30	30	30	30	30	30	30	30	30	30
28	30	30	30	30	30	30	30	30	30	30	30	30	30	30	30	30	30	30	30	30	30	30	30	30
29	30	30	30	30	30	30	30	30	30	30	30	30	30	30	30	30	30	30	30	30	30	30	30	30
30	30	30	30	30	30	30	30	30	30	30	30	30	30	30	30	30	30	30	30	30	30	30	30	30

Table B10.

JULY 1977 KTVY TOWER
NUMBER OF OBSERVATIONS PER HOUR

DATE	YEAR																							
	00	01	02	03	04	05	06	07	08	09	10	11	12	13	14	15	16	17	18	19	20	21	22	23
1	302	303	303	303	304	303	303	303	303	303	303	303	303	303	303	303	303	303	303	303	303	303	303	303
2	304	304	304	304	304	304	304	304	304	304	304	304	304	304	304	304	304	304	304	304	304	304	304	304
3	302	302	302	302	302	302	302	302	302	302	302	302	302	302	302	302	302	302	302	302	302	302	302	302
4	304	304	304	304	304	304	304	304	304	304	304	304	304	304	304	304	304	304	304	304	304	304	304	304
5	304	304	304	304	304	304	304	304	304	304	304	304	304	304	304	304	304	304	304	304	304	304	304	304
6	303	303	303	303	303	303	303	303	303	303	303	303	303	303	303	303	303	303	303	303	303	303	303	303
7	303	303	303	303	303	303	303	303	303	303	303	303	303	303	303	303	303	303	303	303	303	303	303	303
8	303	303	303	303	303	303	303	303	303	303	303	303	303	303	303	303	303	303	303	303	303	303	303	303
9	302	302	302	302	302	302	302	302	302	302	302	302	302	302	302	302	302	302	302	302	302	302	302	302
10	303	303	303	303	303	303	303	303	303	303	303	303	303	303	303	303	303	303	303	303	303	303	303	303
11	301	301	301	301	301	301	301	301	301	301	301	301	301	301	301	301	301	301	301	301	301	301	301	301
12	302	302	302	302	302	302	302	302	302	302	302	302	302	302	302	302	302	302	302	302	302	302	302	302
13	301	301	301	301	301	301	301	301	301	301	301	301	301	301	301	301	301	301	301	301	301	301	301	301
14	303	303	303	303	303	303	303	303	303	303	303	303	303	303	303	303	303	303	303	303	303	303	303	303
15	302	302	302	302	302	302	302	302	302	302	302	302	302	302	302	302	302	302	302	302	302	302	302	302
16	303	303	303	303	303	303	303	303	303	303	303	303	303	303	303	303	303	303	303	303	303	303	303	303
17	302	302	302	302	302	302	302	302	302	302	302	302	302	302	302	302	302	302	302	302	302	302	302	302
18	303	303	303	303	303	303	303	303	303	303	303	303	303	303	303	303	303	303	303	303	303	303	303	303
19	303	303	303	303	303	303	303	303	303	303	303	303	303	303	303	303	303	303	303	303	303	303	303	303
20	302	302	302	302	302	302	302	302	302	302	302	302	302	302	302	302	302	302	302	302	302	302	302	302
21	302	302	302	302	302	302	302	302	302	302	302	302	302	302	302	302	302	302	302	302	302	302	302	302
22	303	303	303	303	303	303	303	303	303	303	303	303	303	303	303	303	303	303	303	303	303	303	303	303
23	303	303	303	303	303	303	303	303	303	303	303	303	303	303	303	303	303	303	303	303	303	303	303	303
24	303	303	303	303	303	303	303	303	303	303	303	303	303	303	303	303	303	303	303	303	303	303	303	303
25	303	303	303	303	303	303	303	303	303	303	303	303	303	303	303	303	303	303	303	303	303	303	303	303
26	303	303	303	303	303	303	303	303	303	303	303	303	303	303	303	303	303	303	303	303	303	303	303	303
27	303	303	303	303	303	303	303	303	303	303	303	303	303	303	303	303	303	303	303	303	303	303	303	303
28	303	303	303	303	303	303	303	303	303	303	303	303	303	303	303	303	303	303	303	303	303	303	303	303
29	303	303	303	303	303	303	303	303	303	303	303	303	303	303	303	303	303	303	303	303	303	303	303	303
30	303	303	303	303	303	303	303	303	303	303	303	303	303	303	303	303	303	303	303	303	303	303	303	303
31	303	303	303	303	303	303	303	303	303	303	303	303	303	303	303	303	303	303	303	303	303	303	303	303

Table B11.

AUGUST 1977 KTVY TOWER
NUMBER OF OBSERVATIONS PER HOUR

DATE	HOUR																							
	00	01	02	03	04	05	06	07	08	09	10	11	12	13	14	15	16	17	18	19	20	21	22	23
1	303	302	302	303	302	303	303	302	303	303	302	302	302	302	302	303	302	303	302	302	303	303	302	302
2	304	303	302	304	302	303	303	304	303	303	301	303	302	303	302	302	302	303	302	302	303	302	303	302
3	303	303	304	303	303	302	304	303	303	303	303	305	6	303	303	301	302	303	302	302	302	303	302	303
4	302	303	303	303	302	301	301	303	303	304	301	301	303	302	302	302	302	302	303	302	302	302	302	302
5	302	302	303	303	302	303	301	303	302	302	302	302	303	303	301	301	303	301	302	302	303	301	302	302
6	302	302	303	301	302	302	302	302	303	302	302	303	302	303	303	302	302	302	302	302	302	302	302	302
7	303	302	303	303	301	303	302	302	303	303	302	303	302	303	303	302	303	301	302	302	302	302	303	303
8	303	302	303	303	303	303	303	302	303	302	302	303	307	303	303	302	303	302	302	302	303	301	303	303
9	303	302	303	303	303	303	303	301	303	302	303	302	303	302	303	302	303	302	302	302	302	303	303	303
10	302	303	303	302	303	302	303	303	302	303	303	302	302	303	303	302	303	303	302	302	302	303	302	302
11	303	302	302	303	301	303	302	303	302	303	302	302	303	303	303	302	303	304	301	303	303	303	303	303
12	302	303	304	303	304	302	303	303	303	302	303	273	31	302	302	303	302	302	302	302	303	303	302	303
13	302	302	302	304	303	303	303	303	302	303	303	303	303	303	303	302	302	303	303	303	303	303	303	303
14	303	303	303	303	303	303	303	304	302	303	303	302	302	303	302	302	302	303	301	303	301	302	303	302
15	301	303	302	303	303	302	302	302	303	302	277	302	302	303	302	302	302	302	302	302	302	303	302	302
16	303	302	301	302	303	302	302	302	303	302	302	301	302	302	301	303	302	302	24	303	302	302	302	302
17	302	302	303	301	302	303	303	303	302	302	272	31	302	301	303	303	302	302	302	303	301	303	302	302
18	302	302	303	303	303	302	302	303	303	303	302	302	303	303	303	301	304	303	302	303	303	302	302	301
19	303	302	303	303	304	303	303	303	303	303	303	303	303	303	301	303	304	303	302	302	302	301	302	303
20	303	303	303	302	303	303	303	302	304	303	303	303	302	304	303	303	303	302	302	301	303	302	302	302
21	304	303	303	304	303	304	303	304	304	302	303	302	302	303	302	303	303	304	304	303	303	302	303	301
22	303	302	303	303	302	302	303	303	303	303	37	13	301	303	303	303	303	303	303	302	303	303	302	303
23	303	303	303	302	303	304	302	302	302	302	301	303	303	302	302	302	302	302	302	302	302	302	303	303
24	302	303	302	303	302	303	301	302	302	302	301	304	302	302	302	302	302	302	302	303	302	302	303	302
25	302	303	302	302	303	303	301	302	302	302	302	301	303	302	302	302	302	302	302	303	302	303	301	301
26	302	302	302	302	303	303	302	302	302	302	302	301	304	301	302	302	302	302	302	302	302	302	302	302
27	302	302	303	302	302	303	302	302	302	302	301	304	302	302	302	302	302	302	302	301	302	302	302	302
28	303	303	303	303	302	303	302	302	302	302	302	304	302	303	303	303	302	302	302	301	302	303	302	303
29	303	303	303	302	302	303	302	302	302	302	302	304	302	303	303	303	302	302	302	302	302	302	302	302
30	303	303	303	302	302	303	302	302	302	302	302	302	302	304	303	303	302	302	302	302	302	302	302	302
31	303	303	303	302	302	303	302	302	302	302	302	302	302	304	303	303	302	302	302	302	302	302	302	302

Table B12.

SEPTEMBER 1977 KTVY TOWER

NUMBER OF OBSERVATIONS PER HOUR

	00	01	02	03	04	05	06	07	08	09	10	11	12	13	14	15	16	17	18	19	20	21	22	23
1	303	303	303	303	303	303	303	303	303	303	303	303	303	303	303	303	303	303	303	303	303	303	303	303
2	303	303	303	303	303	303	303	303	303	303	303	303	303	303	303	303	303	303	303	303	303	303	303	303
3	303	303	303	303	303	303	303	303	303	303	303	303	303	303	303	303	303	303	303	303	303	303	303	303
4	303	303	303	303	303	303	303	303	303	303	303	303	303	303	303	303	303	303	303	303	303	303	303	303
5	303	303	303	303	303	303	303	303	303	303	303	303	303	303	303	303	303	303	303	303	303	303	303	303
6	303	303	303	303	303	303	303	303	303	303	303	303	303	303	303	303	303	303	303	303	303	303	303	303
7	303	303	303	303	303	303	303	303	303	303	303	303	303	303	303	303	303	303	303	303	303	303	303	303
8	303	303	303	303	303	303	303	303	303	303	303	303	303	303	303	303	303	303	303	303	303	303	303	303
9	303	303	303	303	303	303	303	303	303	303	303	303	303	303	303	303	303	303	303	303	303	303	303	303
10	303	303	303	303	303	303	303	303	303	303	303	303	303	303	303	303	303	303	303	303	303	303	303	303
11	303	303	303	303	303	303	303	303	303	303	303	303	303	303	303	303	303	303	303	303	303	303	303	303
12	303	303	303	303	303	303	303	303	303	303	303	303	303	303	303	303	303	303	303	303	303	303	303	303
13	303	303	303	303	303	303	303	303	303	303	303	303	303	303	303	303	303	303	303	303	303	303	303	303
14	303	303	303	303	303	303	303	303	303	303	303	303	303	303	303	303	303	303	303	303	303	303	303	303
15	303	303	303	303	303	303	303	303	303	303	303	303	303	303	303	303	303	303	303	303	303	303	303	303
16	303	303	303	303	303	303	303	303	303	303	303	303	303	303	303	303	303	303	303	303	303	303	303	303
17	303	303	303	303	303	303	303	303	303	303	303	303	303	303	303	303	303	303	303	303	303	303	303	303
18	303	303	303	303	303	303	303	303	303	303	303	303	303	303	303	303	303	303	303	303	303	303	303	303
19	303	303	303	303	303	303	303	303	303	303	303	303	303	303	303	303	303	303	303	303	303	303	303	303
20	303	303	303	303	303	303	303	303	303	303	303	303	303	303	303	303	303	303	303	303	303	303	303	303
21	303	303	303	303	303	303	303	303	303	303	303	303	303	303	303	303	303	303	303	303	303	303	303	303
22	303	303	303	303	303	303	303	303	303	303	303	303	303	303	303	303	303	303	303	303	303	303	303	303
23	303	303	303	303	303	303	303	303	303	303	303	303	303	303	303	303	303	303	303	303	303	303	303	303

REFERENCES

- Asselin, R. (1972). "Frequency filter for time integrations." *Mon. Wea. Rev.*, 100, 487-490.
- Charba, J. (1974). "Application of gravity current model to analysis of squall-line gust front." *Mon. Wea. Rev.*, 102, 140-156.
- Goff, R. C. (1975). "Thunderstorm-Outflow Kinematics and Dynamics." NOAA Tech. Memo ERL NSSL-75, 63. pp.
- Goff, R. C., J. T. Lee and E. A. Brandes (1977). "Gust Front Analytical Study." Report No. FAA-RD-77-119, 126 pp.
- Hane, C. E. (1973). "The squall line thunderstorm: Numerical experimentation." *J. Atmos. Sci.*, 30, 1672-1690.
- Kessler, E. et al. (1961-1964). "Relationships between tropical precipitation and kinematic cloud models." Repts 1-5, Contract DA36-039 SC 89099, Travelers Research Center.
- Ludlam, F. H. (1961). "The hailstorm." *Weather*, 16, 152-162.
- Margules, M. (1905). "Zur sturmtheorie." *Met. Zeit.*, 23, 481-497.
- Mitchell, K. E. and J. B. Hovermale (1977). "A numerical investigation of the severe thunderstorm gust front." *Mon. Wea. Rev.*, 105, 657-675.
- Ogura, Y. and T. Takahashi (1971). "Numerical simulation of the life cycle of a thunderstorm cell." *Mon. Wea. Rev.*, 99, 895-911.
- Orville, H. D. and L. J. Sloan (1970). "A numerical simulation of the life history of a rainstorm." *J. Atmos. Sci.*, 27, 1148-1159.
- Schlesinger, R. E. (1973). "A numerical model of deep moist convection: Part I." *J. Atmos. Sci.*, 30, 835-856.
- (1974). "A numerical model of deep moist convection: Part II." *J. Atmos. Sci.*, 30, 1374-1391.
- (1975). "A three-dimensional numerical model of an isolated deep convective cloud: Preliminary result." *J. Atmos. Sci.*, 32, 934-957.
- Schuman, F. G. and J. B. Hovermale (1968). "An operational six-layer primitive equation model." *J. Appl. Meteor.*, 7, 525-547.
- Steiner, J. T. (1973). "A three-dimensional model of cumulus cloud development." *J. Atmos. Sci.*, 30, 414-435.

Takeda, T. (1965). "The downdraft in convective shower-cloud under the vertical wind shear and its significance for the maintenance of convective system." J. Meteor. Soc. Japan, 43, 302-309.

____ (1966). "The downdraft in the convective cloud and raindrops: A Numerical computation." J. Meteor. Soc. Japan, 44, 1-11.

____ (1971). "Numerical simulation of a precipitating convective cloud: The formation of a long-lasting cloud." J. Atmos. Sci., 28, 350-376.

U.S. Department of Commerce (1977). Storm Data, 19, (No. 5), 14-17; (No. 6), 15.

Wilhelmson, R. (1974). "The life cycle of a thunderstorm in three dimensions." J. Atmos. Sci., 31, 1629-1651.